People's Democratic Republic of Algeria
Ministry of Higher Education and Scientific Research

University of Batna 2 – Mostefa Ben Boulaïd
Faculty of Technology
Department of Electronics

Dissertation

Prepared in LEA Laboratory

Presented in fulfillment of the requirement of the degree of
Doctor of Science in Electronics
Option: Instrumentation

Entitled:

Soft-computing-based approaches to study and model the semiconductor devices

Presented by:

MAOUCHA Abdelhak

Committee members:

Dr. MAHAMDI Ramdane	Professor	University of Batna 2	Chairman
Dr. DJEFFAL Fayçal	Professor	University of Batna 2	Advisor
Dr. TOUAFEK Naima	Assoc Professor(A)	ENSB University of Constantine 3	Examiner
Dr. SAOULI Abdelali	Assoc Professor(A)	University of Constantine 1	Examiner

-2023-

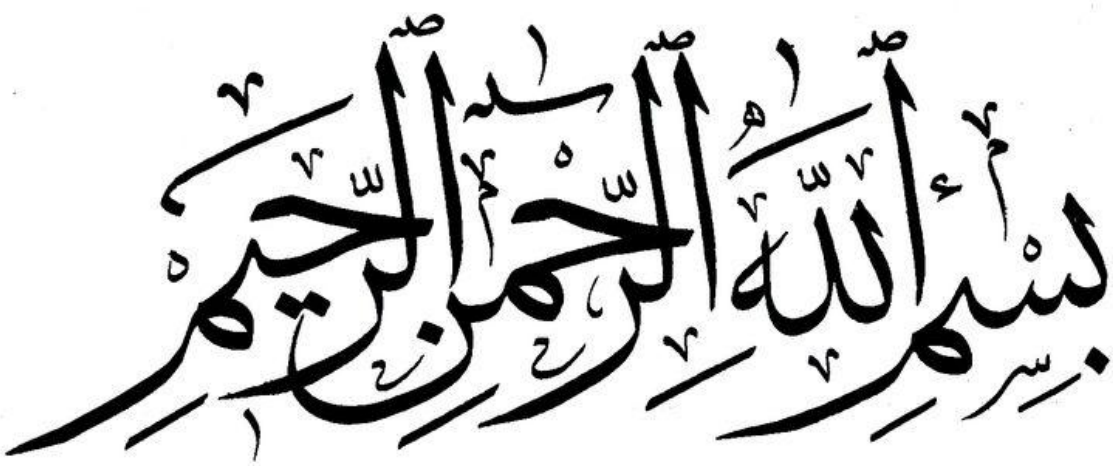
بسم الله الرحمن الرحيم

DEDICATION

إلى شموس نور الله بها دنياي "دادا"، "نانا"، "أبي"، و "أمي".

إلى شموس جعلها الله سندي في هذه الدنيا "إخوتي".

إلى شموس رزقني الله بها فاكتملت فرحتي "زوجتي" و "أبنائي".

I would like to extend my heartfelt gratitude to the luminous stars who have illuminated my life, 'Dada,' 'Nana,' 'Dad,' and 'Mom'.

To the stars whom God has made my steadfast companions in this world, 'my brothers'.

To the stars that God has blessed me with, bringing fullness to my joy, 'my wife' and 'my children'.

Acknowledgments

First and foremost, I thank Almighty God, who granted me health, strength, and willpower to complete this work.

This dissertation would not have seen the light without the exceptional support of my supervisor, **Professor Fayçal DJEFFAL**. His keen attention to detail, vast knowledge, and valuable guidance have been a source of inspiration and kept my work on the right track. He has always been attentive and available throughout the preparation of this dissertation.

I would like to express my gratitude to Mr. MAHAMDI Ramdane, a professor at the University of Batna 2, for accepting to chair the jury of this dissertation. I also thank Dr. TOUAFEK Naima, Associate Professor at the University of Constantine 3, Dr. SAOULI Abdelali, Associate Professor at the University of Constantine 1, for accepting to review and evaluate this work.

Finally, I appreciate the support of Dr. **Toufik BENTRCIA** and Dr. **Hichem FERHATI** for all that they have done to help me for completing this work.

Abstract

Semiconductor modeling and optimization play a crucial role in dealing with semiconductor devices, as they are used to simulate their performances under various operating conditions. This dissertation focuses on improving the performance of semiconductor-based devices, specifically thin-film solar cells. It discusses the use of analytical and numerical modeling techniques, including soft-computing-based optimization algorithms, to boost the performance of these devices. First, a comprehensive overview of the different equations that govern the physical behavior of semiconductors and the use of analytical and numerical modeling techniques in semiconductor device design will be provided, where the advantages and limitations of both techniques and their potential applications in optimizing device performance will be discussed. Finally a detailed review of metaheuristic-based optimization techniques and their potential application in semiconductor device optimization is provided. Next, a novel modeling framework for the design and optimization of copper indium gallium selenide (CIGS)-based thin-film solar cells using a hybrid GBG-PSO-approach is proposed. Moreover the development of new analytical models and the use of numerical simulations to confirm the accuracy of the results is discussed. The chapter also explores the use of non-toxic elements, such as ZnMgO, instead of conventional toxic materials like CdS, to improve solar cell performance. The proposed methodology results in a 31.88% relative improvement in solar cell performance compared to conventional designs. Then, a high-efficiency lead-free perovskite solar cell design based on the optimization of double-absorber material and charge carrier transport layers is proposed, using of eco-friendly and stable lead-free materials. The effect of different hole and electron transport layer materials on double-layered perovskite solar cell performance is investigated. The proposed design methodology leads to a high-performing lead-free perovskite solar cell with a power conversion efficiency of 33.57%. Thereafter, a new design methodology for thin-film tandem solar cells made up of a lead-free perovskite-based top sub-cell and a CZTSSe-based bottom sub-cell is proposed. The chapter discusses the use of numerical simulations to optimize interfaces between the electron and hole transport layers, introducing a graded band-gap profile, a back surface field (BSF) layer, and a non-toxic buffer layer (ZnSe) to improve the performance of the tandem cell. The proposed design methodology leads to a high-performing tandem solar cell with a PCE of 28.42%.

Keywords: Analytical modeling; metaheuristic-based optimization; CIGS; ZnMgO; Alignment; Ofset; Metaheuristic; PSO; Photovoltaic; Lead-free; Perovskite; Solar cell; Double-absorber; Band-alignment; Current matching; Graded band-gap; Cd-free CZTS; Tandem cell; Filtered spectrum.

ملخص

تلعب نمذجة أشباه الموصلات وتجويدها دورًا مهمًا في التعامل مع المركبات الالكترونية ، حيث يتم استخدامها لمحاكاة أدائها في ظل ظروف التشغيل المختلفة، مما يسمح للمهندسين بتحسين تصاميم ها وتحسين كفاءتها وسرعتها وموثوقيتها. تركز هذه الأطروحة على تحسين أداء العناصر القائمة على أشباه الموصلات، وتحديداً الخلايا الشمسية ذات الأغشية الرقيقة. وتناقش استخدام تقنيات النمذجة التحليلية و الرقمية، بما في ذلك خوارزميات التجويد القائمة على الحوسبة اللينة، لتحسين أداء هذه العناصر. في البداية، سيتم تقديم نظرة شاملة على المعادلات المختلفة التي تحاكي السلوك الفيزيائي لأشاه الموصلات واستخدام تقنيات النمذجة التحليلية والعددية في تصميم عناصر أشباه الموصلات، حيث سيتم مناقشة مزايا وعيوب كلتا التقنيتين وتطبيقاتهما المحتملة في تحسين أداء الأجهزة. وأخيرًا سيتم توفير استعراض مفصل لتقنيات التجويد القائمة على الحوسبة اللينة وتطبيقاتها المحتملة في تحسين أداء عناصر أشباه الموصلات. ثم يقترح إطار نمذجة جديد لتصميم وتحسين الخلايا الشمسية ذات الأغشية الرقيقة المستندة إلى النحاس الإنديوم الغاليوم و السيلينيد (CIGS) باستخدام أسلوب الطبقة الممتصة ذات فجوة نطاق متدرجة مقرونة مع تقنية التجويد بسرب الجسيمات (GBG-PSO). كما يتم مناقشة تطوير نماذج تحليلية جديدة و استخدام المحاكاة العددية لتأكيد دقة النتائج. يستكشف الفصل أيضًا استخدام العناصر غير السامة، مثل (ZnMgO)، بدلاً من المواد السامة التقليدية مثل (CdS) لتحسين أداء الخلية الشمسية. تؤدي المنهجية المقترحة إلى تحسين نسبي في أداء الخلية الشمسية مقارنةً بالتصاميم التقليدية بقيمة 31.88٪. ثم بعد ذلك يتم اقتراح تصميم جديد ذي كفاءة عالية للخلايا الشمسية المرتكزة على البيروفسكيت و الخالية من الرصاص، مبني على تحسين المواد الممتصة مزدوجة الطبقات والطبقة الناقلة لحاملات الشحنة باستخدام مواد صديقة للبيئة ومستقرة خالية من الرصاص. يتم التحقق من تأثير مختلف مواد الطبقة الناقلة للثقوب و الإلكترونات على أداء الخلية الشمسية بالبيروفسكيت ذات الطبقتين. تؤدي منهجية التصميم المقترحة إلى الحصول على خلية شمسية بالبيروفسكيت خالية من الرصاص عالية الأداء بكفاءة تحويل طاقوية نسبتها 33.57٪. بعد ذلك يتم اقتراح منهجية تصميم جديدة للخلايا الشمسية المركبة ذات الأغشية الرقيقة ، مكونة من خلية فرعية علوية مبنية على البيروفسكيت الخالي من الرصاص وخلية فرعية سفلية مبنية على (CZTSSe). يتناول الفصل استخدام المحاكاة العددية لتحسين الطبقة البينية الموجودة بين طبقات نقل الإلكترونات والثقوب، مستخدما أسلوب الطبقة الممتصة ذات فجوة نطاق متدرجة إضافة إلى طبقة مجال السطح الخلفي (BSF) وطبقة العزل غير السامة (ZnSe) لتحسين أداء الخلية الشمسية المركبة. يؤدي استخدام هذه الطريقة إلى الحصول على خلية شمسية مركبة عالية الأداء بكفاءة تحويل طاقوية تصل إلى 28.42٪.

الكلمات المفتاحية: النمذجة التحليلية ، التحسينات المستندة إلى الأساليب الذكية ، CIGS، ZnMgO، محاذاة، Ofset، ذكاء اصطناعي ، PSO، الخلايا الكهروضوئية ، الخالية من الرصاص ، البيروفسكيت ، الخلية الشمسية، الممتص المزدوج ، محاذاة الفجوة النطاقية ، مطابقة التيار ، الفجوة النطاقية المدرجة ، CZTS الخالية من الكادميوم، الخلية المركبة، الطيف المصفى.

Résumé

La modélisation et l'optimisation des semi-conducteurs jouent un rôle important dans le traitement des dispositifs à semi-conducteurs, car ils sont utilisés pour simuler leurs performances dans diverses conditions de fonctionnement, permettant aux ingénieurs d'optimiser leurs conceptions et d'améliorer leur efficacité, leur vitesse et leur fiabilité. Cette thèse se concentre sur l'amélioration de la performance des dispositifs à semi-conducteurs, en particulier les cellules solaires à couche mince. Elle aborde l'utilisation de techniques de modélisation analytique et numérique, y compris des algorithmes d'optimisation basés sur le calcule souple, pour optimiser la performance de ces dispositifs. Tout d'abord, une vue d'ensemble complète des différentes équations qui gouvernent le comportement physique des semi-conducteurs et de l'utilisation des techniques de modélisation analytique et numérique dans la conception de dispositifs à semi-conducteurs sera fournie, où les avantages et les limites des deux techniques et leurs applications potentielles dans l'optimisation de la performance des dispositifs seront discutés. Enfin, une revue détaillée des techniques d'optimisation basées sur les métaheuristiques et de leur application potentielle dans l'optimisation de dispositifs à semi-conducteurs est fournie. Ensuite, un nouveau cadre de modélisation pour la conception et l'optimisation de cellules solaires à couche mince à base de (CIGS) en utilisant une approche hybride GBG-PSO est proposé. De plus, le développement de nouveaux modèles analytiques et l'utilisation de simulations numériques pour confirmer l'exactitude des résultats sont discutés. Le chapitre explore également l'utilisation d'éléments non toxiques, tels que le ZnMgO, au lieu de matériaux toxiques conventionnels tels que le CdS, pour améliorer la performance des cellules solaires. La méthodologie proposée permet une amélioration relative de 31,88% de la performance de la cellule solaire par rapport aux conceptions conventionnelles. Après, une conception de cellule solaire à base de perovskite sans plomb à haute efficacité basée sur l'optimisation du matériau double absorbeur et des couches de transport de porteurs de charge est proposée, en utilisant des matériaux sans plomb écologiques et stables. L'effet de différents matériaux de couche de transporteur de trous et d'électrons sur la performance de la cellule solaire à perovskite à double absorbeur est étudié. La méthodologie de conception proposée permet d'obtenir une cellule solaire à perovskite sans plomb performante avec un rendement de conversion de puissance de 33,57%. Puis, une nouvelle méthodologie de conception pour les cellules solaires tandem à couche mince composées d'une cellule supérieure à base de pérovskite sans plomb et d'une cellule inférieure à base de CZTSSe est proposée. Le chapitre discute de l'utilisation de simulations numériques pour optimiser les interfaces entre les couches de transport d'électrons et de trous, en introduisant un profil de bande interdite graduelle, une couche de champ de surface arrière (BSF) et une couche tampon non toxique (ZnSe) pour améliorer les performances de la cellule solaire. La méthodologie de conception proposée conduit à une cellule solaire tandem performante avec un rendement de conversion énergétique (PCE) de 28,42 %.

Mots-clés: Modélisation analytique; optimisation basée sur des métaheuristiques; CIGS; ZnMgO; Alignement; Décalage; Photovoltaïque; Sans plomb; Pérovskite; Cellule solaire; Double absorbeur; Alignement de bande; Bande interdite graduelle; CZTS sans Cd; Cellule tandem; Spectre filtré.

Table of Contents

1.Introduction and state of the art

Semiconductor devices are electronic components made of materials with properties that lie between those of conductors and insulators. These devices form the foundation of modern electronics and are used in a wide range of applications, from simple diodes and transistors in everyday electronics to complex integrated circuits in advanced computing systems [1]. The semiconductor materials used in these devices are typically crystals doped with small amounts of impurities to create regions of either positive or negative charge. By controlling the distribution of charge within these materials, semiconductor devices can be investigated to exhibit a variety of useful electrical properties, including the ability to control the flow of current, amplify signals, and store information [1,2]. Semiconductor devices are fundamental building blocks of modern electronics and have revolutionized the way we live and work. From the micro-processors that power our computers and smartphones to the LEDs that light our homes and streets, they are essential components of the technologies that shape our world [3,4]. The design and optimization of these devices require an accurate understanding of their behavior and performance, which is provided by models that simulate the accurate operation. In this context, traditional modeling based on analytical and numerical approaches have been used to study and model the behavior of semiconductor devices. Analytical models provide analytical solutions to the physical equations governing the behavior of semiconductors, while numerical models solve these equations using numerical algorithms, such as finite difference, finite element, or Monte Carlo methods [1,5]. Although these approaches have been widely used and have provided valuable insights into the behavior of semiconductor devices, they have some limitations, including the inability to handle complex physical phenomena and the difficulty in modeling nonlinear behavior. This situation may yield an inaccurate prediction of the device performance [6]. In order to overcome this issue, Soft computing techniques (SoCo), have been proven to be effective in modeling and optimizing complex systems in various fields. Soft computing is a branch of computer science dealing with approaches that can effectively handle imprecision, uncertainty, and partial truth. Unlike hard computing, which relies on precise mathematical models and algorithms [7], SoCo techniques are designed to mimic the way humans think and make decisions[8]. It encompasses a range of methods, including fuzzy logic, neural networks, genetic algorithms, and machine learning. These techniques can be used to develop systems that

are able to learn and adapt from experience, recognize patterns, and make decisions based on incomplete or uncertain information. SoCo approaches are particularly useful in applications that involve complex, real-world problems where traditional methods may be impractical or ineffective [7,8].

Soft computing has a wide range of applications across various domains [9-16], including but not limited to:

-Engineering: This technique is widely used for tasks such as system control, fault diagnosis, optimization, and prediction. For example, neural networks and fuzzy logic are often used for process control in manufacturing, while evolutionary computation is used for optimizing complex engineering designs.

-Finance: For tasks such as fraud detection, credit scoring, predict stock prices, market trends, and investment decision-making. For example, neural networks and fuzzy logic are used for predicting stock prices, while evolutionary computation is used for optimizing investment portfolios.

-Medicine: It has been used in medical diagnosis and decision-making systems, which can analyze medical data and assist in diagnosing diseases, predicting the risk of developing a disease, and suggesting treatment options.

-Robotics: It is used for tasks such as motion planning, obstacle avoidance, and control. For example, swarm intelligence algorithms are used for multi-robot coordination, while fuzzy logic is used for controlling robot movements.

-Image and speech recognition: Methods such as neural networks and deep learning have been widely used in computer vision and speech recognition applications. They can recognize patterns and identify objects in images and speech with high accuracy.

-Natural language processing: Tasks such as text classification, sentiment analysis, and machine translation. For example, neural networks and fuzzy logic are used for language modeling, while evolutionary computation is used for optimizing machine translation systems.

-Optimization: Genetic algorithms (GA) and particle swarm optimization (PSO) can be used to solve complex optimization problems in various domains.

The semiconductor industry is continuously striving to improve device performance and reduce development time and cost. For addressing these challenges, SoCo techniques have emerged as powerful tools by analyzing large amounts of data and optimizing device parameters.

One of the most used devices in electronics is the transistor. In the context, Soft computing techniques have been used both in the modeling and optimization of transistors. Concerning the modeling process, these techniques have been used to develop accurate and reliable models of transistor behavior under a wide range of operating conditions. For instance, artificial neural networks have been used to learn complex relationships between inputs and outputs from large datasets of transistor performance data, while fuzzy logic and genetic algorithms have been used to capture the non-linear behavior of transistors under different conditions [17-21]. Regarding the optimization, SoCo techniques have been used to optimize the performance of transistors and electronic circuits. For example, genetic algorithms, particle swarm optimization (PSO) and other optimization techniques can be used to search through a large space of transistor designs to find the best configuration for a particular application. Similarly, artificial neural networks can be trained on data to predict the performance of a particular transistor design, allowing designers to make informed decisions about which design to use [21-24].

In the setting of optoelectronic devices, SoCo can be used to model the behavior of devices such as solar cells, photodetectors, and light-emitting diodes (LEDs), and to optimize their performance. It can be used to optimize the design of photodetectors by combining numerical techniques with GA (Genetic Algorithm) or using a combined semi-analytical modeling and PSO-based optimization approaches to improve the sensor performance [25-27]. In photovoltaic domain, as shown in Figure 1, the intense competition in the photovoltaic domain, where researchers are striving to attain the maximum efficiency through the utilization of various materials and improvement techniques. SoCo techniques are particularly useful in this regard, as they can model complex nonlinear relationships between input and output variables. Fuzzy logic, for instance, can provide accurate predictions of the output variables based on the input variables to model the solar cell behavior and extract their parameters [28]. SoCo can handle imprecise and uncertain information and provide accurate control decisions based on the current operating conditions of the PV system (MPPT) [29-31]. While GA

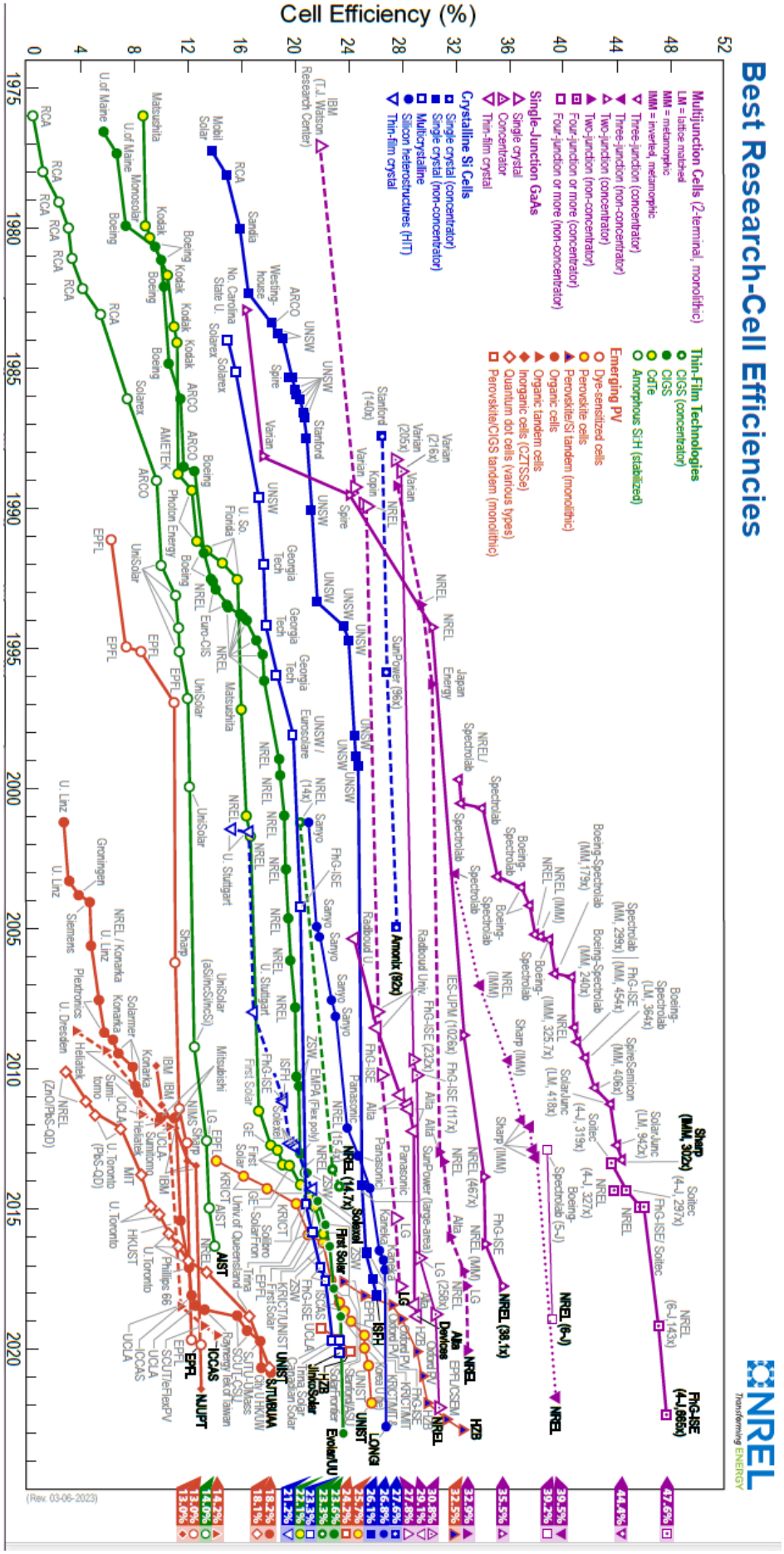

Figure.1 : A timeline chart of the best research cell efficiencies for different photovoltaic technologies from 1976 to present according to the National Renewable Energy Laboratory (NREL) [36].

and PSO can be used to optimize the design of the photovoltaic system, such as the selection of the best combination of materials, the sizing of the system components, and the configuration of the system layout [32-35]. Soft computing approaches can also be used to analyze large datasets and extract meaningful patterns and insights. This can be particularly useful for understanding the behavior of complex optoelectronic devices, and for identifying areas for improvement.

SoCo approaches offer a powerful tool for modeling and optimizing semiconductor devices, improving their efficiency, reliability, and performance in various applications. SoCo can facilitate the development of more efficient and effective optoelectronic devices. These innovations can impact fields such as materials science, energy, telecommunications, computing, consumer electronics, and more. From smartphones and laptops to medical devices and space probes, many of today's innovations have been made possible by soft computing techniques.

2.Dissertation outline

This dissertation is structured into four chapters that outline the conducted research work. The first chapter is dedicated to the modeling and optimization of semiconductors. First, different analytical and numerical modeling techniques are presented, followed by different optimization techniques based on metaheuristics, where their basic concepts are explained in detail. The application of these metaheuristic approaches to optimize semiconductor devices is also introduced.

In the second chapter, new analytical models are developed to study the behavior of solar cells by proposing a new design strategy to enhance the performance of CIGS-based thin film solar cell using the coupling of graded band gap (GBG) engineering with PSO technique. Furthermore, the impact of the band-gap engineering of the buffer layer on the cell's performance is studied. Additionally, the influence of the band-gap profiles for both of the buffer and absorber layers on the device properties is investigated, and finally, the extent improvement of the solar cell performance by combining the global optimization technique PSO with GBG engineering.

The objective of the third chapter is to examine how the performance of lead-free PSCs can be improved by utilizing appropriate carrier transport layers and double absorber lead-free perovskite engineering. The performance is evaluated through numerical modeling and simulations using a design strategy. Finally, by employing the

double-absorber layer engineering and band alignment optimization, the improvement of the device performances is carried out.

Chapter IV of this dissertation addresses novel design strategies to enhance the performance of a tandem cell consisting of two sub-cells, which can be influenced by appropriate carrier transport layers and band alignment. Besides, the study also explores the impact of graded band-gap (GBG) engineering on the overall performance of the device, specifically by applying it to the absorber layer in the bottom sub-cell. The use of a non-toxic buffer layer is also evaluated as a means of improving junction band alignment and enhancing conversion efficiency.

The aim of this dissertation is to investigate the potential of soft-computing-based approaches to study and model the behavior of semiconductor devices. The focus is on developing new models that can accurately represent the complex physical processes involved in these devices and on optimizing their performance.

References

[1] Christopher M Snowden. The Semiconductor Device Modelling. Springer-Vedag Berlin Heidelberg, 1989.

[2] D. Báez-Lópe, F.E. Guerrero-Castro, “Semiconductor Device,” Circuit Analysis with Multisim, Springer. Cham, pp. 117-122, 2011.

[3] Christopher M Snowden. Introduction to Semiconductor Device Modelling, World Scientiic Publishing Co, 1998.

[4] S. Prasad, H. Schumacher, and A. Gopinath, “Review of semiconductor materials and physics,” High-Speed Electronics and Optoelectronics: Devices and Circuits, Cambridge University Press, pp. 3-45 , 2009.

[5] Mordechai Shaul. Applications of Monte Carlo Method in Science and Engineering. InTech, 2011.

[6] Iman Ramezani, Khalil Moshkbar-Bakhshayesh, Naser Vosoughi, Mohammad B. Ghofrani, “Applications of Soft Computing in nuclear power plants: A review,” Progress in Nuclear Energy, vol. 149, pp. 104253, 2022.

[7] Wengang Zhang, Yanmei Zhang, Xin Gu, Chongzhi Wu, Liang Han. Application of Soft Computing, Machine Learning, Deep Learning and Optimizations in Geoengineering and Geoscience. Springer Singapore, 2021.

[8] Satinder Bal Gupta, Shivani, "A Review of Soft Computing Techniques and Applications," INTERNATIONAL JOURNAL OF ENGINEERING RESEARCH & TECHNOLOGY (IJERT) ICRADL, vol. 09, pp. 2278-0181, 2021.

[9] Ramjeet Singh Yadav, "Review of Academic Performance using soft computing techniques," International Journal of Computer Engineering and Applications, vol. 11, 2017.

[10] F. Srairi, M. Meguellati, L. Saidi and F. Djeffal, "Analytical modeling and optimization of new swimming microrobot design using genetic algorithm computations," 14th international conference on Sciences and Techniques of Automatic control and computer engineering STA'2013, 2013,

[11] Santosh Kumar Das, Abhishek Kumar, Bappaditya Das and A. P. Burnwal, "On Soft Computing Techniques in various areas," Computer Science and Information Technology, vol. 3, pp.59-68, 2013.

[12] Ashish Mishra, G. Suseendran and Trung-Nghia Phung, "Soft computing applications and techniques in healthcare," CRC press, Taylor and Francis Group, 2020.

[13] S. Gambhir, SK. Malik, Y. Kumar, "Role of Soft Computing Approaches in HealthCare Domain: A Mini Review," J Med Syst, vol. 40, pp. 287, 2016

[14] Hrishikesh Bhaumik, Siddhartha Bhattacharyya, Mausumi Das Nath, Susanta Chakraborty, "Hybrid soft computing approaches to content based video retrieval: A brief review," Applied Soft Computing, vol. 46, pp. 1008-1029, 2016.

[15] M. Khan, A. Manzoor, K. Rohail, S. M. Ali, A. Iftikhar and M. Alam, "Soft computing applications in education management— A review," IEEE International Conference on Innovative Research and Development *(ICIRD)*, Bangkok, Thailand, pp. 1-4, 2018.

[16] Nurul Hazwani Mohd Shamsuddin, Nor Azizah Ali and Razana Alwee, "An overview on crime prediction methods," 6th ICT International Student Project Conference, pp.1-5, 2017.

[17] T. Bentrcia, F. Djeffal and E. Chebaki, "Multi-objective Design of Nanoscale Double Gate MOSFET Devices Using Surrogate Modeling and Global Optimization," Intelligent Nanomaterials, 2nd Edition, ISBN: 978-1-119-24248-2, Edited: Ashutosh Tiwari, publisher: Wiley, pp. 395-427, 2016.

[18] F. Djeffal, A. Ferdi and M. Chahdi, "A fuzzy-logic-based approach to accurate modeling of a double gate MOSFET for nanoelectronic circuit design,"J. Semicond, vol. 33, pp. 094001, 2012.

[19] F. Djeffal, T. Bendib, R. Benzid, A. Benhaya, "An approach based on particle swarm computation to simulate the nanoscale DG MOSFET-based circuits," Turkish Journal of Electrical Engineering & Computer Sciences, vol. 18, pp. 1131-1141, 2010.

[20] D. Chowdhury, B.P. De, S. Ghosh, N.K. Singh, R. Kar, D. Mandal, "Optimization of Subthreshold Parameters of Graded-Channel Gate-Stack Double-Gate (GC-GS-DG) MOSFET Using PSO-CFIWA," Springer, Singapore, Circuits and Systems. Lecture Notes in Electrical Engineering, vol 904, pp. 41-50, 2023.

[21] T. Bentrcia, F. Djeffal and E. Chebaaki, "ANFIS-based approach to studying subthreshold behavior including the traps effect for nanoscale thin-film DG MOSFETs," J. Semicond. Vol. 34, pp.084001, 2013.

[22] T. Bendib, F. Djeffal and D. Arar, "Subthreshold behavior optimization of nanoscale Graded Channel Gate Stack Double Gate (GCGSDG) MOSFET using multi-objective genetic algorithms," Journal of Computational Electronics, pp. 210-215, Vol. 10, 2011. (Indexed by: Scopus/ISI Thomson/IF= 1.8).

[23] E. Chebaki, F. Djeffal, H. Ferhati, T. Bentrcia, , "Improved analog/RF performance of double gate junctionless MOSFET using both gate material engineering and drain/source extensions," Superlattices and Microstructures vol. 92, pp. 80-91, 2016.

[24] K. Kaharudin, F. Salehuddin, A. M.Zain, and M. A.Aziz, "Application of Taguchi-based Grey Fuzzy Logic for Simultaneous Optimization in TiO2/WSix-based Vertical Double-gate MOSFET," JTEC, vol. 9, no. 2-13, pp. 23–28, 2017.

[25] F. Djeffal, N. Boubiche, H. Ferhati, J. Faerber, F. Le Normand, N. Javahiraly, T. Fix, "Highly efficient and low-cost multispectral photodetector based on RF sputtered a-Si/Ti multilayer structure for Si-photonics applications," Journal of Alloys and Compounds, vol. 876, pp. 160176, 2021.

[26] H. Ferhati, F. Djeffal, "Role of Optimized Grooves Surface -Textured Front Glass in improving TiO2 Thin Film UV Photodetector Performance," IEEE sensors journal, vol. 16, pp. 5618- 5624, 2016.

[27] H. Ferhati, F. Djeffal, "A novel high-performance self-powered ultraviolet photodetector: Concept, analytical modeling and analysis," Superlattices an Microstructures, vol. 112, pp.480-492, 2017.

[28] T. Bendib, F. Djeffal, D. Arar and M. Meguellati, "Fuzzy-Logic-based Approach for Organic Solar Cell Parameters Extraction," Proceedings of the World Congress on Engineering, vol.2, 2013.

[29] G. Dileep, S.N. Singh, "Application of soft computing techniques for maximum power point tracking of SPV system, " Solar Energy, vol. 141, pp. 182-202, 2017.

[30] V. Indragandhi, V. Subramaniyaswamy, R. Logesh, "Resources, configurations, and soft computing techniques for power management and control of PV/wind hybrid system, " Renewable and Sustainable Energy Reviews, vol. 69, pp.129-143, 2017.

[31] M. Balamurugan, Sarat Kumar Sahoo, Sukruedee Sukchai, "Application of soft computing methods for grid connected PV system: A technological and status review," Renewable and Sustainable Energy Reviews, vol. 75, pp.1493-1508, 2017.

[32] A. Maoucha, F. Djeffal, "Multi-objective-optimization-based approach to improve the electrical efficiency for organic solar cells," Journal of Computational Electronics, Vol. 11, pp 336-343, 2012.

[33] H. Ferhati, F. Djeffal, B.L. Drissi, "Performance improvement of Perovskite /CZTS tandem solar cell using low-cost ZnS/Ag/ITO multilayer spectrum splitter," Superlattices and Microstructures, vol. 148, pp. 106727, 2020.

[34] H. Ferhati, F Djeffal, "Exceeding 30% efficiency for an environment-friendly tandem solar cell based on earth-abundant Se/CZTS materials," Physica E: Low-dimensional Systems and Nanostructures vol. 109, 52-58, 2019.

[35] F.Z. Ramadan, F. Djeffal, L.B. Drissi, S. Saidi, H. Ferhati, "Highly efficient ACdTS kesterite solar cell based on a new photovoltaic material," Journal of Physics and Chemistry of Solids, vol. 161, pp. 110458, 2022.

[36] Best Research-Cell Efficiencies chart, Available onlin: https://www.nrel.gov/pv/cell-efficiency.html

CHAPTER I

Modeling and optimization of semiconductor devices

Abstract

This chapter provides an overview of the different analytical and numerical modeling techniques used in the field of semiconductor devices, including their advantages and limitations. The focus is on the application of these methods using semiconductor equations to gain a better understanding of the system and optimize device performance. Additionally, the chapter discusses the classification and basic concepts of metaheuristic-based optimization techniques, such as MOGA, PSO, ML, and ABC-based algorithms, and their potential applications in semiconductor device optimization. The chapter serves as a comprehensive introduction to the methods and techniques used in the field of semiconductor device optimization, providing a solid foundation for further research and development.

I.1 Introduction

Modeling of semiconductor devices involves using mathematical equations and computer simulations to represent the behavior of semiconductor materials and devices. These models allow engineers and scientists to predict and understand the performance of semiconductor devices, under various operating conditions [1-4]. It is an important tool to design and optimize the microelectronic devices. In general, modeling semiconductor devices involves understanding the underlying physics of the materials, including the transport of charge carriers (electrons and holes), the generation and recombination of carriers, the interaction of carriers with impurities, defects, and applied electric fields. It also includes understanding the electrical properties of the materials and how they change with temperature and other parameters [5-7]. There are several approaches to modeling semiconductor devices, including analytical, numerical and physical (empirical) models. Analytical modeling uses mathematical equations to describe the behavior of the device and are often used for simple devices or to gain a basic understanding of the device's behavior. Numerical models explore complex computer algorithms to solve the non linear equations that describe the device's behavior and can be used to model more complex devices or to analyze the device's performance in more details. Physical models use experimental data or measurements to represent the device's behavior and can be used to validate the results of analytical or numerical models [7-9]. Once the model is developed, optimization techniques such as gradient descent, particle swarm optimization, or genetic algorithm are used to find the design and operating conditions that will result in the best performance for the device [10]. This can include finding the optimal dimensions and doping levels for the device to minimize the global resistance and maximize the current flow, or finding the best materials and fabrication processes for the photovoltaic devices to maximize efficiency.

Semiconductor device modeling and optimization techniques is an active area of research and development, as it plays a critical role in the design and optimization of new semiconductor devices and technologies such as transistors, solar cells, and diodes. The goal is to develop more efficient, cost-effective and reliable devices [11-14]. Moreover, the optimization of semiconductor devices is becoming increasingly important for the nanoscale and complex devices. The smaller dimensions of these devices can result quantum effects and complex electron transport behavior, where an accurate modeling and optimization becomes necessary to develop low cost and high performance devices [12,13].

I.2 Analytical modeling

Analytical models are based on mathematical equations and analytical solutions, which are derived using mathematical concepts and techniques such as calculus, linear algebra, and differential equations. These models can be used to make predictions about the behavior of a system, process or phenomenon based on certain assumptions and known inputs. The solutions to the equations are usually in closed-form, meaning they can be expressed in terms of known mathematical functions [15-16]. Examples of analytical models include mathematical models of fluid dynamics, circuit analysis, and economic models. In semiconductor modeling, analytical models can provide a simple and intuitive understanding of the behavior of semiconductor devices, but they typically make simplifying assumptions that may not be valid in all cases [17]. Therefore, they are often used in conjunction with numerical simulations to provide a more accurate prediction of the device performance. There are several important equations used to model semiconductor devices, these equations are part of the set of basic equations used to model semiconductor devices, however depending on the device application and physics of the problem you're modeling, other equations might be used as well.

I.2.1 Poisson's equation

Poisson's equation is a fundamental equation in physics that describes the distribution of electric potential in a region. In a semiconductor, the electric potential is determined by the distribution of charge in the material [1,3,5-8]. Poisson's equation for a semiconductor is given by:

$$div(\mathcal{E}\nabla\psi) = -q(N_D + N_A + n + p) \quad \text{(I.1)}$$

Where ψ is the electric potential, q denotes the elementary charge, ε represents the permittivity of the semiconductor, p and n are the hole and electron concentrations, respectively, N_D and N_A are respectively, the doping concentration of donor and acceptor impurities.

I.2.2 The continuity equation

The continuity equation is a statement of the conservation of charge in a semiconductor. It states that the rate of change of the charge density in a semiconductor is equal to the sum of

the current densities flowing into and out of a small volume [1,3,5-8]. The continuity equation for a semiconductor is given by:

$$\frac{\partial n}{\partial t} = \frac{1}{q} div\overrightarrow{J_n} + G_n - R_n \quad \text{(I.2)}$$

$$\frac{\partial p}{\partial t} = -\frac{1}{q} div\overrightarrow{J_p} + G_p - R_p \quad \text{(I.3)}$$

Where *n, p* are the electron and hole concentration, *Jn* and *Jp* refer to the electron and hole current density, G_n and G_p are respectively the generation rate of electron and holes, and R_n, R_p designate the recombination rate of electron and holes, respectively.

I.2.3 The drift-diffusion equations

The drift-diffusion equations describe the transport of charge carriers (electrons and holes) in a semiconductor. They are based on the balance of the electron and hole current densities and the continuity equation [1,3,5-8]. The drift-diffusion equations for electrons and holes in a semiconductor are given by:

$$\overrightarrow{J_n} = q\mu_n n\vec{E} + qD_n\overrightarrow{\nabla n} \quad \text{(I.4)}$$

$$\overrightarrow{J_p} = q\mu_p p\vec{E} - qD_p\overrightarrow{\nabla p} \quad \text{(I.5)}$$

Where J_n and J_p are the electron and hole current density, respectively, μ_n and μ_p are the electron and hole mobility, D_n and D_p are the electron and hole diffusivities, respectively, and *E* denote the electric potential field.

I.3 Numerical modeling

Numerical modeling, on the other hand, uses complex computer algorithms and simulations to approximate the behavior of a system. The equations and relationships used in numerical models are usually too complex or too uncertain to be solved analytically [18]. Numerical models involve breaking down a system or process into smaller, more manageable parts and solving the equations for each part using a computer algorithm. The solutions to the equations are not in closed-form, meaning that the solutions cannot be expressed in terms of known mathematical functions. Instead, the solutions are approximations that are based on the input data and assumptions of the model [18-19]. Numerical modeling of semiconductor devices

involves using computer simulations to predict the behavior of semiconductor materials and devices. This can be done using a variety of techniques, such as solving the Schrödinger equation for electrons or the drift-diffusion equations to model the transport of charge carriers in a semiconductor using various numerical techniques such as finite difference method, finite element method, boundary element method,. The goal of numerical modeling is to predict the performance and characteristics of semiconductor devices, such as solar cells, transistors, diodes, to aid in the design and optimization of these devices [20].

I.3.1 Finite element method

The engineers have been using the finite element method (FEM) to address issues in structural mechanics even before mathematicians discovered it. The method is favored by engineers because it offers a high degree of geometric adaptability and it is relatively simple to apply to complex problems [21-22]. From a mathematical perspective, the method can be seen as a way to find approximate solutions for a continuous problem through a weighted residual approach, which involves formulating the problem in a variational form $\sum_i w_i \phi_i$ where the ϕ_i are trial functions. The weights w_i are calculated so that they minimize a specific functional [23]. The Rayleigh-Ritz-Galerkin technique is the origin of these methods. The finite element method introduces an innovative aspect where the trial functions are broken down into smaller parts, represented by piecewise polynomials, each defined within a specific subdomain or element. Instead of using functions that cover the entire domain. This specific feature is the reason why the finite element method is so successful in many different fields.

Finite element methods are considered "standard" when no additional techniques, such as upwinding, fitting or inverse averaging, are employed during their development. If any of these techniques are used, then the method is considered "non-standard" [24-25]. The general flowchart of the FEM process typically includes the following steps:

- Discretization of the domain: The domain of the problem, such as a structure or a region in space, is divided into small, manageable elements.
- Selection of shape functions: Shape functions are chosen to approximate the solutions within each element. These functions are chosen based on the type of element, such as a linear or quadratic element, and the type of problem being solved.
- Development of element equations: Element equations are derived for each element using the chosen shape functions and the governing equations for the problem.

- Assembly of global equations: The element equations are assembled to form the global equations. This step involves applying the continuity conditions at the nodes shared by multiple elements.
- Incorporation of boundary conditions: The global equations are modified to account for any boundary conditions. These conditions are used to determine the values of unknowns at specific locations on the boundary.
- Solution of global equations: The global equations are solved for the unknowns. This step can be done using numerical methods such as Gaussian elimination or iterative methods like the conjugate gradient method.
- Interpolation of results: The results are interpolated to the entire domain. This step is done by using the values of the unknowns at the nodes and the shape functions to approximate the solution at all other points within the elements.
- Post-processing: This step is used to analyze the results obtained from the solution and to create visual representation of the solution.

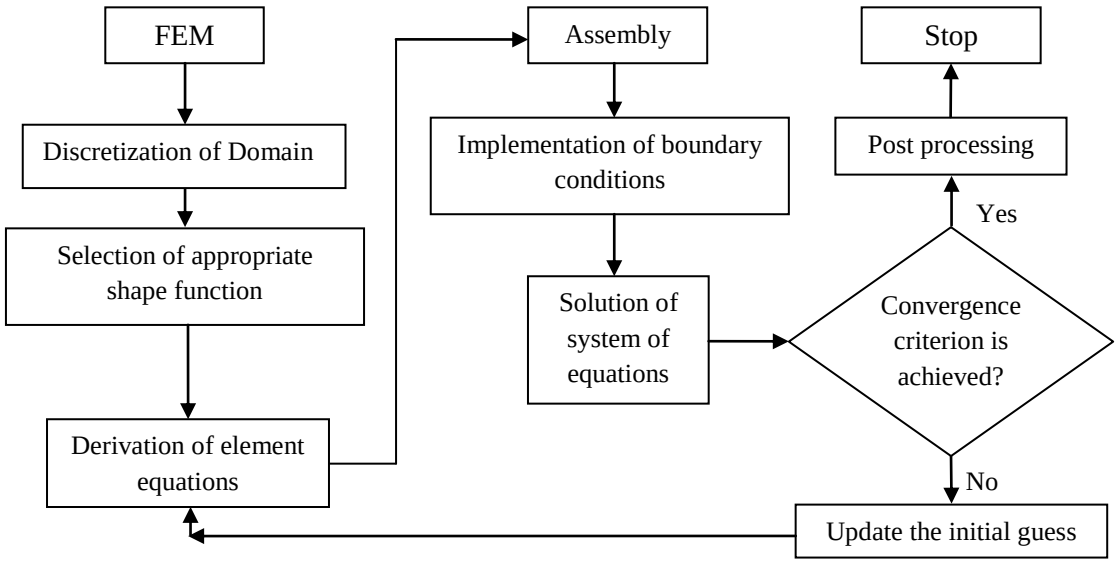

Figure I.1: Flow diagram of finite element method (FEM)

I.3.2 Monte Carlo method

Monte Carlo method (MCM) is a computer simulation approach that uses random sampling to model the behavior of a system. It involves generating random inputs for a model and using them to estimate the output of the system. The technique is named after the city of Monte

Carlo in Monaco, which is known for its casinos and the use of random sampling in games of chance [26-28].

MCM is useful for predicting the behavior of complex systems or analyzing the risk and uncertainty associated with a particular decision. It can be applied to a wide range of fields, including finance, engineering, and science. The accuracy of the results depends on the quality of the model and the number of random samples used in the simulation [29].

Monte Carlo modeling can be used to simulate the behavior of semiconductor devices, such as transistors, diodes, and solar cells. The technique can be used to analyze the performance of the device under different operating conditions, such as temperature, voltage, and material properties [27-30]. It can also be used to study the effects of random variations in the device parameters, such as the dopant concentration or the dimensions of the device, on the device performance.

In semiconductor device simulation, MCM is often used in conjunction with other numerical techniques, such as finite element analysis or drift-diffusion modeling. The Monte Carlo method can be used to sample the input parameters for these models, and the resulting outputs can be used to estimate the statistical properties of the device, such as the mean and variance of its performance characteristics [30].

The basic flowchart for a Monte Carlo algorithm to simulate the behavior of a semiconductor device typically includes the following steps:

- Initialization: The initial conditions of the simulation, such as the device dimensions, doping levels, and applied voltage or current, are set. A random number generator is also initialized.
- Generation of random numbers: A large number of random numbers are generated, which will be used to simulate the movement of carriers (electrons and holes) in the device.
- Calculation of carrier movement: The movement of carriers in the device is calculated based on the random numbers and the physical properties of the materials used in the device, such as their electrical conductivity and carrier mobility.
- Collection of data: Data on the movement of carriers and the resulting electrical current and voltage in the device is collected at regular intervals.

- Analysis of data: The collected data is analyzed to calculate important performance parameters of the device, such as its current-voltage characteristics or its efficiency.
- Repeat steps 2-5 for a large number of iterations: The simulation is repeated for a large number of iterations, typically on the order of millions, to ensure that accurate and reliable data is collected.
- Post-processing: The final data is post-processed, and the results are analyzed. The results are usually presented in the form of graphs and tables
- Comparison and optimization: the results are compared with the design parameters and if there is a mismatch, the design parameters are optimized until the desired results are obtained

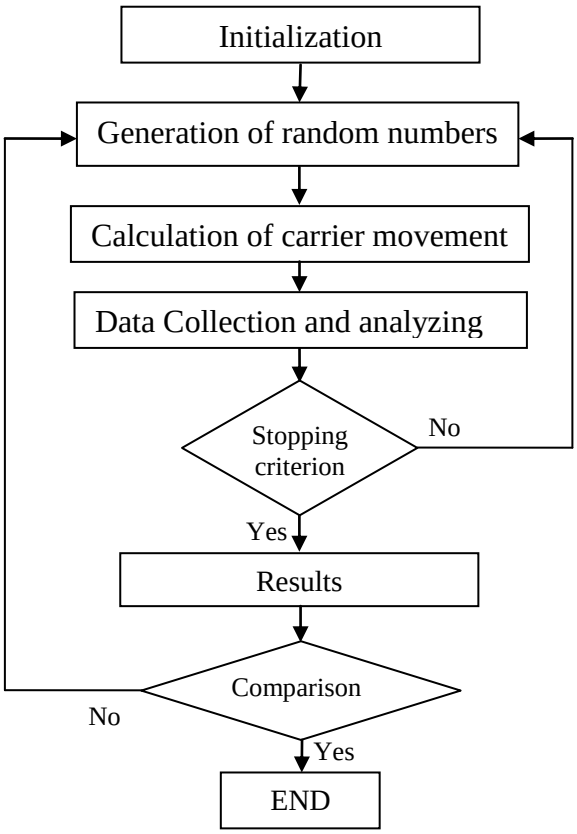

Figure I.2: Flow diagram of Monte Carlo method (MCM)

It's worth noting that more advanced Monte Carlo algorithms can include additional steps such as the incorporation of scattering mechanisms and the use of more complex models to take into account quantum mechanical effects in the device.

I.3.3 Density Functional Theory method

Density Functional Theory (DFT) is a computational method used to study the electronic structure of a wide range of materials, including molecules, solids, and surfaces. It is a theoretical approach that is based on the density of electrons in a system, rather than the wavefunction of individual electrons. DFT is a powerful and widely used method in computational chemistry and materials science because it can accurately predict the properties of a large number of systems with relatively low computational cost [31-33].

The basic idea behind this method is that the total energy of a system can be expressed as a functional of the electron density. This means that the total energy of a system can be calculated by knowing the distribution of electrons within the system. The most common method to solve the DFT is the Kohn-Sham method [31-32], which maps the many-body problem of interacting electrons to a non-interacting system with an effective potential.

One of the most popular functionals used in DFT is the local density approximation (LDA) and the generalized gradient approximation (GGA). These functionals provide a good balance between computational efficiency and accuracy.

Density Functional Theory is widely used in the modeling and simulation of semiconductor devices. It allows to understand the electronic structure and properties of semiconductor materials and devices at the atomic and electronic level [33], which is crucial for the design and optimization of new devices.

One of the main applications of DFT in semiconductor devices is the prediction of electronic band structures and density of states of semiconductor materials. This information is essential for understanding the electronic properties of the materials and their suitability for different types of devices, such as solar cells, transistors, and light-emitting diodes [34].

Another important application of DFT in semiconductor devices is the study of defects and impurities in semiconductor materials. DFT calculations can provide detailed information about the properties and effects of different types of defects, such as point defects, extended defects, and impurities, on the electronic and optical properties of the materials.

DFT can also be used to study the electronic structure and properties of interfaces in semiconductor devices, such as metal-semiconductor interfaces, semiconductor-semiconductor interfaces, and dielectric-semiconductor interfaces [33]. This information is

important for understanding the performance and reliability of devices that involve these interfaces.

DFT is a powerful tool that is widely used in the modeling and simulation of semiconductor devices, allowing to predict and understand the electronic properties of semiconductor materials, defects and impurities, and interfaces, which is crucial for the design and optimization of new devices.

The flow chart for the DFT modeling of semiconductor devices is Detailed below:

- Initialize the crystal structure of the semiconductor device, including the unit cell, lattice vectors, and atomic positions.
- Apply the periodic boundary conditions to the electron density and the potential.
- Choose an appropriate exchange-correlation functional for the DFT calculation.
- Set up the initial electron density and the electrostatic potential due to the applied bias.
- Calculate the effective potential by solving the Poisson equation with the electron density as the source term and adding the external potential and the exchange-correlation potential.
- Solve the Kohn-Sham equations in the periodic crystal potential and obtain the electron density and the total energy.
- Check for convergence by comparing the electron density of the current iteration with that of the previous one.
- If the convergence criterion is not met, go back to step 5 using the new electron density and electrostatic potential as the input.
- If the convergence criterion is met, calculate the output quantities such as band structure, density of states, charge density, etc.
- Repeat the steps above for different interfaces, if necessary, using the slab or supercell method.

this basic flow chart is illustrated in Figure I.3 which, can be adapted to different levels of accuracy and computational resources, as well as specific systems and applications. The choice of the functional approximation and the method of solving the Kohn-Sham equations can also affect the accuracy and computational resources needed, so it's important to choose the appropriate methods and parameters for the specific system and application.

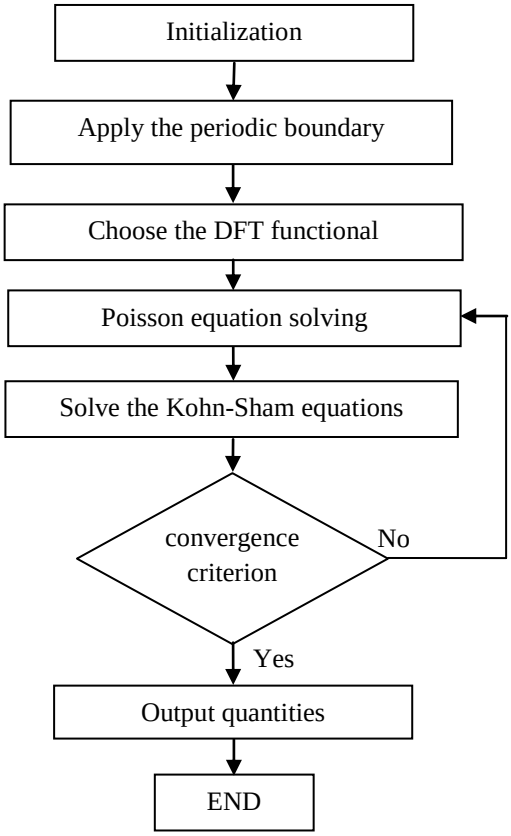

Figure I.3: Flow diagram of Density Functional Theory method

I.4 Metaheuristic technique

Metaheuristics are high-level problem-solving strategies that guide a local heuristic search method to explore the solution space of a problem [35-36]. These algorithms, such as Genetic Algorithms, particle swarm optimization, Simulated Annealing, Artificial Bee Colony, and Ant Colony Optimization [37-40], are often inspired by natural mechanisms and have been shown to be effective in solving global optimization problems. Metaheuristics are not specific to any particular problem and employ strategies to effectively avoid getting stuck at local optima. They also involve efficient strategies for balancing the exploration of new regions of the solution space with the focus on certain regions to find high-quality solutions.

Some examples of popular metaheuristic optimization algorithms include:

Genetic algorithms: These are based on the principle of natural selection and use a process of reproduction, mutation, and selection to evolve a population of solutions over time.

Simulated annealing: This algorithm is based on the process of physical annealing, in which a material is slowly cooled to minimize the defects in its structure. The algorithm starts with a random solution and gradually improves it by making small, random changes and accepting or rejecting the changes based on their impact on the objective function.

Particle Swarm Optimization (PSO): This algorithm simulates the behavior of a swarm of birds or insects searching for food. The algorithm uses a population of solutions (particles) that move around the solution space and adapt their positions based on their own best solutions and the best solutions found by other particles.

Ant Colony Optimization (ACO): This algorithm simulates the behavior of ants as they search for food. The algorithm uses a population of solutions (ants) that move around the solution space and adapt their positions based on the solutions found by other ants and a set of heuristic rules.

Differential Evolution (DE) this is an algorithm based on the genetic concept of natural selection, it uses an iterative process where solutions are evolved by combining properties of existing solutions, instead of recreating solutions randomly.

Artificial Bee Colony (ABC): This algorithm is inspired by the behavior of bees as they search for nectar. It uses a population of solutions (bees) that are divided into three groups: employed bees, onlookers, and scouts. The employed bees and onlookers update their solutions based on the solutions found by other bees, while the scouts explore new areas of the solution space.

Cuckoo Search (CS): This algorithm is inspired by the behavior of cuckoos and their eggs. It uses a population of solutions (cuckoos) that lay eggs in different nests (solutions) and update their positions based on the best solutions found by other cuckoos.

Firefly Algorithm (FA): This algorithm is inspired by the behavior of fireflies as they flash their lights to attract mates. It uses a population of solutions (fireflies) that adapt their positions based on the brightness (objective function value) of other fireflies.

Bat Algorithm (BA): This algorithm is inspired by the behavior of bats as they search for food using echolocation. It uses a population of solutions (bats) that adapt their positions based on the frequency and loudness (objective function value) of their echolocation calls.

Harmony Search (HS): This algorithm is inspired by the process of improvisation in music. It uses a population of solutions (musical notes) that are combined together to form different harmonies (solutions).

Hybrid Metaheuristics: These are optimization algorithms that combine multiple metaheuristics in order to take advantage of the strengths of each individual algorithm.

Metaheuristic optimization algorithms are useful for solving problems with high-dimensional search spaces and complex objective functions. They can also handle constraints and have the ability of handling multiple objectives. Moreover, they do not require the objective function to be differentiable or have a specific structure, and they are often used in applications such as function optimization, engineering design, and machine learning.

All these examples, as well as the previously mentioned ones, are all metaheuristic optimization algorithms that can be used to solve a wide range of optimization problems with different characteristics. The choice of the algorithm is determined by the characteristics of the problem and the specific requirements of the application. Some algorithms may work better for certain types of problems or have specific advantages in certain scenarios.

I.4.1 Multi Objective Genetic Algorithm optimization (MOGA)

MOGA is a variant of genetic algorithm which is adapted to handle optimization problems with multiple objectives. Its basic principle is similar to that of a traditional genetic algorithm (GA) [37], where a population of solutions is evolved over time using operations such as selection, crossover, and mutation. However, in MOGA multiple objective functions are optimized simultaneously, rather than a single objective function. The population of solutions is represented by a set of points in a multi-dimensional space, where each point corresponds to a set of values for the parameters of the problem. These points can also be represented as individuals in the population [41-43].

The algorithm starts with a random population of individuals, then it applies genetic operators to evolve the population over multiple generations until it reaches a satisfactory solution. The selection process uses a combination of elitist and non-elitist selection methods, where a fraction of the best individuals from the current population is carried over to the next generation (Elitist selection) and the remaining individuals are selected based on their fitness values, the individuals are then mated to generate offspring (Non-elitist selection). Crossover and Mutation are genetic operators used to generate offspring in MOGA. A crossover

operator is used to combine the genetic information of two parents to create new offspring, while a mutation operator is used to introduce small random variations in the genetic makeup of the individuals.

In semiconductor device optimization, MOGA can be used to find the optimal design of a device by adjusting its various design parameters to achieve the desired performance while satisfying constraints such as cost and manufacturability. For example, in the case of a solar cell, MOGA can be used to optimize the doping levels, layer thicknesses and material properties of the various layers in the solar cell in order to maximize its efficiency while minimizing its cost. The algorithm can also consider other constraints such as the maximum allowable recombination rate and series resistance. MOGA can also be used to optimize the performance of other semiconductor devices such as LEDs, transistors, and photodetectors [43-44]. It can also be used to optimize the performance of integrated circuits by adjusting the layout and routing of the various components on the chip. One of the advantages of using MOGA for optimization of semiconductor devices is that it can handle multiple objectives and constraints simultaneously, which is particularly useful for problems where the objectives are conflicting. It also can handle continuous, discrete and mixed variables which makes it suitable for a wide range of semiconductor devices optimization problems.

The flowchart of a typical Multi-Objective Genetic Algorithm (MOGA) is as follows:

- Initialize the population: A initial set of solutions is randomly generated and evaluated according to the multiple objectives.
- Selection: The solutions are ranked based on their fitness, and the best solutions are selected to be included in the next generation.
- Crossover: A crossover operation is performed on the selected solutions to create new solutions.
- Mutation: A mutation operation is performed on the new solutions to introduce genetic diversity.
- Evaluation: The new solutions are evaluated according to the multiple objectives.
- Stopping Criteria: Check if stopping criteria are met, such as a maximum number of generations or a satisfactory solution being found.
- Repeat steps 2-6 until stopping criteria are met.

- Pareto Front: The solutions found by the MOGA are used to construct the Pareto Front, which shows the trade-off between the multiple objectives.
- Decision making: The Pareto Front is presented to the decision maker, who selects the best solution according to their preferences.

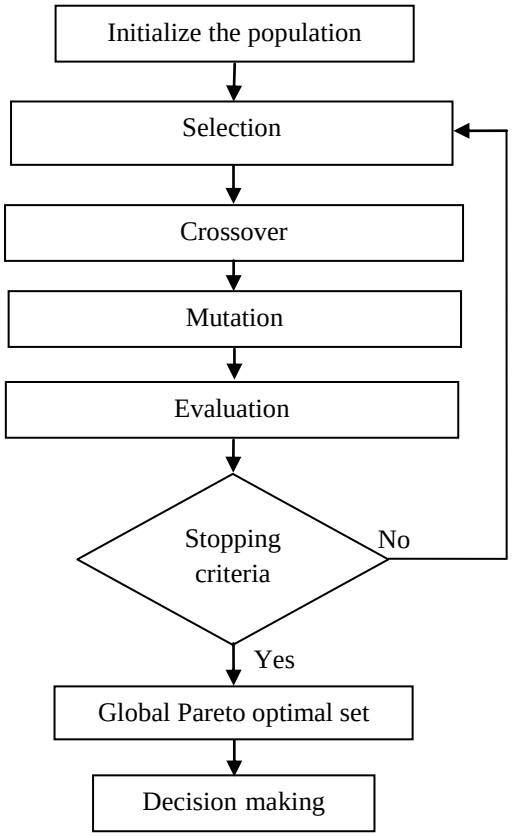

Figure I.4: Flow diagram of Multi Objective Genetic Algorithm (MOGA).

I.4.2 Particle Swarm Optimization (PSO)

It is a metaheuristic optimization algorithm that is inspired by the behavior of a swarm of birds or insects searching for food. The algorithm uses a population of solutions, called "particles," that move around the solution space and adapt their positions based on their own best solutions and the best solutions found by other particles [45].

The basic idea behind this method is that each particle represents a possible solution to the problem, and the algorithm uses the principles of social interactions and communication to direct the movement of the particles. Each particle has a position in the solution space and a velocity that determines the direction and magnitude of its movement. The position of a particle is updated based on its current velocity and its previous position.

The PSO algorithm uses two main concepts: the personal best solution and the global best solution. The personal best solution of a particle is the best solution that it has found so far, and the global best solution is the best solution found by any particle in the population.

The movement of a particle is updated based on its current velocity, its personal best solution and the global best solution. The velocity of a particle is updated using the following equation:

$$V_i^{k+1} = wV_i^k + c_1 r_1^k (p_{li}^k - X_i^k) + c_2 r_2^k (p_{gi}^k - X_i^k) \quad \text{(I.6)}$$

$$X_i^{k+1} = X_i^k + V_i^{k+1} \qquad \text{for } i=1...n \quad \text{(I.7)}$$

where n denotes to the swarm size, the particle position and velocity are presented by X_i^k and V_i^k , p_{li}^k and p_{gi}^k are particle's best position and particles group's best position in the swarm respectively, c_1 and c_2 represents the cognitive and social acceleration factors, r_1 and r_2 reveal the random numbers, which are picked from the range [0,1], w represents the inertia weight applied to balance the global exploration and X_i^k is the actual position of the particle in the swarm.

In the context of semiconductor devices, PSO can be used to optimize various design parameters such as doping concentration, layer thickness, and material properties, in order to achieve the desired device performance. For example, in the case of a solar cell, PSO can be used to optimize the doping levels, layer thicknesses and material properties of the various layers in the solar cell in order to maximize its efficiency while minimizing its cost. PSO has been used to optimize a wide variety of semiconductor devices, such as solar cells, LEDs, and transistors. It has been shown to be effective in solving optimization problems with complex and non-linear objective functions [46-48]. Some of the advantages of PSO are its simplicity, easy of implementation and the ability to handle continuous and discrete variables.

Like other optimization algorithms, the choice of the PSO algorithm depends on the specific problem and the preferences of the decision maker. It is important to note that, PSO algorithm could be sensitive to the initial parameters, such as the number of particles, the maximum velocity, the inertia weight and the cognitive and social factors. The algorithm`s basic flow chart is illustrated in Figure I.5

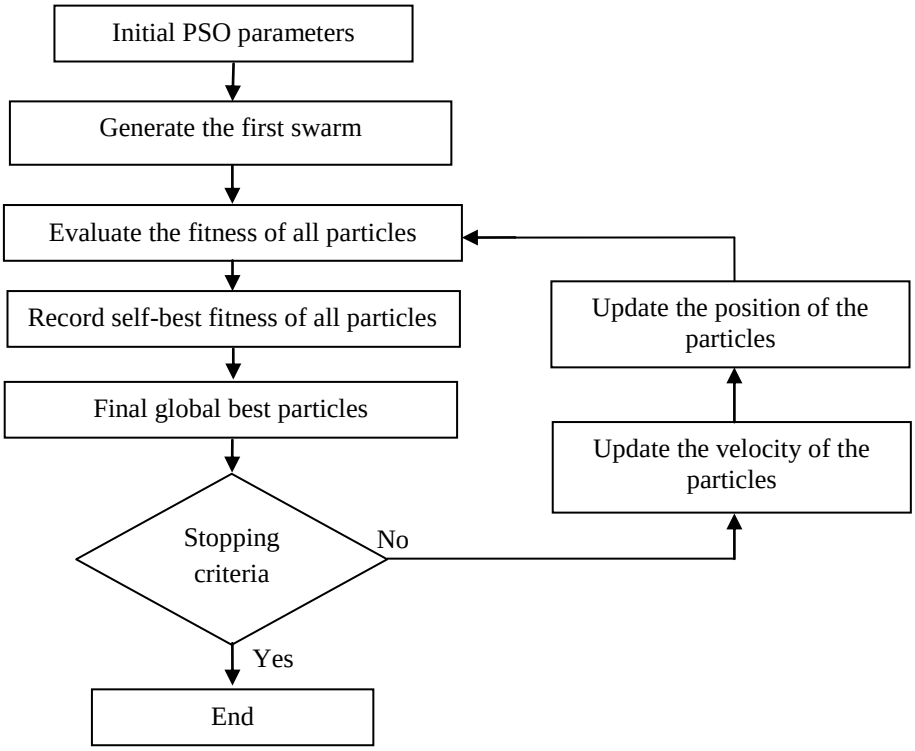

Figure I.5: Flow diagram of Particle Swarm Optimization (PSO)

I.4.3 The Artificial Bee Colony (ABC) algorithm

Artificial Bee Colony is a metaheuristic optimization algorithm that is inspired by the behavior of bees as they search for nectar. The algorithm uses a population of solutions, where each solution is represented by a "bee". The algorithm uses a set of heuristic rules to control the movement of the bees in the solution space, and it is designed to efficiently explore and exploit the solution space to find the best solution to the problem [49-50].

The ABC algorithm has three main components: the employed bees, the onlooker bees, and the scout bees [49]. The employed bees are responsible for updating the solutions of their corresponding food sources. They generate new solutions by modifying the current solutions. The onlooker bees observe the solutions of the employed bees and choose the food source with the highest quality. Then, they generate new solutions based on the chosen food source. The scout bees are responsible for discovering new food sources by randomly generating new solutions. They are used to overcome the stagnation problem that can occur when the algorithm gets stuck in a local optimum.

The algorithm uses a probabilistic selection mechanism that encourages exploration and exploitation of the solution space. It starts with a random set of initial solutions and uses the

employed and onlooker bees to iteratively improve the solutions. The scout bees are used to discover new solutions and to overcome the stagnation problem that can occur when the algorithm gets stuck in a local optimum. The algorithm stops when a stopping criterion is met, such as reaching a certain number of iterations or achieving a certain level of quality in the solution.

ABC algorithm has been applied to solve a wide range of optimization, it uses a set of equations to control the movement of the bees in the solution space and to update the solutions [49-52]. The main equations used in the algorithm are:

The equation for the initial solutions: $X = X_{min} + \lambda (X_{max} - X_{min})$ This equation is used to generate the initial solutions for the problem, where X_{min} and X_{max} are the lower and upper bounds of the solution space. The initial solutions are randomly generated within the solution space by multiplying a random number λ between 0 and 1 with the difference of the upper and lower bounds, and then adding it to the lower bound. The variable n is the number of solutions and corresponds to the number of bees in the colony.

The equation for the new solutions generated by the employed bees: $V = X + \sigma (X - X_r)$

This equation generates new solutions by modifying the current solutions. The bee chooses a randomly another bee's solution (X_r) and generate a new solution by adding (or subtracting) the difference between X and X_r multiplied by a random number σ between -1 and 1. This equation aims to exploit the best features of the neighborhood of the current solutions, and it guarantees that the new solutions will be similar to the current solutions.

The equation for the new solutions generated by the onlooker bees: $V = X + \sigma (X_{best} - X)$

This equation generates new solutions by modifying the best solution found so far (X_{best}) . The bee chooses the solution that has the highest fitness (X_{best}) and generates a new solution by adding (or subtracting) the difference between the best and the current solution multiplied by a random number λ between 0 and 1. This equation aims to explore other regions of the solution space, that potentially contain better solutions.

The equation for the fitness or quality: $Fitness(i) = f(X(i))$ Where $f(X(i))$ is the objective function to optimize and i is the solution or food source to evaluate.

The equation for the selection probability: P(i) = Fitness(i) / Σ Fitness(k) where i is the solution or food source and k is the index of the food source. This equation is used to determine the probability of selecting a certain food source.

In the scout bee Phase the abandonment counter of all employed bees is checked against a limit set by the designer. If an employed bee's counter exceeds the limit, replace it with a randomly generated solution. The flowchart of ABC algorithm is given in Figure I.6.

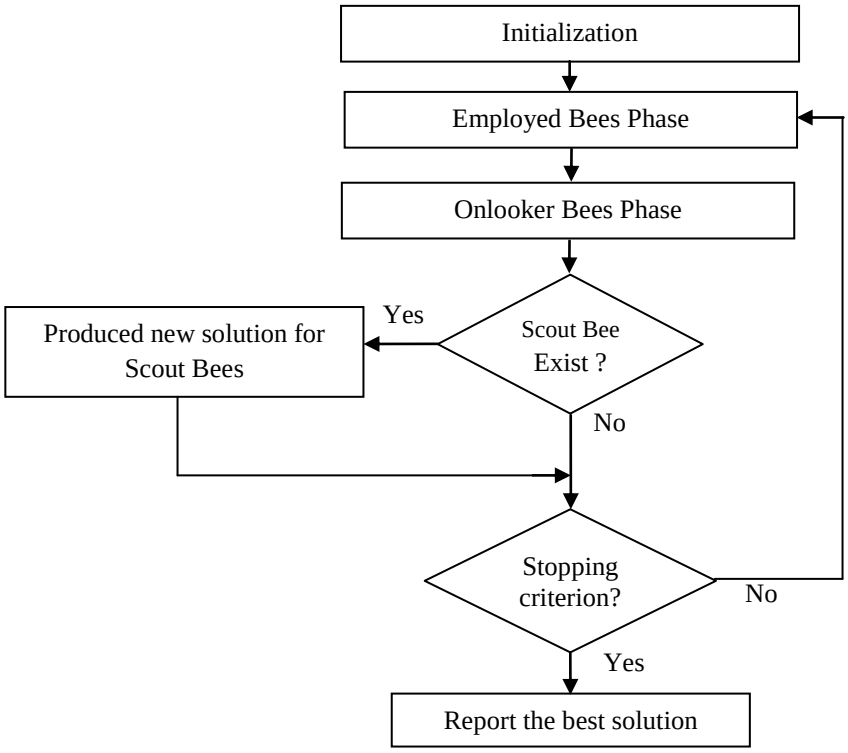

Figure I.6: Flow diagram of Artificial Bee Colony (ABC) algorithm

I.4.4 Machine learning (ML)

It is a subfield of artificial intelligence (AI) that focuses on the development of algorithms and models that can learn from data and make predictions or decisions without being explicitly programmed [53-55]. It encompasses a wide range of techniques and methodologies, including supervised learning, unsupervised learning, semi-supervised learning, and reinforcement learning [54].

Supervised learning: It is the task of inferring a function from labeled training data, the algorithm tries to find a relationship between the input and output variables. The goal is to

generalize this function to new examples, this can be done with classification and regression problems.

Unsupervised learning: it is the task of inferring a function to describe hidden structure from unlabeled data. Clustering and dimensionality reduction are example of unsupervised learning tasks

Semi-supervised learning: is a variation of supervised learning where only a small portion of the data is labeled, the algorithm uses this limited labeled data and the vast amount of unlabelled data to make predictions.

Reinforcement learning: It is the task of creating agents that learn how to behave in an environment, so as to maximize some notion of cumulative reward. This can be applied to a wide range of problems, from controlling a robot to playing games or optimizing a business process.

These are some examples of machine learning techniques, it also has a lot of subfields such as deep learning, computer vision, natural language processing, etc.

Machine learning algorithms can be used for a wide range of tasks, such as image recognition, speech recognition, language translation, natural language processing, and many other applications that require decision making and predictions. They have been used in many different industries, including finance, healthcare, transportation, and e-commerce [54-57].

For semiconductor device modeling, researchers have been using ML techniques to model and predict the behavior of various semiconductor devices, such as solar cells, transistors, diodes, and other optoelectronic devices [55-58]. ML can be used in a number of ways, including:

- Modeling and optimization of device performance: it can be used to model and optimize the performance of semiconductor devices by predicting their response to different inputs and identifying the optimal design parameters.
- Characterization and diagnosis of device behavior: it can be used to analyze and diagnose the behavior of semiconductor devices, such as detecting defects or identifying failure modes.
- Inverse Modeling : Machine learning can be used to find the input parameters that give rise to a specific set of output measurements.

- Data-Driven approaches: Data-driven methods, such as neural networks and other deep learning algorithms, can be used to analyze large datasets and extract useful information about the devices.

Researchers have been using various ML techniques, such as neural networks, decision trees, and support vector machines to model and predict the behavior of semiconductor devices. The use of ML for semiconductor device modeling has the potential to significantly improve the design and optimization of these devices.

Machine learning can be very useful in device modeling and optimization as it can handle high-dimensional input-output data and can provide an accurate prediction even if the physics-based models are not available or too complicated to use.

A flowchart for a basic machine learning process may include the following steps:

- Define the problem and gather data: Identify the problem you want to solve and collect the relevant data that will be used to train and test the model.
- Prepare the data: Clean and preprocess the data to make it suitable for modeling. This may include tasks such as handling missing values, normalizing the data, and removing outliers.
- Select a model: Choose an appropriate machine learning model based on the type of problem you are trying to solve and the characteristics of your data.
- Train the model: Use the prepared data to train the model. This may involve using techniques such as cross-validation to tune the model's parameters.
- Evaluate the model: Use a set of test data to evaluate the performance of the model and determine how well it is able to make predictions on new, unseen data.
- Fine-tune the model and repeat steps 4 and 5 until satisfactory performance is achieved: This step involves adjusting the model's hyperparameters, or the parameters that are not learned during training, in order to improve its performance. This may include adjusting the learning rate, number of hidden layers, or number of neurons in a neural network.
- Use the trained model to make predictions on new, unseen data: Once the model has been trained and fine-tuned, it can be used to make predictions on new, unseen data. This can be used for tasks such as image classification, speech recognition, or natural language processing. The basic flow chart is illustrated in Figure I.7

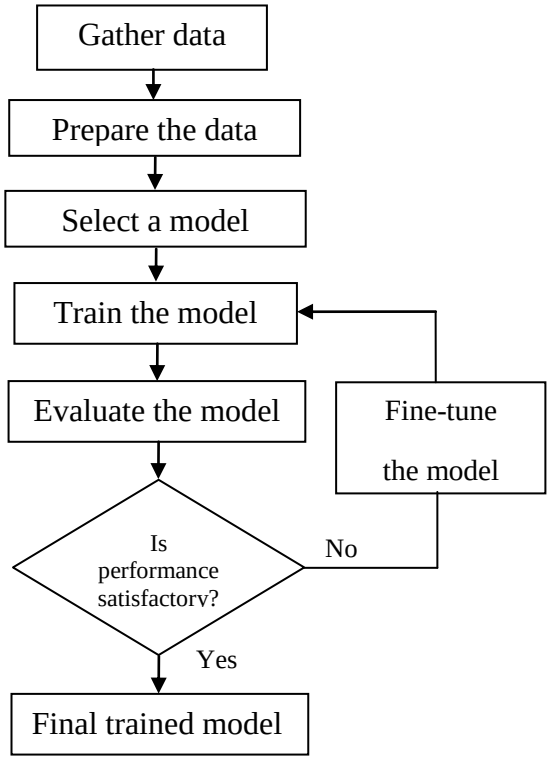

Figure I.7: Flow diagram of Machine learning (ML).

These are the general steps, the specific implementation details can vary depending on the problem and the chosen algorithm.

I.5 conclusion

In this chapter, we have represented the different equations that govern the physical behavior of a semiconductor. we have discussed the use of analytical and numerical modeling techniques in the field of semiconductor devices. The Analytical modeling involves the use of mathematical equations to model the performance of the device, while numerical modeling involves using computational methods such as the finite element, Monte Carlo, and density functional theory to simulate the complex behavior. Both techniques have their own advantages and limitations, and the choice of the appropriate technique is mainly depending on the specific problem being addressed and the desired level of accuracy. Analytical modeling can provide closed-form solutions and is generally faster, but may not be able to accurately capture complex or nonlinear phenomena. Numerical modeling can provide more accurate results, but can be more computationally expensive and may require iterative methods. In this chapter, we have discussed the application of these methods using

semiconductor equations. The use of both analytical and numerical methods can provide a better understanding of the system and can be used to optimize the device performance.

The second section of this chapter has provided a comprehensive review of metaheuristic-based optimization techniques and their classification. The different global optimization approaches, such as MOGA, PSO, ML, and ABC-based algorithms, have been thoroughly discussed and their basic concepts have been explained in detail. The application of these metaheuristic approaches to optimize semiconductor devices has also been introduced. The use of these techniques can significantly improve the performance of semiconductor devices and aid in the design and optimization of new devices. The chapter has effectively defined the basic concepts associated with these approaches and provided insight into their potential applications in the field of semiconductor device optimization.

References

[1] E.A.B.Cole. Mathematical and Numerical Modelling of Heterostructure Semiconductor Devices: From Theory to Programming. Springer London, 2009.

[2] Franco BREZZI, Luisa Donatella MARINI, Paola PIETRA,"NUMERICAL SIMULATION OF SEMICONDUCTOR DEVICES," Computer Methods in Applied Mechanics and Engineering, vol. 75, pp. 493-514, 1989.

[3] Florin Babarada, "Semiconductor Processes and Devices Modeling," Semiconductor Technologies, edited by Grym Jan, InTech, pp. 1-26, 2010.

[4] D. Vasileska, D. Mamaluy, H. R. Khan, K. Raleva, S. M. Goodnick, " Semiconductor Device Modeling , " Journal of Computational and Theoretical Nanoscience, vol. 5, pp. 1–32, 2008.

[5] S. Selberherr. The Stationary Semiconductor Device Equations. Springer-Verlag Wien GmbH, 1986.

[6] Samira Shamsir, Md Sakib Hasan, Omiya Hassan, et al, "Semiconductor Device Modeling and Simulation for Electronic Circuit Design," Modeling and Simulationin Engineering - Selected Problems, edited by Jan Valdman and Leszek Marcinkowski, IntechOpen, pp. 207-221, 2020.

[7] Christopher M Snowden. The Semiconductor Device Modelling. Springer-Vedag Berlin Heidelberg, 1989.

[8] P. A. Markowich, c. A. Ringhofer, C. Schmeiser. Semiconductor Equations. Springer-Verlag Wien, 1990.

[9] Norainon Mohamed, Muhamad Zahim Sujod, Mohamad Shawal Jadin, "Iterative Solution Method in Semiconductor Equations," Semiconductor Technologies, edited by Grym Jan, InTech, pp. 29-32, 2010.

[10] M. S. Khan, F. Jabeen, S. Ghouzali, Z. Rehman, S. Naz and W. Abdul, "Metaheuristic Algorithms in Optimizing Deep Neural Network Model for Software Effort Estimation," in IEEE Access, vol. 9, pp. 60309-60327, 2021.

[11] Xiao-Feng Xie, Wen-Jun Zhang and De-Chun Bi, "Optimizing semiconductor devices by self-organizing particle swarm," Proceedings of the 2004 Congress on Evolutionary Computation (IEEE Cat. No.04TH8753), Vol.2 , pp. 2017-2022, 2004.

[12] D. Jiang, W. Lin and N. Raghavan, "Semiconductor Manufacturing Final Test Yield Optimization and Wafer Acceptance Test Parameter Inverse Design Using Multi-Objective Optimization Algorithms," IEEE Access, vol. 9, pp. 137655-137666, 2021.

[13] Martin Burger, Michae Hinze, Rene Pinnau, "Optimization models for semiconductor dopant profiling," Semiconductor Technologies, edited by Carlo Cercignani. Ester Gabetta, Birkhauser Boston, pp. 91-116, 2007.

[14] S. E. De León-Aldaco, H. Calleja and J. Aguayo Alquicira, "Metaheuristic Optimization Methods Applied to Power Converters: A Review," IEEE Transactions on Power Electronics, vol. 30, no. 12, pp. 6791-6803, 2015.

[15] Christopher M. Snowden. Introduction to Semiconductor Device Modelling. word Scientiic Pubishing Co. Pte. Ltd. 1998.

[16] H. Ferhati, F. Djeffal, L.B. Drissi, "A new approach to the modeling and simulation of multi-junction solar cells," Optik, vol. 200, pp. 163452, 2020.

[17] H. Ferhati, F . Djeffal, " An efficient analytical model for tandem solar cells," Materials Research Express, vol. 6, pp. 076424, 2019.

[18] Joachim N. Burghartz, "Technology Computer Aided Design," Guide to State-of-the-Art Electron Devices , edited by Joachim N. Burghartz, Wiley-IEEE Press, pp.97-106, 2013.

[19] H. Ferhati, F. Djeffal, " Novel high-performance SOI junctionless FET-based phototransistor using channel doping engineering: Numerical investigation and sensitivity analysis," Optik, vol. 138, pp. 119-126, 2017.

[20] H. Ferhati, F. Djeffal, T. Bentercia, " Numerical Investigation of A New Junctionless Phototransistor for High-Performance and Ultra-Low Power Infrared Communication Applications," TELKOMNIKA, vol. 14, pp. 1213-1216, 2016.

[21] J. J. Barnes and R. J. Lomax, "Finite-element methods in semiconductor device simulation," IEEE Transactions on Electron Devices, vol. 24, pp. 1082-1089, 1977.

[22] D. -M. Yu, X. -M. Pan and X. -Q. Sheng, "An Accurate and Stable Finite Element Method for Self-Heating Effects Simulation of Semiconductor Devices," International Conference on Electromagnetics in Advanced Applications (ICEAA), Granada, Spain, pp. 1107-1110, 2019.

[23] N. Mohamed and M. Z. Sujod, "Finite Elements in Semiconductor Devices," International Conference on Information Management and Engineering, Kuala Lumpur, Malaysia, pp. 108-110, 2009.

[24] Norainon Mohamed, Muhamad Zahim Sujod, "Finite Elements In Semiconductor Devices," International Conference on Information Management and Engineering, 2009.

[25] J.J.H. Miller, W.H.A. Schilders, S. Wang, "Application of Finite Element Methods to the Simulation of Semiconductor Devices," Reports on Progress in Physics, edited by Grym Jan, InTech, vol. 62, pp. 287-300, 1999.

[26] Mordechai Shaul. Applications of Monte Carlo Method in Science and Engineering. InTech, 2011.

[27] C. Moglestue. Monte Carlo Simulation of Semiconductor Devices. Chapman & Hali, 1993.

[28] PAOL LUGLI, "The Monte Carlo Method for Semiconductor Device and Process Modeling," IEEE TRANSACTIONS ON COMPUTER-AIDED DESIGN, vol. 9, pp. 1164-1177, 1990.

[29] R. W. Kelsall, "The Monte Carlo method for semiconductor device simulation," IEE Colloquium on Physical Modelling of Semiconductor Devices, pp. 1-5, 1995.

[30] Geir U. Jensen, Bjørnar Lund, Tor A. Fjeldly, Michael Shur, "Monte Carlo simulation of semiconductor devices, Computer Physics Communications," Computer Physics Communications, vol. 67, pp. 1-61, 1991.

[31] Kieron Burke, et al. The ABC of DFT. University of California, 2007.

[32] Freyss. M, "Density functional theory," NEA, State-of-the-Art Report on Multi-scale Modelling of Nuclear Fuels, Nuclear Energy Agency of the OECD (NEA) , pp. 225-235, 2015.

[33] S. Farah, Z. Dibi, H. Ferhati, F. Djeffal, "DFT-FDTD modeling of a new broadband mid-infrared IGZO thin-film phototransistor based on black phosphorus capping layer incorporating intermediate metallic film," Journal of Physics and Chemistry of Solids, vol. 162, pp. 110528, 2022.

[34] A. Kebabi, A. Bentabet, F. Djeffal, H. Ferhati, N. Benmekideche, A. Benmakhlouf, A. Chala, *"*DFT study of X-doped (X= Cu, Ag, Au) boron nitride nanotubes for spintronic and optoelectronic applications*,"*. Optik, vol. 225, pp. 165863, 2021.

[35] C. Blum and A. Roli, "Metaheuristics in combinatorial optimization: Overview and conceptual comparison," ACM Computing Surveys, vol.35, pp.268-308, 2003.

[36] H. Ferhati, F. Djeffal, L.B. Drissi, "Metaheuristic-based decision maker framework for the development of multispectral IGZO thin-film phototransistors," Journal of Science: Advanced Materials and Devices, vol. 7, pp. 100414, 2022.

[37] J. H. Holland, "Adaptation in natural and artificial systems: an introductory analysis with applications to biology, control, and artificial intelligence," University of Michigan Press, 1975.

[38] S. Kirkpatrick, C. D. Gelatt and M. P. Vecchi, "Optimization by Simulated Annealing," Science, vol. 220, pp. 671-680, 1983.

[39] C. Blum and A. Roli, "Metaheuristics in combinatorial optimization: Overview and conceptual comparison," ACM Computing Surveys, vol. 35, pp. 268-308, 2003.

[40] I. Boussaıd, J. Lepagnot and P. Siarry, "A survey on optimization metaheuristics," Information Sciences, vol. 232, pp. 82-117, 2013.

[41] F. Djeffal, M. Meguellati, A. Benhaya, "A two-dimensional analytical analysis of subthreshold behavior to study the scaling capability of nanoscale graded channel gate stack DG MOSFETs," Physica E, vol. 41, pp. 1872–1877, 2009.

[42] P.-C. Chang, J.-C. Hsieh, C.-Y. Wang, "Adaptive multi-objective genetic algorithms for scheduling of drilling operation in printed circuit board industry, " Appl. Soft Comput, vol. 7, pp. 800–806, 2007.

[43] K. Atashkari, N. Nariman-Zadeh, A. Pilechi, A. Jamali, X. Yaob, "Thermodynamic Pareto optimization of turbojet engines using multi-objective genetic algorithms, " Int. J. Therm. Sci, vol. 44, pp. 1061–1071, 2005.

[44] A. Maoucha, F. Djeffal, "Multi-objective-optimization-based approach to improve the electrical efficiency for organic solar cells," J Comput Electron, vol. 11, pp. 336–343, 2012.

[45] M. Clerc and J. Kennedy, "The particle swarm - explosion, stability, and convergence in a multidimensional complex space," J. IEEE Trans. Evolut. Comput, vol. 73, pp. 57-70, 2002.

[46] F. Djeffal, N. Lakhdar, M. Meguellati, A. Benhaya, “Particle swarm optimization versus genetic algorithms to study the electron mobility in wurtzite GaN-based devices,” Solid-State Electronics, vol. 53, pp. 988-992, 2009.

[47] F. Djeffal, T. Bendib, R. Benzid and A. Benhaya, “An approach based on particle swarm computation to study the nanoscale DG MOSFET-based circuits,” Turk. J. Elec. Eng & Comp Sci., vol. 18, pp. 1131-1140, 2010.

[48] H. Ferhati, F. Djeffal, “Graded band-gap engineering for increased efficiency in CZTS solar cells,” Optical Materials, vol. 76, pp. 393-399, 2018.

[49] Xin-She Yang, “, “Nature-Inspired Computation and Swarm Intelligence Algorithms, Theory and Applications,” Academic Press, pp. 361-390, 2020.

[50] Mustafa Servet Kiran, Ahmet Babalik, “Improved Artificial Bee Colony Algorithm for Continuous Optimization Problems,” Journal of Computer and Communications, vol. 2, pp. 108-116, 2014.

[51] Xuanhu He, Wei Wang, Jiuchun Jiang, Lijie Xu, “An Improved Artificial Bee Colony Algorithm and Its Application to Multi-Objective Optimal Power Flow,” Energies, vol. 8, pp. 2412–2437, 2015.

[52] Samrat L. Sabat, Siba K. Udgata, Ajith Abraham, “Artificial bee colony algorithm for small signal model parameter extraction of MESFET,” Engineering Applications of Artificial Intelligence, vol. 23, pp. 689–694, 2010.

[53] P. P. Shinde and S. Shah, "A Review of Machine Learning and Deep Learning Applications," Fourth International Conference on Computing Communication Control and Automation (ICCUBEA), Pune, India, pp. 1-6, 2018.

[54] S. Sah, "Machine Learning: A Review of Learning Types," Preprints, pp. 1-7, 2020.

[55] Peiyuan Xu, " Review on Studies of Machine Learning Algorithms," *J. Phys.: Conf. Ser*, vol. 1187, pp. 1-6, 2019.

[56] Chen He, Hanbin Hu, Peng Li, “Applications for Machine Learning in Semiconductor Manufacturing and Test,” Electron Devices Technology and Manufacturing Conference (EDTM), 2021.

[57] Y. S. Bankapalli and H. Y. Wong, "TCAD Augmented Machine Learning for Semiconductor Device Failure Troubleshooting and Reverse Engineering," International Conference on Simulation of Semiconductor Processes and Devices (SISPAD), 2019.

[58] E. Knapp, M. Battaglia, S. Jenatsch and B. Ruhstaller, "Machine Learning Assisted Material and Device Parameter Extraction from Measurements of Thin Film Semiconductor Devices," International Conference on Numerical Simulation of Optoelectronic Devices (NUSOD), 2022.

CHAPTER II

Highly efficient Cd-Free ZnMgO/CIGS solar cells via effective band-gap tuning strategy

Abstract:

In this chapter we propose a new modeling framework based on combining graded band-gap (GBG) engineering and metaheuristic optimization to improve the Cd-Free ZnMgO/CIGS solar cell performances. Analytical and numerical calculations are carried out to assess the influence of band-gap profiles of both buffer and active layers on the electronic and optical properties of the studied solar cell. This investigation shows a great improvement of solar cell efficiency by increasing the optoelectronic Figures of Merit (FoMs) through tuning and optimizing the band-gap profiles and the conduction band offset (CBO) at the ZnMgO/CIGS interface. Moreover, metaheuristic-based optimization models are developed to optimize the GBG profiles and enhance the optical and electrical performances of the solar cell. In this context, we recorded very satisfactory results, where the optimized design with GBG paradigm offers a high efficiency of 31.88% compared to 23.35% provided by the conventional CdS/CIGS solar cell. Therefore, this study provides a new strategy in enhancing the efficiency of thin-film solar cells by exploiting the graded band-gap engineering combined with metaheuristic optimization approach.

II.1 Introduction

The current demand for energy in the world with the depletion of the earth's resources from non-renewable energies, put researchers in face to severe challenges for getting sustainable and eco-friendly alternatives [1-5]. Among the proposed solutions are thin-film solar cells (Amorphous Si, perovskite, CZTS, CdTe and CIGS), which are witnessing increasing interest due to their low-cost and less material utilization [2-10]. In this context, the perovskites and CZTS have received a great attention from researchers in the last few years due to many advantages. Regarding perovskites, the use of synthetic materials that do not require complex metallurgy or refining processes, and also require a very small amount of material in the manufacture, and low-cost fabrication processes using low temperature budgets. As for the CZTS, it is composed of only abundant and non-toxic elements, having a larger tuning band-gap close to the optimal single junction value of ~1.5 eV. In contrast, there are some shortcomings that make copper indium gallium selenide (CIGS) the best choice compared with other thin film materials, among which we have material toxicity, device hysteresis and material stability within perovskite. While for the CZTS, we have the efficiency value which is really far from its theoretical limit (η~30%). This is mainly due to sever interface recombination effects, lattice mismatching, the conduction band offset (CBO) at the buffer/absorber interface and the Sulfur diffusion at CZTS/Mo back contact which can increase the total series resistance of the CZTS solar cell [9-13]. At front of the efficiency race, CIGS solar cells attracted additional interest because of several characteristics like their high conversion efficiency, stability of performance, very flexible modules availability, low-cost industrial manufacturing, durability due to the "powder" build up with no wafers to crack or damage, weight down to 2.9 kg/m^2, and a better reliability against high temperature effects. The fabrication of CIGS absorber layer can be carried out by vacuum or non-vacuum processes [14-17]. The achieved current maximum efficiency provided by the CIGS-based solar cells is about 23.35%. This recorded PCE value was confirmed by the Japanese National Institute of Advanced Industrial Science and Technology [18,19]. To improve the efficiency value, many studies have been performed by changing the films parameters: thickness, doping, band-gap energy, acceptor density or by introducing intermediate layers between the absorber and buffer films. For the CIGS active layer, modifying the band-gap, can be done by adjusting the Ga/(Ga + In) ratio, where the band-gap energy can be tuned from 1.01 eV

to 1.68 eV [20-21]. Moreover, several published works have been focused in improving the buffer layer properties. This region can boost the cell performance by suggesting other non-toxic materials instead of the conventional CdS film, such as (ZnO, ZnS, ZnSe,InS, SiC,..) [22-24]. The Zn-based compounds are proper substitute buffer layers with similar electronic and physical properties due to their high band-gap as compared to CdS, we can also find other compounds used as buffer layer like ITO, CdZnS, ZnSnO and ZnMgO. In fact, these materials exhibit a high transmittance for blue spectrum [22-26].The role of the buffer layer defined as an n-type semiconductor material in heterojunction CIGS solar cells; it is used to form the p-n junction with the p-type absorber layer (CIGS) while pushing the maximum amount of incoming light into the absorbing layer. Therefore, this layer must have low surface recombination, minimal electrical resistance, and minimal absorption losses. Moreover, the buffer has an important role in the bands alignment between the absorber and the window layer, as well as protecting the junction against the chemical reactions and mechanical damage, which leads to improve the carriers transport mechanism in the solar cell [27-28]. To the best of our knowledge, no investigations based on combining double band-gap engineering (absorber and buffer layers) with metaheuristic optimization approach have been developed to improve the CIGS solar cell performances, where the powerful of metaheuristic-based techniques for the optimization of complex engineering problems has proven its efficacy in several published works [21,29-31]. For this purpose, a double graded band-gap (GBG) aspect is applied on both buffer and absorber layers to investigate the influence of the band engineering on the device performances. For the buffer layer, we have used the ZnMgO alloy material because of its ability to tune the band-gap values by adjusting the Mg levels during the deposition process. By doing so, it would be possible to better align the junction bands, and also help to more absorption of short wavelength incident photons [23]. Moreover, a global metaheuristic optimization technique is combined with the GBG engineering to boost up the power efficiency in the investigated structure. The advantage of the proposed approach resides on the determination of the optimized graded band-gap profiles for both layers to maximize the PCE value by enhancing the absorption behavior, and prevent the recombination losses effects at the interface. The proposed modeling framework based on coupled GBG profile engineering with metaheuristic computation approach can be helpful to develop high performance thin-film solar cells.

II.2 CIGS solar cell design and modeling frameworks

The choice of the buffer layer is very important for the p-n junction formation and charge carrier separation in chalcogenide $CuIn_xGa_{1-x}Se_2$ solar cells. The most used buffer is the cadmium sulfide (CdS), that yields to reduced open-circuit voltage because of a negative conduction band offset (CBO) at the $Cu(In,Ga)S_2$/CdS interface. In this context, an alternative buffer layer was proposed to reduce this loss [32]. For this purpose, we proposed an engineering $Zn_{1-x}Mg_xO$ buffer layer by using a graded band-gap profile. For more details, the schematic of the proposed structure with a double graded band-gap aspect is shown in Figure II. 1(a). The proposed solar cell structure consists of CIGS layer as an absorber deposited on soda lime glass (SLG) substrates coated Mo from the bottom of the cell. The ZnMgO buffer layer is deposited on the absorber layer, where both layers are suggested with a graded band-gap based on a linear profile, as it is shown in Figure II. 1(b), (c). At the top, the front finger contact formed for the aluminum-doped ZnO (AZO) which, is a good TCO with low cost, nontoxic, and highly durable compared to commercial tin-doped indium-oxide (ITO) [21,23-24]. In Figure II.1 (a), GBG_1 and GBG_2 represent the material graded band-gap in the buffer and the absorber layer respectively, Eg_{1max} and Eg_{1min} are the ZnMgO material band-gap values at the top and bottom of the buffer layer, respectively, while Eg_{2max} and Eg_{2min} are respectively the maximum and minimum band-gap values of the CIGS absorber layer at the following interfaces (ZnMgO/CIGS) and (CIGS/Mo). The t_{ZnMgO}, and t_{CIGS} are n-ZnMgO layer thickness, and p-CIGS absorber region thickness, respectively. Based on the literature, the ZnMgO band-gap can be adjusted in the range of 3.34 eV and 4 eV [25,33-34].

In order to estimate the photocurrent generated by the cell, we need to calculate the materials optical parameters. Accordingly, by using of a well-known expression provided by Tauc et al. we estimate the absorption coefficient as a function of the wavelength for un-polarized incident light model which, is represented as follows [35-36].

$$\alpha(\lambda)=\begin{cases}0 & \frac{hc}{\lambda}<E_g \\ \frac{B\lambda}{hc}\left(\frac{hc}{\lambda}-E_g\right)^{1/2} & \frac{hc}{\lambda}>E_g\end{cases} \qquad \text{(II.1)}$$

where c represents the light speed, λ refers to the optical wavelength, h denotes the Planck's constant, B and E_g are respectively a constant and the material band-gap which, are depending on the semiconductor intrinsic properties *(ZnMgO* and *CIGS*) [37].

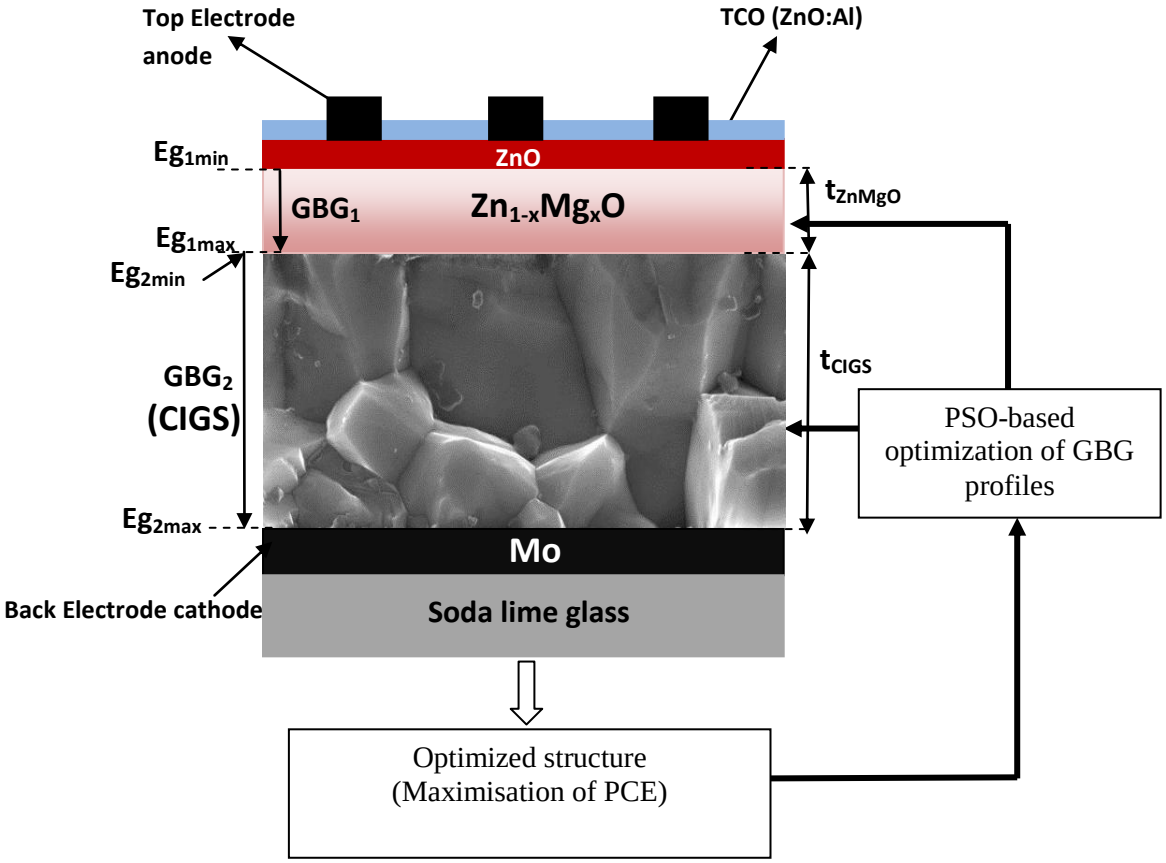

(a)

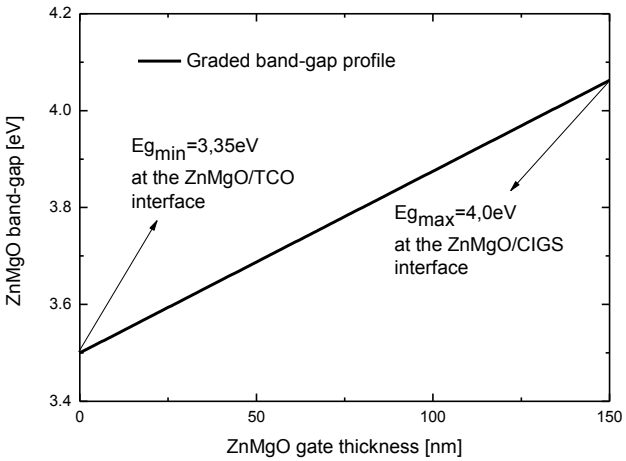

(b)

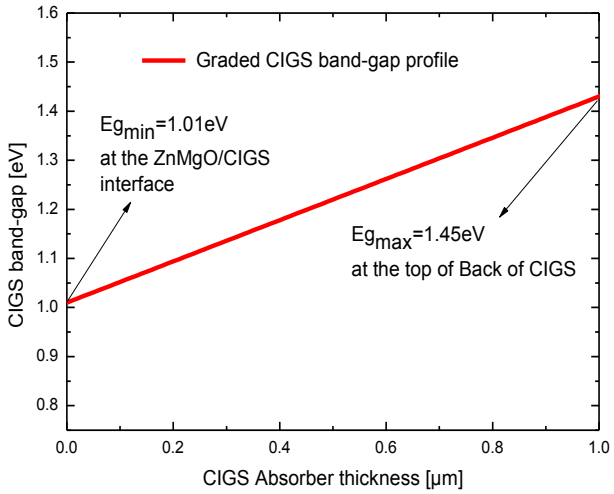

(c)

Figure II.1: (a) Cross-sectional view of the investigated ZnMgO/CIGS thin-film solar cell associated with the optimization approach. **(b)** Band gap grading profile of the inserted ZnMgO buffer layer. **(c)** Band gap grading profile of the CIGS Absorber layer using varied Ga/(In+Ga) ratios.

We can estimate both buffer and absorber layer absorption coefficient using the graded band-gap engineering reported in [21], [36] and [38-40], by exploiting the modified absorption coefficient expressed as follows

$$\alpha(\lambda) = \begin{cases} 0 \; for \; 0 < \dfrac{hc}{\lambda} < E_{\mathrm{gmin}} \\ \dfrac{2}{3}\left(\dfrac{B\lambda}{hc}\left(\dfrac{hc}{\lambda} - E_{\mathrm{g}}\right)^{1/2}\right)\left(\dfrac{\left(\frac{hc}{\lambda} - E_{\mathrm{gmin}}\right)}{\left(E_{\mathrm{gmax}} - E_{\mathrm{gmin}}\right)} - E_g\right)^{1/2} \; for \; E_{\mathrm{gmin}} < \dfrac{hc}{\lambda} < \dfrac{3E_{\mathrm{gmax}} - E_{\mathrm{gmin}}}{2} \\ \dfrac{B\lambda}{hc}\left(\dfrac{hc}{\lambda} - E_{\mathrm{g}}\right)^{1/2} \; for \; \dfrac{hc}{\lambda} > \dfrac{3E_{\mathrm{gmax}} - E_{\mathrm{gmin}}}{2} \end{cases} \quad \text{(II. 2)}$$

After estimating the absorption coefficients of the amended design including graded band-gap profile, of the two regions (buffer and absorber), and by combining both Poisson's and continuity equations, the photocurrent can be expressed by the following expression [41].

$$I_{ph} = \int_{\lambda_{\min}}^{\lambda_{\max}} I_d(\lambda) + I_b(\lambda) + I_a(\lambda) \quad \text{(II.3)}$$

where I_d, I_b and I_a are photocurrents within the depletion, base and emitter regions, respectively.

The photocurrent within the depletion region can be given as follows

$$I_d(\lambda) = q\phi(\lambda)(1 - R(\lambda)) \exp\left(-\alpha_{ZnMgO}(\lambda)W_n\right)\left[1 - \left(\exp\left(\alpha_{ZnMgO}(\lambda)W_n - \alpha_{CIGS}(\lambda)W_p\right)\right)\right] \quad \text{(II.4)}$$

where W_p and W_n are the depletion widths extended in both absorber and buffer layers respectively [39]. The $\alpha_{CIGS}(\lambda)$ and $\alpha_{ZnMgO}(\lambda)$ are respectively absorption coefficients associated with CIGS and ZnMgO materials determined using (*Eq* II.2), $R(\lambda)$ is the reflection coefficient and $\phi(\lambda) = \dfrac{P_i(\lambda)}{qE(\lambda)}$ represents the number of the incident photons with $E(\lambda) = \dfrac{1.24[eV.\mu\mathrm{m}]}{\lambda}$ and $P_i(\lambda)$ is the solar spectral irradiance approximation [40-42].

The photocurrent generated in the buffer ZnMgO region is calculated using the final explicit equation

$$I_a(\lambda) = \left[\frac{q\phi(\lambda)\left(1 - R(\lambda)\right)\alpha_{ZnMgO}(\lambda)L_P}{\left(L_P{}^2\alpha_{ZnMgO}(\lambda)^2 - 1\right)}\right] \times \left[\frac{\left(\frac{S_P L_P}{D_P} + \alpha_{ZnMgO}(\lambda)L_P\right) - \exp\left(-\alpha_{ZnMgO}(\lambda)t_{ZnMgO}\right)\left(\frac{S_P L_P}{D_P}\, ch\left(\frac{t_{ZnMgO}}{L_P}\right) + sh\left(\frac{t_{ZnMgO}}{L_P}\right)\right)}{\left(\frac{S_P L_P}{D_P}\right)sh\left(\frac{t_{ZnMgO}}{L_P}\right) + ch\left(\frac{t_{ZnMgO}}{L_P}\right)} - \alpha_{ZnMgO}L_P \exp\left(-\alpha_{ZnMgO}(\lambda)t_{ZnMgO}\right)\right] \quad \text{(II.5)}$$

where L_P represents the diffusion length of the ZnMgO material, D_p diffusion coefficient and t_{ZnMgO} is buffer layer thickness, S_p is the recombination velocity which, can be calculated from $D_P \frac{d(P_n - P_{n0})}{dy} = S_P(P_n - P_{n0})$, and at the depletion width (W_n) of the buffer region, where we can neglect the excess carrier density ($P_n - P_{n0} = 0$).

The photocurrent generated within the CIGS neutral p-region, can be estimated in the same way by the following formula

$$I_b = \left(\frac{\phi(\lambda)\left(1 - R(\lambda)\right)\alpha_{\mathrm{CIGS}}(\lambda)L_{np}}{\left(\alpha_{\mathrm{CIGS}}(\lambda)^2 L_{np}{}^2 - 1\right)}\right) \exp\left(-\alpha_{\mathrm{CIGS}}(\lambda)\, d_{\mathrm{p}}\right) \times \left[\alpha_{\mathrm{CIGS}}(\lambda)\, L_{neff} - \frac{\left(\frac{S_n L_{np}}{D_{np}}\right)\left(ch\left(\frac{d_z}{L_{np}}\right) - \exp\left(-\alpha_{\mathrm{CIGS}}(\lambda)\, d_z\right)\right) + sh\left(\frac{d_z}{L_{np}}\right) + \alpha_{\mathrm{CIGS}}(\lambda)\, L_{neff} \exp\left(-\alpha_{\mathrm{CIGS}}(\lambda)\, d_z\right)}{\left(\frac{S_n L_{np}}{D_{np}}\right) sh\left(\frac{d_z}{L_{np}}\right) + ch\left(\frac{d_z}{L_{np}}\right)}\right] \quad \text{(II.6)}$$

where d_p is calculated by using the following formula $d_p = t_{ZnMgO} + W_n + W_p$, d_z is the quasi-neutral zone width related to the absorber layer CIGS, L_{np} and D_{np} are the diffusion length and coefficient of the absorber region respectively, and S_n is the recombination velocity for minority carrier associated with the absorber region CIGS. The latter was modified for the proposed GBG design as follows [21]

$$S_{neff} = S_n - \mu_n \xi \quad \text{(II.7)}$$

where μ_n is the electron mobility, ξ is the electric field produced from using of graded band-gap profile provided as [40,43]

$$\xi = \frac{dE_g}{dx} \tag{II.8}$$

The new diffusion length after introducing the impact of the electric field on the material can be estimated using the following equation [21,36],[38-40].

$$L_{neff} = \frac{L_n}{\sqrt{1+\left(\frac{L_n\xi}{2V_{th}}\right)^2} - \frac{L_n\xi}{2V_{th}}} \tag{II.9}$$

The saturation current also occurred from the use of GBG engineering can be calculated by using this formula [21].

$$I_{seff} = I_s\left(\frac{2V_{th}}{E_{g\max} - E_{g\min}}\right) \tag{II.10}$$

with

$$I_s = qN_cN_v\left(\frac{1}{N_{CIGS}}\sqrt{\frac{D_p}{\tau_p}}\right)\exp\left(-\frac{E_{g2\min}}{V_{th}}\right) + qN_cN_v\left(\frac{1}{N_{ZnMgO}}\sqrt{\frac{D_n}{\tau_n}}\right)\exp\left(-\frac{E_{g1\min}}{V_{th}}\right) \tag{II.11}$$

where N_c, N_v are respectively, the effective densities of states in conduction and valence bands of both ZnMgO and CIGS regions, N_{ZnMgO} and N_{CIGS} denote the doping concentration of buffer and absorber layers, respectively, E_{g2min} and E_{g1min} represent the band-gap associated with both CIGS and ZnMgO materials. Knowing the saturation current estimation, we can estimate the open circuit voltage by the following expression

$$V_{oc} = V_{th}\ln\left(\frac{I_{ph}}{I_{seff}} - 1\right) \tag{II.12}$$

Now the current voltage characteristics of the investigated solar cell under illumination can be calculated by the following implicit equation

$$I(V) = I_{ph} - I_{seff}\left[e^{\frac{V-I\,R_s}{nV_{th}}} - 1\right] - \frac{V - IR_s}{R_{sh}} \tag{II.13}$$

where, R_s and R_{sh} are the series and shunt resistances respectively, V_{th} represents the thermal voltage, n is the ideality factor.

In order to evaluate the accurateness of the developed model, the *I-V* characteristic provided by our analytical model is compared and validated using experimental data [44], as it is shown in Figure II.2 From this figure, it can be demonstrated that a good agreement between both analytical results and experimental data is successfully achieved. Moreover, the obtained results show that the developed model is able to simulate the solar cell electrical and optical behavior. We can also notice that the developed model well simulates the current-voltage dependence compared to the experimental results.

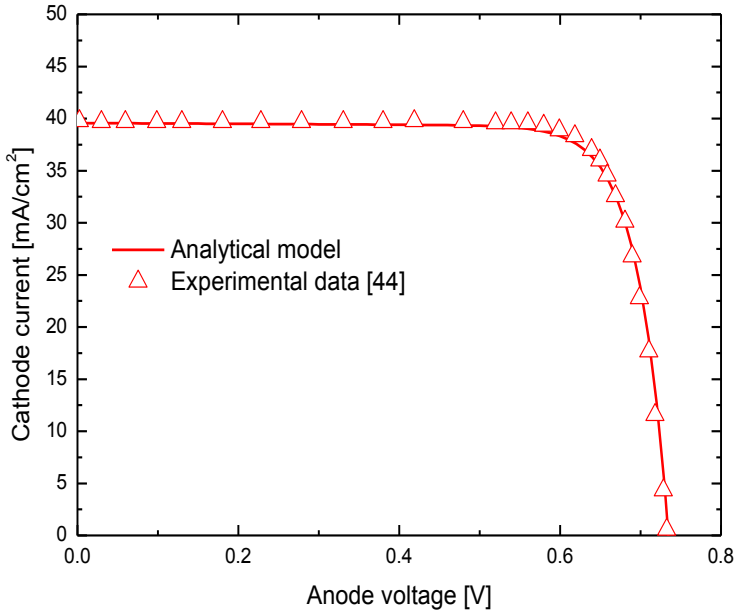

Figure II.2: I-V characteristics of experimental data and simulation results associated with the conventional CdS/CIGS solar cell.

II.3 Results and discussions

In this section, the effect of GBG for both of buffer and absorber layers is investigated. In other words, the goal of this framework is firstly to study the impact of the absorber layer grading band gap on the cell performance. Secondly the impact of the band-gap engineering of the buffer layer on the cell performance, thirdly the influence of the band-gap profiles of both buffer and absorber layers on the device properties, and finally the solar cell enhancement by combining the global optimization PSO technique

with the GBG engineering. Figure II.3 (a) plots the variation of PCE as a function of E_C offset and the associated CIGS band-gap, where the Eg_{CIGS} ranges from 1.10 to 1.5 eV. It can be seen that the PCE increases with the increasing of the Ga percentage, allowing the Eg_{CIGS} to widen, until it reaches its maximum value of 23.2% at E_C offset = 0.1 eV, where it starts to decrease. This is due to the reduced generation rate when the CIGS band-gap is increased. In addition, the E_C offset (CBO) has an important effect in increasing the interface recombination so that, CBOs between 0 and 0.3 eV improves photovoltaic performance. When the CBO exceeds more than 0.3 eV, a high energy barrier is formed, which may hinder the cross of photogenerated electrons in CIGS. On the other hand, a negative value of CBO leads to reduce the life time of the photo-induced carriers [28,31], [45-46]. Otherwise, in Figure II.3 (b) presenting PCE as a function of CBO and ZnMgO band-gap with fixed CIGS band gap value of 1.2 eV, the PCE continues to increase with increasing of the Mg concentrations to reach a maximum value of 25.3% with the maximum range of ZnMgO band-gap E_{g1max}.

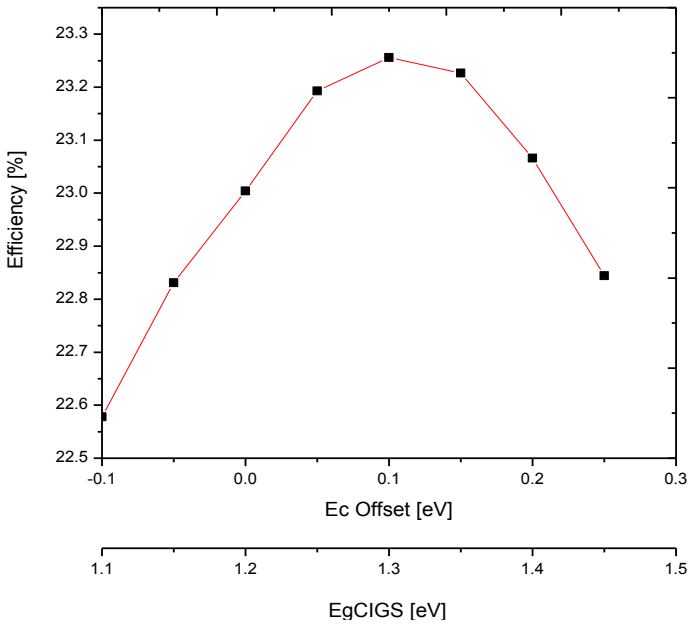

(a)

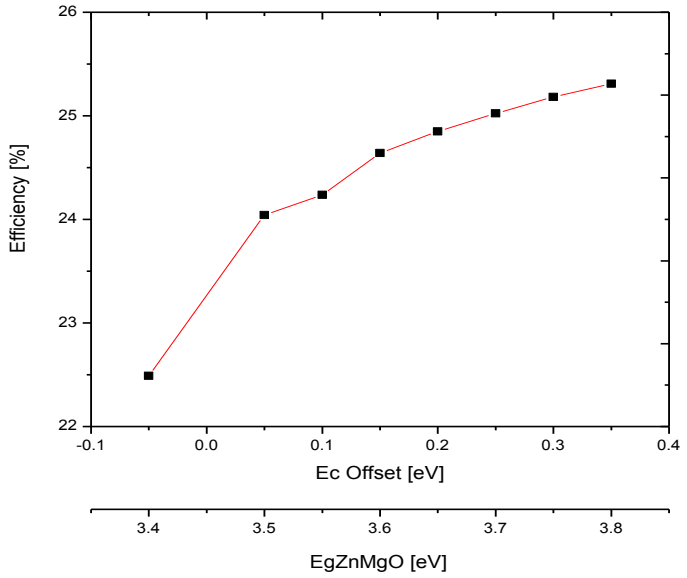

(b)

Figure II.3: (a) Power efficiency versus CIGS band-gap using dissimilar Ga/(In+Ga) ratio values. **(b)** Variation of power efficiency as a function of the ZnMgO band-gap at the buffer/absorber using various Mg concentrations and fixed CIGS band gap value of 1.2eV.

This can be explained by the enhanced carrier life-time provided by the graded band-gap aspect. In other words, the graded band-gap aspect of ZnMgO buffer and CIGS absorber materials has a profound implication on the carrier extraction mechanism of the solar cell, inducing a built in electric field that facilitates the separation of photo-induced carriers. This can contribute in reducing recombination effects and thereby decreasing Voc deficit. Figure II.4 represents the *I-V* characteristics of the conventional CdS/CIGS solar cell in comparison with the proposed structures in different graded band-gap, the buffer GBG (GBG-ZnMgO/CIGS), and the GBG for both buffer and absorber layer (GBG-ZnMgO/GBG-CIGS). The comparison illustrated by this figure demonstrates that the proposed structures exhibit an improved open circuit voltage (more than 1 V), due to the best alignment of the conduction bands in the ZnMgO/CIGS interface and between the buffer and absorber layers, where the appropriate CBO can allow avoiding degradation related to interfacial recombination losses [28,47]. On the contrary, we notice a clear decrease in the short circuit current compared to the conventional solar cell, particularly the GBG-ZnMgO/CIGS which is attributed to the effect of the GBG since the increase of the band gap establishes a reduction of short

circuit current. However, for the other engineered structure i.e. GBG-ZnMgO/GBG-CIGS, the GBG applied from the back contact prevents the recombination and enhances the transmission of electrons leading to improving the short circuit current [48]. But in general, the PCE is increased for both GBG designs. For further improvement to boost the efficiency, and to find the best combination of electrical and optical parameters, a global optimization approach using particle swarm optimization (PSO)-based metaheuristic technique, is combined with GBG engineering for both buffer and absorber layers with the aim of pushing the solar cell efficiency to its maximum. That what will be more detailed in the next sub-section.

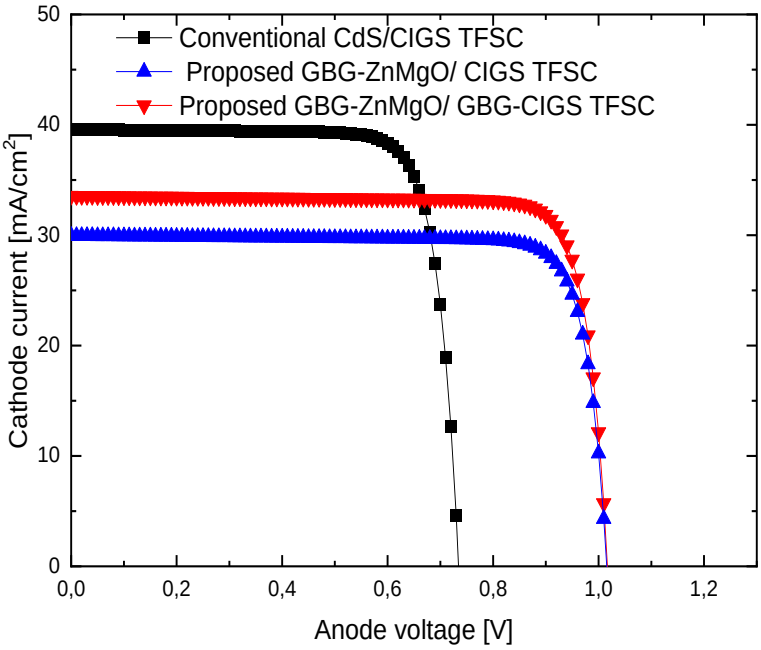

Figure II.4: I-V characteristics comparison between the investigated TFSCs based on GBG-ZnMgO/CIGS, GBG-ZnMgO/GBG-CIGS and the conventional CdS/CIGS structures.

II.3.1 PSO decision-making framework for the design of CIGS solar cell

In order to reach the effective limit of CIGS-based solar cell, we have to find the best combination among the different parameters of the solar cell. Such task can be achieved by exploiting the metaheuristic methods. One of the most powerful optimization technique, which is widely used in the optoelectronic and nanoelectronic field, is the particle swarm optimization (PSO)-based approach [49-52]. This method is an evolutionary computational technique inspired by nature and mainly from social

behavior to fly flocks of birds and insects. Kennedy and Eberhart were the first to propose this technique [53]. Although its simple mechanism, it has proven its worth in studying complex and non-linear systems, especially in engineering fields. PSO algorithm is based on searching for the optimal solution by modifying particle motion across a well-defined space, according to the flight experiences of each particle in the swarm and its companion group, affected by two factors: best site found for each particle, the other is the best site of the companions group. Accordingly, the particles velocity and position are adjusted using the following equations

$$V_i^{k+1} = wV_i^k + c_1 r_1^k (p_{li}^k - X_i^k) + c_2 r_2^k (p_{gi}^k - X_i^k) \quad \text{(II.14a)}$$

$$X_i^{k+1} = X_i^k + V_i^{k+1} \qquad \text{for i=1...n} \quad \text{(II.14b)}$$

where p_{li}^k and p_{gi}^k are particle's best position and particles group's best position in the swarm respectively, *n* refers to the swarm size, X_i^k and V_i^k denote, respectively, the particle position and velocity, and X_i^k represents the actual position of the particle in swarm, c_1 and c_2 represents the cognitive and social acceleration factors, respectively, *w* is the inertia weight applied to balance the global exploration, r_1 and r_2 denote the random numbers distributed in the range of [0,1]. In this perspective, the proposed CIGS solar cell with graded band-gap aspects will be optimized by maximizing the power efficiency, where the fitness function is given as follows

$$Fitness(X) = \frac{1}{\eta(X)} \quad \text{(II.15)}$$

where X_i =(Eg_{1min}, Eg_{1max}, t_{ZnMgO}, N_{ZnMgO}, Eg_{2min}, Eg_{2max}, t_{CIGS}, N_{CIGS}) of the i^{th} generation represents the design parameter vector.

In order to ensure that the parameters values do not exceed their physically acceptable limits, we have to keep them in a given range which is given as the following $x \in [x_{mmin}, x_{mmax}]$, $x_i \in X$ which means that each design variable should be confined within a given range.

To examine the effectiveness of the proposed approach in improving the CIGS solar cell performance, we have compared in Figure II.5 (a) the *I-V* characteristics of the optimized design (GBG-ZnMgO/GBG-CIGS-based solar cell), with that of the conventional CdS/CIGS structure. This figure confirms that a significant improvement has been achieved by using the coupled dual-GBG aspect with global optimization technique, where the cell performance has been significantly improved thanks to the best configuration of different solar cell parameters and the best band-gap profile identification. So that the improvement is achieved in both short circuit current, open-circuit voltage and fill factor (FF). Moreover, the buffer/absorber interfaces optimization by using ZnMgO as a graded band-gap buffer layer has enabled avoiding the interface recombination losses, which has enhanced the open-circuit voltage.

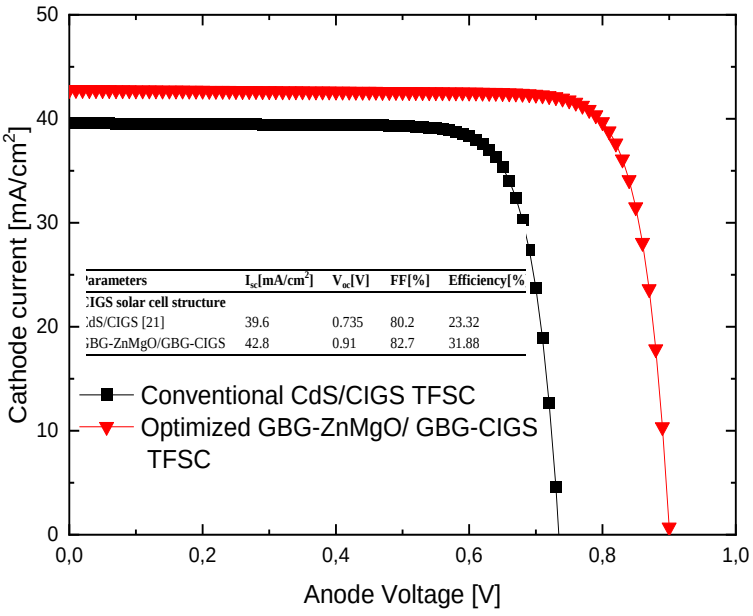

(a)

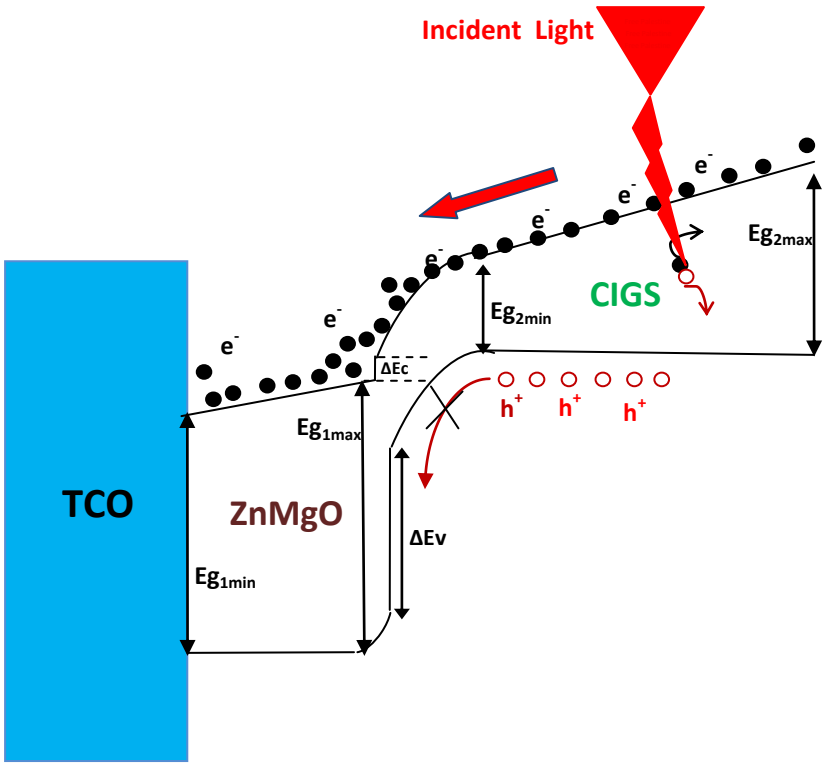

(b)

Figure II.5: (a) I-V characteristics of the optimized GBG-ZnMgO/GBG-CIGS-based TFSC compared to that of the conventional CdS/CIGS structure. **(b)** Band structure of the optimized GBG-ZnMgO/GBG-CIGS interface.

To assess the performance of our optimized TFSC design with respect to other studies, we compare in Table II.1 the results obtained in this chapter with those of other studies in terms of the solar cell performance. We can notice from this table the clear superiority of our optimized design over the other studied solar cells mentioned in [54-59]. In this context, we recorded a very high efficiency of about 32% and significant improvements in short current of 42.8 mA/cm^2, open circuit voltage of 0.91V, and an FF of 82.7%. These improvements can be explained by the fact that adopted GBG paradigm allowed an additional electric field generated by a linear gradient of the potential in the absorber layer, which leads to a reduction in series resistance that enhances the separation and transfer mechanisms of photo-excited carriers resulting in an increase in the carrier life time. Moreover, the smooth mobility of electrons provided by the optimized band alignment, as it is shown in Figure II.5 (b). Because many studies have proven the possibility of modifying the band-gap for both ZnMgO and CIGS in the range of 3.34 eV to 4 eV and 1.01 eV to 1.68 eV, respectively, our optimized TFSC

design is considered technologically feasible [20-21], [25] and [33-34]. Therefore, we expect the outcomes demonstrated in this study, to provide solutions and enable designers to further improve the solar cells performance [60].

Table II.1: Performance comparison between the proposed ZnMgO/CIGS TFSCs based on the GBG aspect and other CIGS TFSCs with different buffer materials reported in the literature.

Parameters	**I_{sc} [mA/cm^2]**	**V_{oc}[V]**	**FF[%]**	**Efficiency[%]**
CdS/CIGSsolarcell				
Experimental [44]	39.6	0.734	80.4	23.35
Numerical results	39.6	0.735	80.2	23.32
CIGS solar cell with several buffers				
ZnO/In_2S_3 [54]	35.16	0.55	56.73	11.02
ZnS/(Zn,Mg)O [55]	31.9	0.63	72..6	14.6
CdS/i-ZnO [55]	30.5	0.666	74.4	15.1
ZnSe [56]	36.02	0.669	50.33	12.13
FTO/In_2S_3/CdS [57]	34.35	0.637	82.59	18.08
ZnO:Al/CBD-ZnS [58]	34.9	0.671	77.6	18.1
NiO/ZnO/CdS [59]	36.49	0.635	70.6	16.35
Optimized GBG-ZnMgO/GBG-CIGS solar cell	42.8	0.91	82.7	31.88

II.4 Conclusion

In this chapter, we have proposed a novel modeling framework design strategy to improve the CIGS-based TFSC performances based on hybrid GBG-PSO-approach. New analytical models have been developed to investigate the solar cell behavior, where the accuracy of the obtained results was confirmed using numerical simulations. In addition, we have employed the ZnMgO instead of the conventional toxic CdS buffer

layer, including the graded band-gap engineering aspect, which made it very compatible with CIGS absorber layer in terms of band alignment and light management behavior. The good combination between metaheuristic-based approach and GBG aspect, for both CIGS and ZnMgO layers opened up new insights for improving TFSCs performances. In this context, we recorded very satisfactory results, where the optimized design with GBG paradigm offers a high relative improvement of 36.5% in comparison with that of the conventional CdS-based design. Accordingly, the proposed strategy will provide new guidelines for the development of high-performance thin-film solar cells based on non-toxic elements.

References

[1] M. A. Green, E. D. Dunlop, J. Hohl-Ebinger, M. Yoshita, N. Kopidakis and X. Hao, "Solar cell efficiency tables (Version 56)," Progress In Photovoltaics, vol.28, pp. 3-15, 2020.

[2] P. K. Nayak, S. Mahesh, H. J. Snaith and D. Cahen , "Photovoltaic solar cell technologies: analysing the state of the art," Nature Review Materials, vol. 4, pp. 269-285, 2019.

[3] K. Branker, M. Pathak and J. M. Pearce, "A review of solar photovoltaic levelized cost of electricity," Renew. Sustain. Energy Rev, vol. 15, pp.4470-4482, 2011.

[4] M. A. Green, "Tracking solar cell conversion efficiency," Nature Reviews Physics, vol. 2, pp. 172–173, 2020.

[5] P. Jackson, D.Hariskos, E. Lotter, S. Paetel, R. Wuerz, R. Menner, "New world record efficiency for Cu (In,Ga)Se2 thin-film solar cells beyond 20%," Prog Photovoltaics Res Appl, vol. 19, pp. 894-897, 2011.

[6] F. Belarbia, W. Rahal, D. Rached, S. benghabrit, M. Adnane, "A comparative study of different buffer layers for CZTS solar cell using Scaps-1D simulation program," Optik - International Journal for Light and Electron Optics, vol. 216,pp. 164743, 2020.

[7] H. Ferhati, F. Djeffal, L. B. Drissi, "Performance improvement of Perovskite/CZTS tandem solar cell using low-cost ZnS/Ag/ITO multilayer spectrum splitter," Superlattices and Microstructures, vol. 148, pp. 106727, 2020.

[8] K. Kacha, F. Djeffal, H. Ferhati, D. Arar, M. Meguellati, "Numerical investigation of a double-junction a: SiGe thin-film solar cell including the multi-trench region," Journal of Semiconductors, vol. 36,pp. 064004, 2015.

[9] J. Lakshmi Prasanna, Ekta Goel Amarjit Kumar, Amel Laref , Chella Santhosh , Pranay Ranjan , Atul Kumar, "Bandgap graded perovskite solar cell for above 30% efficiency," Optik, vol. 269, pp. 169891, 2022.

[10] H. Sun, K. Deng, J. Xiong, and L. Li, "Graded Bandgap Perovskite with Intrinsic n–p Homojunction Expands Photon Harvesting Range and Enables All Transport Layer-Free Perovskite Solar Cells," *Adv. Energy Mater*, vol. 1, pp. 1903347, 2020.

[11] O.K. Simya, A. Mahaboobbatcha, K. Balachander, "Compositional grading of CZTSSe alloy using exponential and uniform grading laws in SCAPS-ID simulation," Superlattices and Microstructures, vol. 92, pp. 285-293, 2016.

[12] B. Maharana, R. Jha, S. Chatterjee, "Metal oxides as buffer layers for CZTS based solar cells: A numerical analysis by SCAPS-1D software," Optical Materials, vol. 131, pp. 112734, 2022.

[13] H. Ferhati, and F. Djeffal, "Role of intermediate metallic sub-layers in improving the efficiency of kesterite solar cells: concept and optimization," Materials Research Express, vol. 5, pp.036417, 2018.

[14] S. Niki, M. Contreras, I. Repins, M. Powalla, K. Kushiya, S. Ishizuka, K. Matsubara, "Cd- Free Cu(In, Ga)(Se, S)2 thin-film solar cell with record efficiency of 23.35%," Prog.Photovolt Res. App, vol.18, pp.453–466, 2010.

[15] J.H. Shi, Z.Q. Li, D. W. Zhang, Q.Q. Liu, Z. Sun, S.M. Huang, "Fabrication of Cu(In, Ga)Se_2 thin films by sputtering from a single quaternary chalcogenide target" Prog. Photovolt. Res. App, vol.19, pp. 160-164, 2011.

[16] C.J. Hibberd, E. Chassaing, W. Liu, D.B. Mitzi, D. Lincot, A.N. Tiwari, "Non-vacuum methods for formation of Cu(In, Ga)(Se, S)$_2$ thin film photovoltaic absorbers," Prog. Photovolt. Res. App, vol.18, pp. 434–452, 2010.

[17] M. Zahedifar, E. Ghanbari, M. Moradi, M. Saadat, "Optimized annealing regime of $CuGaSe_2$ nanoparticles prepared by solvothermal method," Phys. Status Solidi A, vol.212, pp.657-661, 2015.

[18] El-H.Ihalane, L.Atourki, H.Kirou, A. Ihlal, K. Bouabid, "Numerical study of thin films CIGS bilayer solar cells using SCAPS," Materials Today, vol. 3, pp. 2570-2577, 2016.

[19] M. Nakamura, K. Yamaguchi, et al, "Cd- Free Cu(In, Ga)(Se, S)2 thin-film solar cell with record efficiency of 23.35%," IEEE J. Photovoltaics ,vol.9 , pp.1863–1867, 2019.

[20] W. Liu, H. Li, B. Qiao, S. Zhao, Z. Xu, D. Song, "Highly efficient CIGS solar cells based on a new CIGS bandgap gradient design characterized by numerical simulation," Solar Energy, vol.233, pp.337-344, 2022.

[21] H. Ferhati, F. Djeffal, "Graded band-gap engineering for increased efficiency in CZTS solar cells," Optical Materials, vol.76, pp.393-399, 2018.

[22] M. Moradia, R. Teimouria, M. Saadata, M. Zahedifar, "Buffer layer replacement: A method for increasing the conversion efficiency of CIGS thin film solar cells," Optik, vol.136, pp.222-227, 2017.

[23] R. Prasad, Rajarshi Pal, Udai P. Singh, "Performance optimization of single graded CIGS absorber and buffer layers for high efficiency: A numerical approach," Superlattices and Microstructures, vol.161, pp.107094, 2022.

[24] F. Ghamsari-Yazdel, A. Fattah, "Performance enhancement of CIGS solar cells using ITO as buffer layer," Micro and Nanostructures, vol.168, pp. 207289, 2022.

[25] R. Prasad, A. K. Das, Udai P. Singh, "Impact of buffer layers on the performance of graded CIGS solar cells: a numerical approach," Applied Physics A, vol.127, pp. 816, 2021.

[26] K. Kacha, F. Djeffal, H. Ferhati, L. Foughali, A. Bendjerad, A. Benhaya, "Efficiency improvement of CIGS solar cells using RF sputtered TCO/Ag/ TCO thin-film as prospective buffer layer," Ceramics International, vol.48, pp. 20194, 2022.

[27] N. Khoshsirat, N. A. Md Yunus, M. N. Hamidon, S. Shafie, N. Amin, "Analysis of Absorber and Buffer Layer Band Gap Grading on CIGS Thin Film Solar Cell Performance Using SCAPS," Pertanika J. Sci. & Technol, vol.23, pp. 241-250, 2015.

[28] B.Salhi, "The Photovoltaic Cell Based on CIGS: Principles and Technologies," Materials, vol.15, pp. 1908, 2022.

[29] H. Ferhati, F. Djeffal, L.B. Drissi, "Metaheuristic-based decision maker framework for the development of multispectral IGZO thin-film phototransistors," Journal of Science: Advanced Materials and Devices, vol.7, pp. 100414, 2022.

[30] F. Djeffal, H. Ferhati, "A new high-performance phototransistor design based on both surface texturization and graded gate doping engineering," J. Comput. Electron, vol. 15, pp. 301-310, 2016.

[31] H. Ferhati , F. Djeffal, "Exceeding 30 % efficiency for an environment-friendly tandem solar cell based on earth-abundant Se/CZTS materials," Physica E: Low-dimensional Systems and Nanostructures, vol.109, pp.52-58, 2019.

[32] M. Sood, P.Gnanasambandan, D. Adeleye, S. Shukla, N. Adjeroud, R. Leturcq, S. Siebentritt, "Electrical barriers and their elimination by tuning (Zn,Mg)O buffer composition in Cu(In,Ga)S_2 solar cells: systematic approach to achieve over 14% power conversion efficiency," *J. Phys. Energy*, vol.3, pp. 045005, 2022.

[33] A. Kadri, H. Ferhati, F. Djeffal, "Giant responsivity of a new optically controlled graphene UV-phototransistor using graded band-gap ZnMgO gate," Sensors and Actuators A, vol. 325, pp. 112701, 2021.

[34] W. Seok Choi, J-G. Yoon, "Optical characterization of band gap graded ZnMgO films," Solid State Communications, vol. 152, pp. 345-348, 2012.

[35] J. Tauc, A. Menth, "States in the gap," J. Non-Cryst. Solids, vol.8-10, pp.569-585, 1972.

[36] Arturo Morales-Acevedo, "A Simple Model of Graded Band-Gap CuInGaSe2 Solar Cells," Energy Procedia, vol. 2, pp. 169-176, 2010.

[37] M. Courel, J. A. Andrade-Arvizu and O. Vigil-Galán, "The role of buffer/kesterite interface recombination and minority carrier lifetime on kesterite thin-film solar cells," Mater. Res. Express, vol.3, pp. 095501, 2016.

[38] A. Morales-Acevedo, "Effective absorption coefficient for graded band-gap semiconductors and the expected photocurrent density in solar cells," Sol.Energy Mater. Sol. Cell, vol. 93, pp. 40-44, 2009.

[39] A. L.Sufer, A. K. Abdullah, "Computer Simulation of the effect of band gap grading of the CIGS absorber layer on the performance of Cds/CIGS thin film solar cell," Al-Rafida Eng, vol. 20, pp. 44-60, 2012.

[40] A. Aissat, H. Arbouz, J.P. Vilcot," Optimization and improvement of a front graded bandgap CuInGaSe2 solar cell," Solar Energy Materials and Solar Cells, vol. 180, pp. 381-385, 2018.

[41] J. Tauc, A. Menth, "States in the gap," J. Non-Cryst. Solids, vol.8-10, pp.569-585, 1972.

[42] A. Benmir, M. S. Aida, "Analytical modeling and simulation of CIGS solar cells," Energy Procedia, vol. 36, pp. 618-627, 2013.

[43] A. Morales-Acevedo, "Analytical model for the photocurrent of solar cells based on graded band-gap CdZnTe thin films," Sol. Energy Mater. Sol. Cell, vol. 95, pp. 2837-2841, 2011.

[44] J. Hwang, Y. Cho, D. Shin, I. Jeong, J. H. Park, J-S. Cho, J. Gwak, J. H. Yun, K. Han, H. S. Chang, K. Kim, "Improved carrier transport in CIGS solar cells induced by Ag treatment," Journal of Alloys and Compounds, vol. 886, pp. 161193, 2021.

[45] N. Naghavi, D. Abou-Ras , N. Allsop , N. Barreau , et al "Buffer layers and transparent conducting oxides for chalcopyrite Cu(In,Ga)(S,Se)2 based thin film photovoltaics: Present status and current developments," Prog. Photovolt. Res. Appl, vol.18, pp.411-433, 2010.

[46] T. Minemoto , A. Okamoto , H. Takakura, "Sputtered ZnO-based buffer layer for band offset control in Cu(In,Ga)Se_2 solar cells," Thin Solid Films, vol.519, pp. 7568-7571, 2011.

[47] H. Ferhati, F. Djeffal, L.B. Drissi, "A new approach to the modeling and simulation of multi-junction solar cells, "Optik, vol. 200, pp. 163452, 2020.

[48] J. Liu, M. Zhang, X. Feng, "Simulation of graded bandgap on the performance of back-wall superstrate CIGS solar cells," Optik, vol. 172, pp. 1172-1178,2018.

[49] F. Djeffal, N. Lakhdar, M. Meguellati, A. Benhaya, "Particle swarm optimization versus genetic algorithms to study the electron mobility in wurtzite GaNbaseddevices," Solid State Electron, vol. 53, pp. 988-992, 2009.

[50] F. Djeffal, T. Bendib, R. Benzid, A. Benhaya, "An approach based on particle swarm computation to study the nanoscale DG MOSFET-based circuits," Turk. J.Electron. Eng. Comput. Sci, vol. 18, pp. 1131-1140, 2010.

[51] F. Djeffal, N. Lakhdar, A. Yousfi, "An optimized design of 10-nm-scale dualmaterial surrounded gate MOSFETs for digital circuit applications," Phys. E Low-Dimens. Syst. Nanostruct, vol. 44, pp. 339-344, 2011.

[52] H. Ferhati, F. Djeffal, "Role of optimized grooves surface -textured front glass in improving TiO_2 thin film UV photodetector performance," IEEE Sensor. J, vol. 16, pp. 5618-5624, 2016.

[53] M. Clerc, J. Kennedy, "The particle swarm - explosion, stability, and convergence in a multidimensional complex space," J.IEEE Trans. Evolut. Comput, vol. 73, pp. 6-58, 2002.

[54] J. H. Kim, D. Shin, B. T. Ahn, "Surface morphology control of In2S3 buffer layer by Sn incorporation and its application to cadmium-free Cu(In,Ga)Se2 thin-film solar cells," Current Applied Physics, vol. 16, pp. 1040-1045, 2016.

[55] W. Witte, D. Hariskos, M. Powalla, "Comparison of charge distributions in CIGS thin-film solar cells with ZnS/(Zn, Mg)O and CdS/i-ZnO buffers," Thin Solid Films,vol.519, pp. 7549–7552, 2011.

[56] M. Mostefaoui, H. Mazari, S. Khelifi, A. Bouraiou, R. Dabou, "Simulation of High Efficiency CIGS Solar Cells with SCAPS-1D Software," Energy Procedia,vol.74, pp.736–744, 2015.

[57] M.A. Ashraf and I. Alam, "Numerical simulation of CIGS, CISSe and CZTS-based solar cells with In2S3 as buffer layer and Au as back contact using SCAPS 1D," Eng. Res. Express, vol. 2, pp.035015, 2022.

[58] T. Nakada, M. Mizutani, "18% efficiency Cd-free Cu(In, Ga)Se2 thin-film solar cells fabricated using chemical bath deposition (CBD)-ZnS buffer layers," Japanese J. Appl. Physics, vol.41, pp.97–100, 2002.

[59] S-M. Youn, M-J. Park, J. H. Kim and C. Jeong, "Performance enhancement of CIGS thin-film solar cells with a functional-window NiO thin layer," Journal of Alloys and Compounds, vol.886, pp.154803, 2020.

[60] A. Maoucha, H. Ferhati, F. Djeffal, and F. AbdelMalek, "Highly efficient Cd-Free ZnMgO/CIGS solar cells via effective band-gap tuning strategy," Journal of Computational Electronics, vol. 22, pp. 887–896, 2023.

CHAPTER III

Performance enhancement of a new lead-free perovskite solar cell

Abstract:

In this chapter we investigate the effectiveness of a lead-free perovskite solar cell based on $MAGeI_3$/$CsSnGeI_3$ double-absorber structure engineering and an optimized band alignment design. Moreover, in this study we have explored different electron and hole transport layers (ETL and HTL) and their impact on the solar cell performances using accurate numerical simulations. Also, using the SnO_2 and Cu_2O as ETL and HTL, respectively, provides excellent solar cell performances. Further, optimizations in terms of both absorber layer thicknesses, energy band alignment and defect density have also been performed. Besides, the obtained optimum parameters have been implemented in the proposed lead-free perovskite solar cell structure (FTO/ SnO_2 (electron transport layer) / $MAGeI_3$-$CsSnGeI_3$ double-absorber layer/ Cu_2O (hole transport layers)/Au). The performance parameters provided by the proposed structure are compared with the already existing perovskite solar cells, where remarkable enhancements in the device performances were achieved with power conversion efficiency (PCE)= 33.57%, open-circuit voltage (V_{OC})=1.32V, short-circuit current (J_{SC})= 28.11 mA/cm^2 and Fill factor (FF)= 90.37 %. Therefore, these findings open the perspective for developing alternative efficient lead-free perovskite solar cells, which are highly suitable for newly emerging non toxic and low-cost thin-film photovoltaic applications.

III.1 Introduction

Nowadays, thin-film solar cells have received a great deal of research interest, opening new avenues to achieve enhanced power conversion efficiency, while maintaining cost-effective fabrication process, which is highly suitable extended application domains including thermal energy and photovoltaic engineering [1-5]. Thin-film solar cells have revealed several advantages compared to that provided by the conventional wafer-based technology, such as low production cost and less material utilization, which is the most important requirements for high-performance photovoltaic applications [1-5]. Recently, a lot of efforts for developing new materials have been intensified to further boosting up the efficiency to cost ratio of thin film solar cells [2-8]. In this context, lead-based perovskites have observed remarkable progress due to their good electrical and optical properties such as high absorption coefficient, low exciton binding energy, long charge diffusion lengths, bandgap tunability, high carrier mobility and low-cost elaboration process, where the power conversion efficiency provided by the lead-based perovskite solar cell (PSC) has already reached 25.5% [9]. Despite these exciting properties, lead-based perovskite solar cells still face some limitations, which are mainly due to their degradation and the toxic nature of lead [10-12]. To overcome these challenges, researches have turned out towards using alternative lead-free perovskite materials such as Cesium Germanium halide perovskites, which have proven to be good alternatives to lead-based perovskites due to their tunable band-gap, higher optical absorbance behavior and excellent optical conductivity [13]. In addition, the successful elaboration of lead-free perovskites MAGeI3 (CH3NH3GeI3) and CsSnGeI3 has opened new routes in developing high-performance thin film solar cells [13,14]. This is mainly due to their fascinating electrical, optical and processing characteristics like band-gap tunability, high carrier mobility, high Vis-IR absorption coefficient and good stability behavior in comparison to MAPbI3 [14]. Moreover, the hybrid Ge-based perovskite reveals commensurable photovoltaic performance similar to Pb and Sn, also, Ge exhibits chemical similarities to both neighboring group elements, lead and tin [14]. So far, several solar cells based on these lead-free perovskites were numerically and experimentally investigated based on various electronic configurations using different ETL and HTL structures as charge carriers transport layers, showing a great promise for achieving enhanced PCE values [10-15]. Despite these benefits, the use of inadequate transport layers leads to induce severe degradation-related to and energy misalignment and lattice mismatching effects. Therefore, new design strategies are required to

overcome these challenges and enhance the performance of lead-free perovskite solar cells. In this context, this chapter aims at investigating the impact of double absorber lead-free perovskite engineering and band alignment, by using the appropriate carriers transport layers, on the photovoltaic performances of lead-free PSCs. To do so, accurate numerical modeling and simulations are carried out to assess the device performance using the proposed design strategy. It is revealed that the proposed approach based on combining double-absorber layer engineering aspect and band alignment optimization shows enhanced solar cell performances.

III.2 Numerical modeling framework

Numerical tools constitute the backbone for the simulation of novel devices. This fact is justified by offering not only the possibility of studying various optical and electrical properties of materials but also contributing to the reduction of time needed to conduct optimization experiments. In addition, numerical tools can be used very efficiently to predict the device behavior as a function of time without opting for its practical fabrication and testing. In this context, SCAPS-1D can be considered as one of the most prominent software tools dedicated for the simulation of semiconductor properties. It is based on solving fundamental equations of semiconductors namely the Poisson equation, the electron and hole continuity equations through numerical differentiation and the Gummel type iteration method [16,17]. These equations can be formulated as

$$\frac{dp_n}{dt} = G_p - \frac{p_n - p_{n0}}{\tau_p} - p_n u_p \frac{dE}{dx} - u_p E \frac{dp_n}{d_x} + D_p \frac{d^2 p_n}{dx^2} \quad \text{(III.1)}$$

$$\frac{dn_p}{dt} = G_n - \frac{n_p - n_{p0}}{\tau_n} - n_p u_n \frac{dE}{dx} - u_n E \frac{dn_p}{d_x} + D_n \frac{d^2 n_p}{dx^2} \quad \text{(III.2)}$$

$$\frac{d}{dx}\left(\varepsilon(x)\frac{d\phi}{dx}\right) = q[p(x) - n(x) + N_{d^+}(x) - N_{a^-}(x) + N_t(x) - N_t(x)] \quad \text{(III.3)}$$

where ε is the dielectric permittivity, q denotes the electron charge, G stands for the rate of generation, D represents the diffusion coefficient, φ represents the electrostatic potential, E is the electric field, $p(x)$ and $n(x)$ are the free holes and electrons, $pt(x)$ and $nt(x)$ designate the trapped holes and electrons, $Nd+$ and $Na-$ are the donor and acceptor ionized doping concentrations, and x represents the thickness.

Our objective in this chapter is to propose a new solar cell design by optimizing the band energy alignment at the interface using the appropriate charge carriers transport

layers and two different lead-free perovskite films placed directly one above the other, where the layer with wide band gap is on top as illustrated in Figure III.1(a).

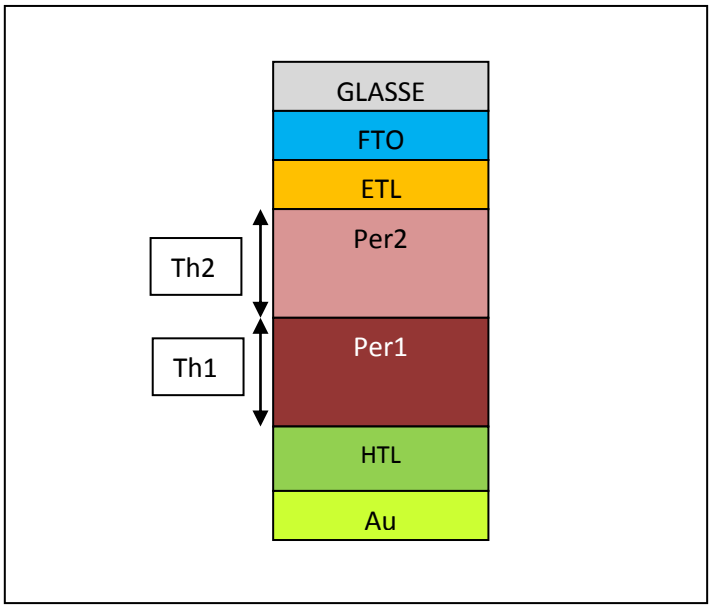

(a)

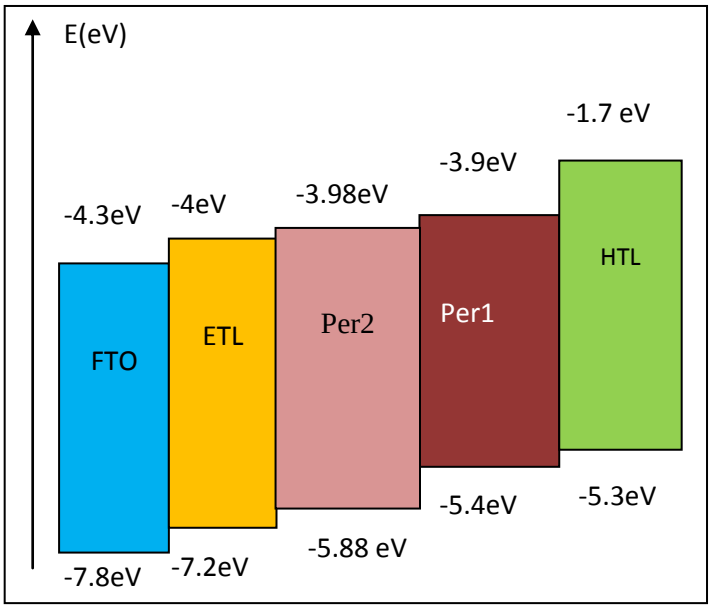

(b)

Figure III.1: A schematic view (a): proposed structure; (b): band gap energy alignment.

The properties of these two perovskite layers have been carefully chosen from literature [18,19] to achieve higher performance in terms of stability and efficiency. The band

energy alignment is well respected as shown in Figure III.1(b). The first absorber is a halide perovskite MAGeI3 (CH3NH3GeI3) which has the potential to replace toxic lead-based PSCs. Furthermore, it holds numerous advantages like tunable band gap, optical absorption, effective mass, and stability in comparison to MAPbI3. The hybrid Ge-based perovskite reveals commensurable photovoltaic performance similar to Pb and Sn as the germanium element belongs to the same subgroup with lead and tin [20,21]. The second absorber is CsSnGeI3, where such free-lead perovskite highlights superior performance and exceptional air stability over its pure counterparts CsSnI3 and CsGeI3 [18,22]. The schematic view of the proposed PSC is given in Figure III.1(a), where the two perovskite layers MAGeI3/CsSnGeI3 are sandwiched between FTO/ETL from the upper side and HTL/Au from the bottom of the structure. STO and CuSCN are used as ETL and HTL, respectively. Electrical and optical parameters of materials used in our simulations are summarized in Table III.1.

Table III.1: Set of Material parameters adopted for the simulations.

Parameters	**FTO [24]**	**STO(ETL) [19]**	**Per2 [19]**	**Per1 [18]**	**CuSCN(HTL) [23]**
Thickness (µm)	0.200	0.05	0.75	0.75	0.100
Bandgap Eg(eV)	3.5	3.2	1.90	1.5	3.5
Electron affinity χ (eV)	4.3	4.0	3.98	3.90	4.0
Dielectric permittivity	9	8.7	10	28	9.0
CB effective density of states (cm^{-3})	2.2×10^{18}	1.7×10^{19}	1×10^{16}	3.1×10^{18}	2.2×10^{18}
VB effective density of states (cm^{-3})	1.8×10^{19}	2.0×10^{20}	1×10^{16}	3.1×10^{18}	1.8×10^{19}
Electron mobility ($cm^2/V.s$)	20	5.3×10^{3}	1.62×10^{5}	974	20
Hole mobility ($cm^2/V.s$)	10	6.6×10^{2}	1.01×10^{5}	213	10
Donor Concentration N_D (cm^{-3})	1×10^{18}	2×10^{16}	1×10^{9}	0	0
Acceptor Concentration N_A (cm^{-3})	0	0	1×10^{9}	1×10^{19}	1×10^{19}

The numerical simulations are performed under AM 1.5 solar spectrum at 1000W/m2 incident light power, and 300 K room temperature.

III.3 Results and discussions

Figure III.2 shows the obtained J-V characteristics of the simulated PSCs based on wide band gap PSC ($MAGeI_3$), low band gap PSC ($CsSnGeI_3$), and the double layered PSC ($MAGeI_3/CsSnGeI_3$) structures.

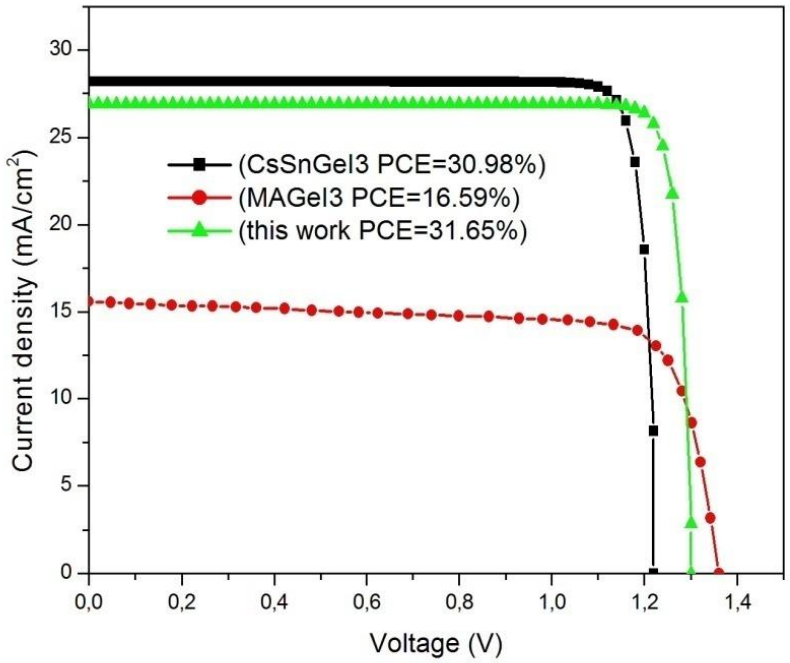

Figure III.2: current density–voltage characteristics of several lead-free perovskite solar cells

The defect densities at the considered interfaces are presented in Table III.2. Besides, Table III.3 summarizes the photovoltaic parameters associated with the investigated PSC structures. It is clearly shown from Figure III.2 and Table III.3 that the short circuit current of ($CsSnGeI_3$) PSC is much greater than that offered by ($MAGeI_3$) PSC. This is mainly due to the high absorption capabilities of $CsSnGeI_3$ material as compared to $MAGeI_3$. While, the open circuit voltage associated with $MAGeI_3$-based PSC is superior to that provided by $CsSnGeI_3$-based PSC. This behavior can be attributed to the high band gap of wide band-gap of $MAGeI_3$ (1.9 eV) as compared to that of $CsSnGeI_3$ perovskite material (1.5 eV) counterpart. In addition, MAGeI3-based PSC exhibits better band alignment promoting reduced interface recombination effects, which allows reduced V_{OC} deficit.

Table III.2: Defect density values for the layers and at the interface of the investigated PSC structure.

Parameters	**ETL [19]**	**HTL [18]**	**HTL/Per1 [18]**	**Per2/ETL [19]**	**Per1 [18]**	**Per2 [19]**
Defect Type	Neutral	Neutral	Neutral	Neutral	Neutral	Neutral
Capture cross section σ_n(cm^{-2})	1×10^{-15}	1×10^{-15}	1×10^{-18}	1×10^{-15}	1×10^{-15}	1×10^{-15}
Capture cross section σ_p(cm^{-2})	1×10^{-15}	1×10^{-15}	1×10^{-16}	1×10^{-15}	1×10^{-15}	1×10^{-15}
Energetic distribution	*Single*	*Single*	*Single*	*Single*	*Single*	*Single*
Energy level with respect to E_v (eV)	*0.6*	*0.650*	*0.6*	*0.6*	*0.6*	*0.6*
Characteristic energy (eV)	*0.1*	*0.1*	0.1	*0.1*	*0.1*	0.1
Total density N_t (cm^{-3})	1×10^{15}	1×10^{14}	1×10^{12}	1×10^{11}	1×10^{14}	1×10^{15}

Despite this, it is demonstrated from Table III.3 that the use of CsSnGeI3 absorber can pave the way for achieving an enhanced efficiency value of 30.98% as compared to the conventional structure based on MAGeI3 perovskite material (16.59%). On the other hand, the proposed structure based on double layered PSC (MAGeI3/CsSnGeI3) can offer a high efficiency value of 31.65% using the same layers thicknesses and under the same conditions. This enhancement is attributed to the role of double layered structure for offering the dual-benefit of enhanced absorption capabilities and reduced recombination effects at the perovskite/ETL interface. Therefore, this is a motivating result to implement our design methodology using double layered Perovskite jointly with numerical optimization. Initially, we set the two absorbent layers of the same thickness as 0.750 µm, we get a short circuit current close to the first PSC (CsSnGeI3) and an open circuit voltage close to the second PSC (MAGeI3).

As a matter of fact, ETL and HTL layers plays a crucial role in determining the performance of PSCs. Aiming at further boosting the photovoltaic performances of the proposed lead-free PSC design based on double layered absorber paradigm, various ETLs and HTLs are explored. It is found that the use of cuprous oxide Cu2O as HTL is the best choice for achieving enhanced efficiencies for PSC [18]. This is because of its small activation energy of the interfacial recombination defined as the difference between the absolute value of the band gap of the absorber layer and that of the valence band offset (VBO) [25].

Table III.3: Comparison of solar cell parameters for various PSC based on dissimilar absorber layers.

	V_{OC}(V)	J_{SC}(mA/cm^2)	FF(%)	PCE(%)
CsSnGeI3(Per1) [18]	1.22	28.19	89.52	30.98
MAGeI3(Per2) [19]	1.36	15.58	77.88	16.59
(MAGeI3/CsSnGeI3) This work	1.30	26.89	90.23	31.65

The activation energy for carrier recombination can be expressed as:

$$VBO = Ev(HTL) - Ev(Absorber\ Layer) \quad (4)$$

where *Ev(HTL*), and *Ev(Absorber Layer)* designate the energy valance band minimum of the HTL and the Absorber Layer, respectively. Hence, in the rest of simulations we keep using Cu_2O, while different ETLs such as SnO_2, PCBM, TiO_2 and IGZO are alternately used. The input parameters associated with the latter ETL materials are recapitulated in Table III.4.

Table III.4: Set of ETL Material parameters adopted in the simulation.

Parameters	**SnO2 [19]**	**PCBM [25]**	**IGZO [18]**	**SnO2 [23]**	**TiO2 [26]**
Thickness (µm)	0.05	0.05	0.05	0.05	0.05
Bandgap Eg(eV)	3.6	2	3.05	3.4	3.2
Electron affinity χ (eV)	4.5	3.9	4.16	4.0	3.9
Dielectric permittivity	9	3.9	10	9	9
CB effective density of states (cm^{-3})	2.2×10^{18}	2.5×10^{21}	1×10^{19}	2.2×10^{18}	1×10^{21}
VB effective density of states (cm^{-3})	1.8×10^{19}	2.5×10^{21}	1×10^{19}	1.8×10^{19}	2×10^{20}
Electron mobility (cm^2/V.s)	100	0.2	50	100	25
Hole mobility (cm^2/V.s)	25	0.2	5	25	100
Donor concentration N_D (cm^{-3})	1×10^{20}	2.93×10^{17}	1×10^{17}	1×10^{15}	1×10^{19}
Acceptor concentration N_A (cm^{-3})	0	0	0	0	0

The simulation results obtained for the proposed PSCs based on double layer absorber aspect with the proposed ETL materials are given in Table III.5.

Table III.5: Performance comparison between PSCs based on different ETLs.

Parameters	V_{OC}(V)	J_{SC}(mA/cm^2)	FF(%)	PCE(%)
SnO_2 [19]	1.27	27.00	87.91	30.19
PCBM	1.31	24.22	87.95	28.02
IGZO	1.33	27.07	90.25	32.52
SnO_2 [23]	1.33	27.08	90.64	32.69
SiGe [30]	0.78	49.80	83.50	28. 57
TiO_2	1.33	26.97	90.64	32.56

From this table, it can be seen that the PSC with the PCBM ETL provides the lowest PCE, while PSC with the SnO_2 [23] ETL offers the highest efficiency. The performance of PSCs with TiO_2 ETL and IGZO are also acceptable, whereas we recorded a good short circuit current using SnO_2 [19] and a relatively lower open circuit voltage affecting the solar cell efficiency. The conduction band offset (CBO) level of almost all ETL materials used in this chapter is in excellent band alignment with that of the $MAGeI_3$ Perovskite, except for SnO_2 [19] as elucidated in Figure III.3. The CBO is defined by equation (5), which denotes the difference between CB level of ETL and that of the perovskite.

$$CBO = Ec(ETL) - Ec(Absorber\ Layer) \qquad (III.5)$$

Basically, when the CBO is negative (CB level of ETL is lower than that of perovskite), an energy cliff will be formed at the ETL/Perovskite interface and conversely, an energy spike will be formed if CBO is positive. Thus, an energy cliff is formed at the SnO2/Perovskite and IGZO/Perovskite interfaces, while energy spikes are generated at the other ETL/Perovskite interfaces. The flow of photo-generated electrons is not be hindered by the energy cliff.

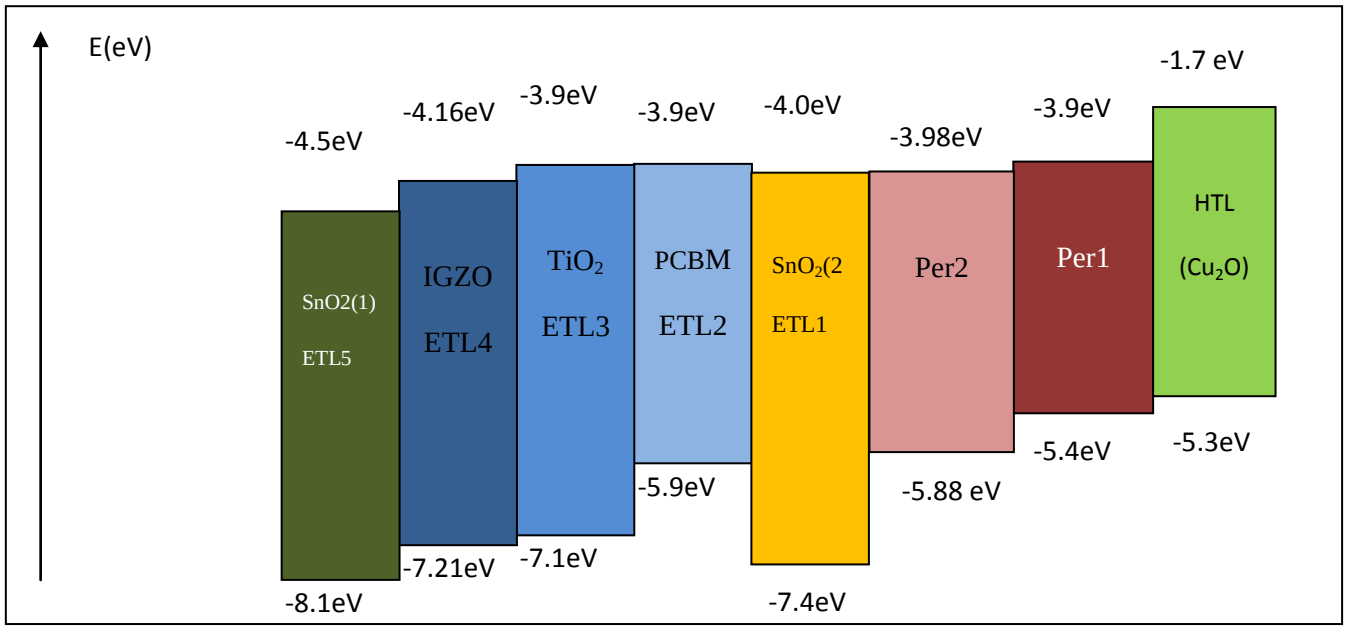

Figure III.3: ETLs perovskite energy band alignment.

However, the activation energy for carrier recombination (the difference between the band gap of perovskite and the absolute value of CBO) becomes lower than the band gap of perovskite, which makes interface recombination effects as the dominant mechanism of the PSC device [27,28]. Thus, Voc deficit increases with the recombination rate increase, which is the case for PSC with SnO2 ETL exhibiting low electron affinity [19]. On the other hand, the energy spike is formed at the other ETLs/Perovskite interfaces, which acts as a barrier for the photo-generated electrons. However, the activation energy for carrier recombination is equal to the band gap of the perovskite. The activation energy is higher than that calculated by the energy cliff, which can definitely improve the performance of the cell. It is also proved that the energy spike in a small range has less effect on the transfer of photo-generated electrons but has greater impact on the carrier recombination rate [27]. It is revealed from Table III.5 that the use of TiO2 and SnO2 [23] offer higher efficiencies. This is mainly related to their CB level, which is perfectly aligned with perovskite CB and their carrier mobility is higher than other ETL materials. Nevertheless, as the CBO continues to increase, the performance will decrease to achieve high VOC and PCE. The CB level of ETL should not be deeper than CB level of perovskite like the case of SnO2 [19]. Both TiO2 and PCBM have a small absolute CBO value but the low PCE of yield in PCBM is attributed to its dielectric constant, low mobility, and low band gap [28] compared to

other ETLs studied in this chapter. Therefore, SnO2 is selected as the optimal ETL material for the proposed lead-free PSC based on double layered absorber engineering.

III.3.1 Impact of perovskite layer thickness

The absorber layer plays a crucial role in determining the performance of solar cells, and particularly those composed of Ge-based perovskite photo-absorbing material [28]. In this framework, its thickness can influence greatly the absorption capabilities of the device and thereby the performance of the solar cell (Jsc Voc FF and PCE). To obtain the optimum geometrical parameters of the inserted double layered perovskite absorber, the optimization ratio of both absorber layer thicknesses is shown in the following equation:

$$R = \frac{\mathrm{Th}\,1}{\mathrm{Th}\,1+\mathrm{Th}\,2} \quad \text{where (Th1+Th2=1.5µm)} \qquad \text{(III.6)}$$

with Th1 and Th2 are the thickness of CsSnGeI3 and MAGeI3, respectively. For comparison purposes, the sum of the two layers thicknesses is kept fixed equal to 1.5 µm, which corresponds to the value of the thickest layer CsSnGeI3 [18]. It can be clearly observed from Figure III.4 that the increase in the ratio leads to enhance the efficiency of the proposed PSC-based on double layered absorber structure.

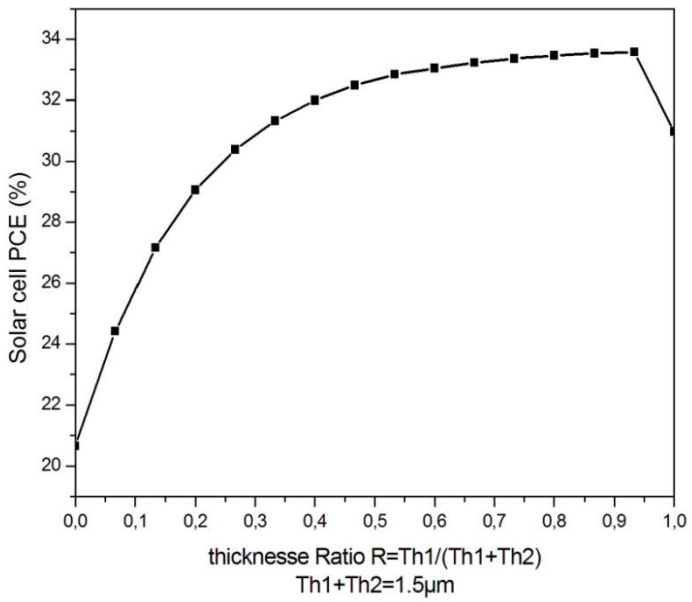

Figure III.4: Solar cell PCE as a function of the thickness ratio of the two perovskite layers.

After the specific value of R=0.5 µm, the efficiency saturates until reaching the maximum value at R=1.4 µm. after the latter critical value, the efficiency decreases to reach its lower value of 16.69%, corresponding to the conventional structure with $MAGeI_3$ perovskite absorber. Accordingly, it is revealed that the best PCE of the double layered perovskite solar cell is 33.57%, where the thicknesses of the two layers are 1.4µm and 0.1µm for the $CsSnGeI_3$ and $MAGeI_3$, respectively.

The J-V curve of the double layered perovskite solar cell with different lead-free perovskite solar cell is exposed in Figure III.5.

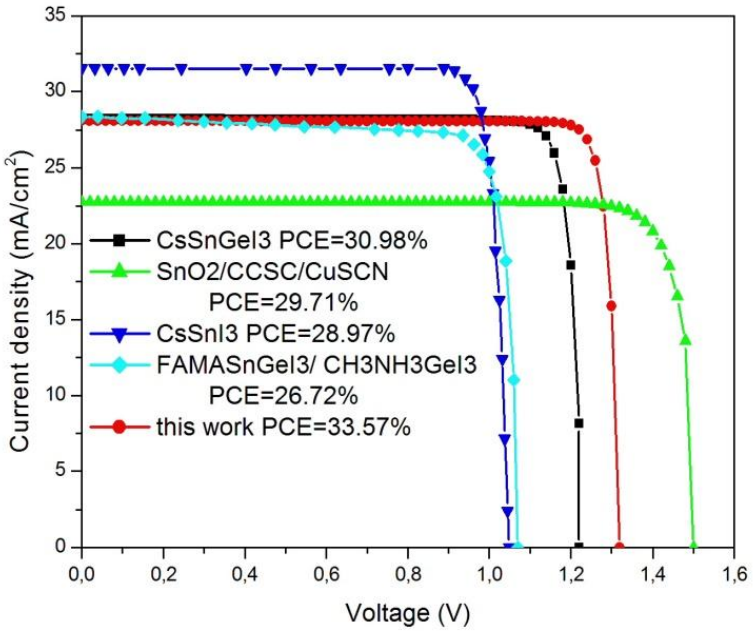

Figure III.5: I-V characteristics of the proposed PSC design based on optimized HTL, ETL and double layered absorber compared to other lead-free perovskite solar cells.

It can be noticed by referring to the detailed results of Table III.6 that our PSC structure has the best FF and PCE with values 90.37% and 33.57%, respectively. This enhanced value of the FF can be explained by the improved resistive behavior of the investigated structure, where the use of Ge-based perovskites can promote low series resistance. The optimized structure also exhibits one of the best Voc with 1.32 V and an excellent Jsc with 28.11mA/cm^2. This indicates the effectiveness of the proposed PSC based on an optimized absorber with double layered structure and appropriate HTL and ETL for promoting high-efficiency lead-free perovskite solar cells [31].

Table III.6: Performance comparison between the optimized device and various lead-free perovskite SCs.

Devices	V_{OC}(V)	J_{SC}(mA/cm^2)	FF(%)	PCE(%)
$CsSnGeI_3$ [18]	1.22	28.19	89.52	30.98
FTO/SnO_2/CCSC/CuSCN/ (Au) [23]	1.5	23.47	84.19	29.71
$CsSnI_3$ [29]	1.048	31.53	87.66	28.97
Au/Cu_2O/$FAMASnGeI_3$/ $CH_3NH_3GeI_3$/ZnO/FTO [19]	1.07	28.36	84.46	26.72
$CH_3NH_3PbI_3$+SiGe+ SiGeSn [30]	0.78	49.80	83.50	28. 56
This work	1.32	28.11	90.37	33.57

III.4 Conclusion

In this chapter, a new high-efficiency lead-free perovskite solar cell design based on the optimization of both double-absorber material and the charge carriers transport layers is proposed. In this context, lead-free materials that are eco-friendly and characterized by their stability are used. The effect of different HTL and ETL materials on the double layered PSC performance is exhaustively investigated, and the appropriate absorber thickness from the best ratio of the two perovskite layers thickness is selected. The proposed PSC with double-absorber aspect demonstrated high photovoltaic performances with a current density of Jsc of 28.11 mA/cm2, and a voltage of Voc of 1.32V, and FF of 90.37%, and a PCE of 33.57%. These findings are obtained by selecting the Cu2O, and SnO2 as the most suitable HTL and ETL, respectively, which contributed to enhance the performance of the solar cell by promoting an optimized band alignment and reduced recombination effects. In addition, the use of a double layered perovskite absorber with optimized thickness configuration enables achieving better absorption capabilities and a high degree of freedom for optimizing the band alignment at the ETL/absorber/HTL interfaces. Therefore, we believe the proposed

design methodology has great application potential in the development of high-performance lead-free perovskite solar cell.

References

[1] K. Branker, M. Pathak and J. M. Pearce, "A review of solar photovoltaic levelized cost of electricity," Renew. Sustain. Energy Rev., vol. 15, pp.4470-4482, 2011.

[2] P. K. Nayak, S. Mahesh, H. J. Snaith and D. Cahen , "Photovoltaic solar cell technologies: analysing the state of the art," Nature Review Materials, vol. 4, pp. 269-285, 2019.

[3] M. A. Green, "Tracking solar cell conversion efficiency," Nature Reviews Physics, vol. 2, pp. 172–173, 2020.

[4] H. Ferhati, F. Djeffal, L.B. Drissi, "Performance improvement of Perovskite/CZTS tandem solar cell using low-cost ZnS/Ag/ITO multilayer spectrum splitter, " Superlattices and Microstructures, vol. 148, pp. 106727, 2020.

[5] K. Kacha, F. Djeffal, H. Ferhati, D. Arar, M. Meguellati, " Numerical investigation of a double-junction a: SiGe thin-film solar cell including the multi-trench region," Journal of Semiconductors, vol. 36,pp. 064004, 2015.

[6] H. Ferhati, F. Djeffal and K. Kacha, "Optimizing the optical performance of ZnO/Si-based solar cell using metallic nanoparticles and interface texturization," Optik, vol. 153, pp. 43-49, 2018.

[7] H. Ferhati and F. Djeffal, "Graded band-gap engineering for increased efficiency in CZTS solar cells," Optical materials, vol.76, pp. 393-399, 2018.

[8] M. C. Beard, J. M. Luther and A. J. Nozik, "The promise and challenge of nanostructured solar cells," Nature Nanotechnology, vol. 9, pp. 951–954, 2014.

[9] National Renewable Energy Laboratory. Perovskite Efficiency Chart; National Renewable Energy Laboratory: Golden, CO, USA, 2020.

[10] T. Zhang, H. Li, H. Ban, Q. Sun, Y. Shen, M.K. Wang, "Efficient CsSnI 3 -based inorganic perovskite solar cells based on a mesoscopic metal oxide framework via incorporating a donor element", J. Mater. Chem. vol. 8, pp. 4118–4124, 2020.

[11] F. Giustino, H.J. Snaith, " Toward lead-free perovskite solar cells, " ACS Energy Lett., vol. 1, pp.1233–1240.2016.

[12] Baig, F., Y. H. Khattak, B. Marí, S. Beg, A. Ahmed and K. Khan, "Efficiency Enhancement of CH3NH3SnI3 Solar Cells by Device Modeling, " Journal of Electronic Materials, vol. 47, pp. 5275-5282, 2018.

[13] W. Ming, H. Shi, M.H. Du, " Large dielectric constant, high acceptor density, and deep electron traps in perovskite solar cell material CsGeI3, " J. Mater. Chem, vol. 4, pp. 13852–13858, 2016.

[14] S. Bhattarai, T.D. Das, "Optimization of carrier transport materials for the performance enhancement of the MAGeI3 based perovskite solar cell, " Solar Energy, vol. 217, pp. 200-207, 2021.

[15] S. Bhattarai, R. Pandey, J. Madan, F. Ahmed, S. Shabnam, "Performance improvement approach of all inorganic perovskite solar cell with numerical simulation," Materialstoday communications, vol.33, pp. 104364, 2022.

[16] M. Burgelman, P. Nollet, and S. Degrave, "Modelling of polycrystalline semiconductor solar cells," Solid Films, vol. 361-362, pp. 527–532, 2000.

[17] F. Liu, J. Zhu, J. Wei, Y. Li, M. Lv, S. S. Yang et al., "Numerical simulation: toward the design of high-efficiency planar Perovskite solar cells," Applied Physics Letters, vol. 104, pp. 253508-253516, 2014.

[18] H. Sabbah, "Numerical Simulation of 30% Efficient Lead-Free Perovskite $CsSnGeI_3$-Based Solar Cells," Materials, vol.15, pp.3229, 2022.

[19] N. Singh, A. Agarwal, M. Agarwal "Numerical simulation of highly efficient lead-free all-Perovskite tandem solar cell," Solar Energy, vol 208, pp. 399–410, 2020.

[20] S. Raghvendra, C. Pathak, S. K. Pandey "Design, Performance, and Defect Density Analysis of Efficient Eco-Friendly Perovskite Solar Cell," IEEE Trans on Electron Devices, Vol. 67, pp. 2837 - 2843, 2020.

[21] T. Krishnamoorthy et al, "Lead-free germanium iodide Perovskite materials for photovoltaic applications," Journal of Materials Chemistry A, vol. 3, pp.23829-23832, 2015.

[22] Milimo Amos Nalianya et al, "Numerical study of lead free $CsSn_{0.5}Ge_{0.5}I_3$ Perovskite solar cell by SCAPS-1D," Optik - International Journal for Light and Electron Optics, vol. 248 , pp. 168060-168072, 2021.

[23] Subhash C. Yadav et al, " Stable lead-free $Cs_4CuSb_2Cl_{12}$ layered double Perovskite solar cells yielding theoretical efficiency close to 30%," j.optmat ,vol.132, pp.112676-112685, 2022.

[24] S. Abdelaziz , A. Zekry , A. Shaker , M. Abouelatta, "Investigating the performance of formamidinium tin-based Perovskite solar cell by SCAPS device simulation," Optical Materials, vol. 101, pp.109738-109746, 2020.

[25] He. Y, Xu. L, Yang. C, Guo. X, Li. S, "Design and Numerical Investigation of a Lead-Free Inorganic Layered Double Perovskite $Cs_4CuSb_2Cl_{12}$ Nanocrystal Solar Cell by SCAPS-1D," Nanomaterials, vol. 11, pp. 2321-2340, 2021.

[26] A.C. Piñón Reyes. A.C, R.C. Ambrosio Lázaro , K. Monfil Leyva et al, "Study of a Lead-Free Perovskite Solar Cell Using CZTS as HTL to Achieve a 20% PCE by SCAPS-1D Simulation," Micromachines, vol. 12, pp. 1508-1528, 2021.

[27] Y. Gan et al, "Numerical Investigation Energy Conversion Performance of Tin-Based Perovskite Solar Cells Using Cell Capacitance Simulator," Energies, vol. 13, pp. 5907-5924, 2020.

[28] A-A. Kanoun et al, "Toward development of high-performance Perovskite solar cells based on $CH_3NH_3GeI_3$ using computational approach," Solar Energy, vo. 182, pp. 237–244, 2019.

[29] S. Srivastava et al, "Comparative Performance Analysis of Lead-Free Perovskites Solar Cells by Numerical Simulation, " Journal of Applied Physics, vol. 131, pp.175001-175024, 2022.

[30] G. Kumar, J. Kaur, R. Basu, "Performance Analysis of Planar Heterojunction Perovskite Solar Cell Featuring Double Hole Transport Layer & Backplane, " Silicon, vol. 14, pp. 463–474, 2022.

[31] A. Maoucha, F. Djeffal, H. Ferhati "Numerical Investigation of a new Double-Absorber Lead-free Solar Cell via SCAPS-1D, " International Conference on Electrical Engineering, Computing Science and Automatic Control (CCE), Mexico city, Mexico, 2023.

.

CHAPTER IV

Lead-free perovskite/Cd-free CZTSSe tandem cell exceeding 28% efficiency through current matching and band-gap optimization

Abstract:

Tandem solar cells are capable of dividing the solar spectrum over multiple sub-cells with distinct band-gaps, leading to more efficient conversion of sunlight into electricity compared to single-junction solar cells. In this chapter, we investigate a new eco-friendly tandem solar cell design utilizing lead-free perovskite (LFP)/CZTSSe that can achieve very high efficiency levels, while remaining cost-effective. The proposed design consists of a LFP-based top cell with wide band-gap of 1.8 eV, and a Cd-free CZTSSe-based bottom cell with graded band-gap profile. Using numerical modeling, the standalone top and bottom cells were calibrated to validate our simulations with experimental data, an investigation was conducted to examine how the performance of the device is affected by sub-cell parameters such as structures, thickness, unabsorbed spectrum by top cell and GBG paradigm. The two cells have been improved, leading to an increase in the tandem efficiency and a rise in the matching current. The results show that the highest efficiency value of 28.4% was obtained with top and bottom cell thicknesses of 950 nm and 1µm, respectively. Our study introduces a novel approach to improving the efficiency of tandem solar cells at an affordable cost. The proposed design methodology resolves optical and electrical losses and toxicity issues and also offers better efficiency.

IV.1 Introduction

The increasing need for energy has created significant environmental concerns regarding the use of fossil fuels [1]. As a result, it has become essential to develop renewable energy sources that are highly efficient, cost-effective, and eco-friendly [1-2]. In this context, photovoltaic (PV) technology is conceded as a potential alternative for clean energy generation. Si-PV is currently the leading player in the PV industry, reaching an efficiency record of 26.6%, which is getting closer to the Schokley-Queisser limit of single-junction solar cells 33% [2-6]. The only way to exceed this limit is by combining two or more individual solar cells with dissimilar band-gaps. This is known as multi-junction technology that allows the absorption of different ranges of wavelength bands, while maintaining reduced thermalization losses [7-10]. Initially, the upper limit for the theoretical efficiency of double-junction tandem solar cells was approximately 42%, but recent theoretical calculations have extended this limit to 46% [11-12]. In addition, the elaboration of low cost solar cells required the development new design approaches based on thin-film technology using non-toxic and eco-friendly materials such as lead-free perovskites, CIGS, SnS and CZTS [13-15].

Perovskite solar cells with an efficiency record of 25.7% have recently been introduced as a promising option for developing high performance low-cost solar cells [16]. These cells use readily available materials and can be produced using simple and low-cost techniques. Perovskite materials are highly promising as wide band-gap top cells or narrow band-gap bottom cells in tandem devices [17-22], due to their band-gap tenability between 1.2 and 2.2 eV. This latter property makes perovskite material as one of the top candidates for developing tandem solar cells capable of capturing a broad spectral range. Several tandem configurations based on perovskite top cell and Si, CIGS, or CZTS bottom cells, have shown the potential to attain efficiencies surpassing 32.5% [23-25]. However, the advancement of stable and highly efficient perovskite-based tandem solar cells is impeded by reliability issues such as toxicity and degradation-related aging effects [20-26]. To address these concerns, scientists have focused their research efforts on lead-free perovskites to eliminate the toxicity of lead. Transition metals like Sn and Ge have been utilized as substitutes for lead due to their comparable electronic structures and their capacity to form new lead-free perovskites. CZTS p-type chalcogenide semiconductor is gaining a great deal of attention for thin-

film photovoltaic due to its abundance in the earth, low cost, non-toxic nature, high absorption coefficient (greater than $10^4 cm^{-1}$), tunable band-gap and unique optical characteristics [27-29]. More importantly, its inherent advantages make it a potential solution for balancing high-efficiency and low fabrication cost in solar cell technology [29-33]. However, the recorded values (12.6%) are still lower than that offered by the CIGS thin film solar cell counterpart (23.4%) [27-30]. This can be attributed to several limitations, such as short minority carrier lifetime and high series resistance caused by the formation of MoS_2 at the CZTS/Mo interface.

This work involves the use of a top sub-cell that utilized a lead-free perovskite (LFP) material ($Cs_2AgBi_{0.75}Sb_{0.25}Br_6$) with a band-gap of 1.8 eV. For the bottom sub-cell, we used a CZTSSe material with a band-gap of 1.097 eV. This study focuses on exploring the effect of band alignment on the photovoltaic performance of both sub-cells, by utilizing appropriate carrier transport layers. Additionally, the research also examines the influence of band-gap engineering on the device's overall performance by applying the graded band-gap (GBG) aspect to the absorber layer in the bottom sub-cell. Moreover, the inclusion of a non-toxic buffer layer offers the potential to improve the alignment of junction bands and enhance conversion efficiency. We conducted a simulation study using SCAPS-1D. It is found that the optimized tandem design offers improved efficiency, making it a viable option for developing low-cost, reliable, and high-performance tandem solar cells.

IV.2 Tandem cell architecture and simulation methodology

IV.2.1 Device Structure and Materials

Tandem solar cell configurations can achieve higher efficiencies compared to single-junction cells because their capability for avoiding thermalization effects. In the study, LFP/CZTS tandem architecture is proposed to harvest the solar spectrum. The top cell, made of a high band-gap lead-free perovskite material, generates photocurrent from the short-wavelength region of sunlight, while the longer-wavelength photons are transmitted to a bottom solar cell based on kesterite earth abundant material. The diagram in Figure IV.1(a) illustrates the proposed Top sub-cell LFP configuration of ZnS and copper oxide (Cu_2O) as electron and hole transport layers, respectively. The LFP $Cs_2AgBi_{0.75}Sb_{0.25}Br_6$ material was employed as the absorber layer [34]. To achieve high efficiency, the electron and hole transport films will be carefully switched later.

The proposed bottom sub-cell structure comprises soda lime glass (SLG) substrate, Mo back contact, CZTSSe absorber layer, ZnSe buffer layer replacing the CdS toxic buffer layer, intrinsic ZnO layer, Al-doped ZnO (AZO) layer acting as TCO, and a 500 nm-thick Al collection grid [35]. The parameters t_{LFP} and t_{CZTSSe} are respectively, LFP absorber and CZTSSe thicknesses. Besides, the proposed structure consists of a graded band gap CZTS absorber with $E_g(y)$ linear profile as it is showb in Figure IV.1(c). In this context, Eg_1 and Eg_2 denote the limits band-gap values of the CZTSSe material. Alternatively, the second alteration in design comprises modifying the absorber layer of the bottom cell by implementing an optimized graded band-gap profile of the CZTSSe material and introducing a back surface field (BSF) between the absorber and the bottom electrode cathode Mo. This is done with the intention of achieving two objectives simultaneously, which are the optimization of the conduction band offset (CBO) and the minimization of bulk recombination, which can be further decreased by implementing a BSF, as shown in Figure IV.1(b).

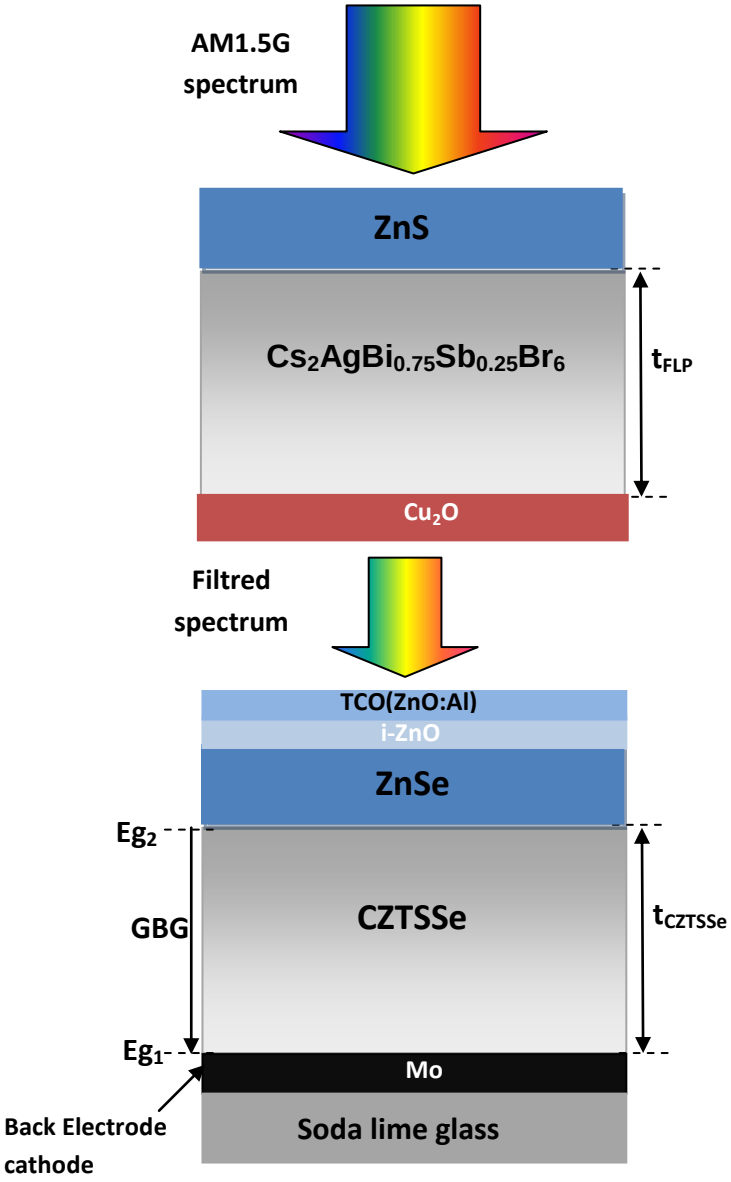
AM1.5G spectrum
ZnS
$Cs_2AgBi_{0.75}Sb_{0.25}Br_6$
t_{FLP}
Cu_2O
Filtred spectrum
TCO(ZnO:Al)
i-ZnO
ZnSe
Eg_2
GBG
CZTSSe
t_{CZTSSe}
Eg_1
Mo
Soda lime glass
Back Electrode cathode

(a)

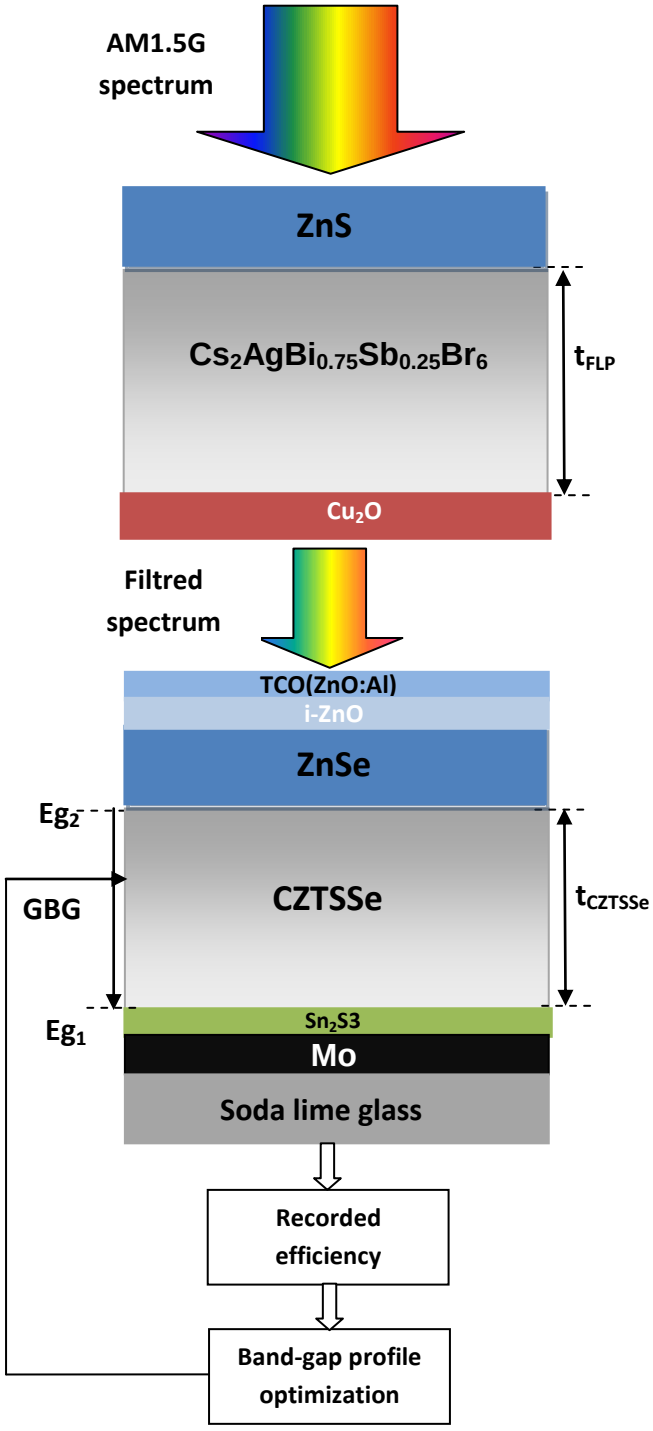
AM1.5G spectrum
ZnS
$Cs_2AgBi_{0.75}Sb_{0.25}Br_6$
t_{FLP}
Cu_2O
Filtred spectrum
TCO(ZnO:Al)
i-ZnO
ZnSe
Eg_2
GBG
CZTSSe
t_{CZTSSe}
Eg_1
Sn_2S3
Mo
Soda lime glass
Recorded efficiency
Band-gap profile optimization

(b)

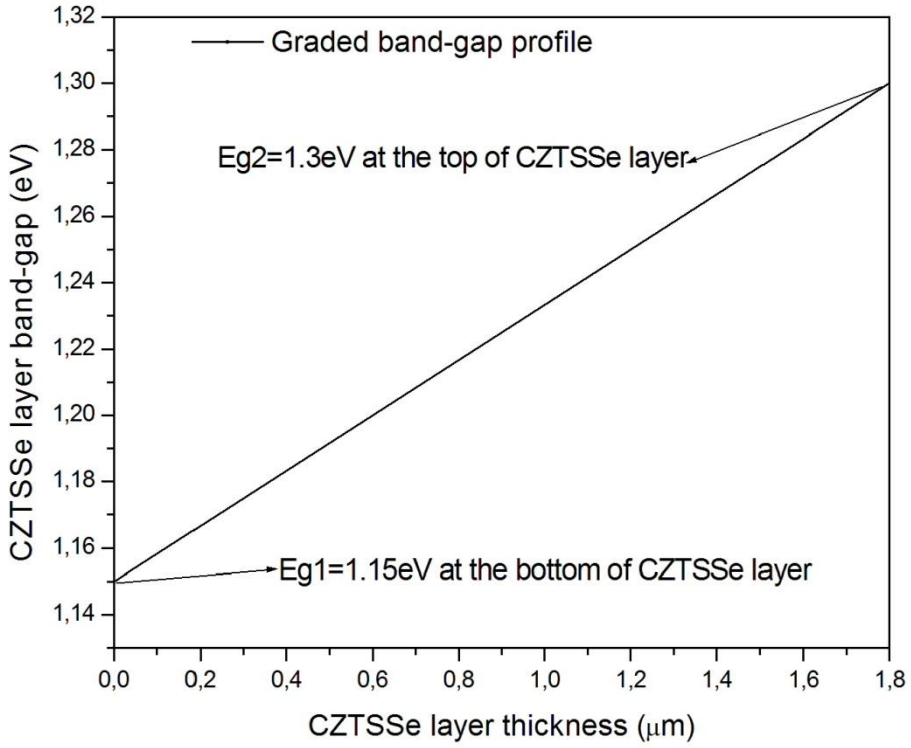

(c)

Figure IV.1: (a) Cross-sectional view of the investigated LFP/CZTSSe tandem solar cell with a random graded band-gap aspect. **(b)** Cross-sectional view of the optimized LFP/CZTSSe tandem solar cell. **(c)** Band gap grading profile of the CZTSSe Absorber layer.

To accurately simulate the suggested tandem structure, one could represent the examined LFP/kesterite structure as a series combination of two distinct single-junction solar cells having different band-gap energies (one made of LFP and the other made of CZTSSe material). In this context, the top layer of the solar cell is exposed to the AM1.5G standard spectrum while the bottom layer is exposed to the remaining unabsorbed spectrum. The unabsorbed or the transmitted spectrum simulates the optical behavior of the top layer. To do so, an optical transmission filter is used, which is calculated using the following equation [36-37].

$$S(\lambda)=S_0(\lambda).exp(-\alpha_{ITO}.d_{ITO}).exp(-\alpha_{SnO2}.d_{SnO2}).exp(-\alpha_{ETL}.d_{ETL}).exp(\alpha_{perov}.d_{perov}).exp(-\alpha_{HTL}.d_{HTL}) \quad (IV.1)$$

where α is the absorption coefficient of each material, $S_0(\lambda)$ is the global AM1.5G spectrum, and d represents the thickness of deferent solar cell layers. The basic characteristics of the structures, which were obtained from previously published literature [34, 38-41] are provided in Table IV.1 and Table IV.2.

Table IV.1: Set of the bottom sub-cell parameters adopted for the simulations.

Parameters	Sn_2S_3 (BSF)	CZTSSe	ZnSe	i-ZnO	ZnO-Al
Thickness (µm)	0.010	1	0.05	0.05	0.300
Bandgap Eg(eV)	1.09	1.097	2.9	3.3	3.3
Electron affinity χ (eV)	4.26	4.0	4.02	4.4	4.4
Dielectric permittivity	12.5	13.6	10	9	9.0
CB effective density of states (cm^{-3})	1×10^{19}	2.2×10^{18}	2.2×10^{18}	2.2×10^{18}	2.2×10^{18}
VB effective density of states (cm^{-3})	1×10^{19}	1.8×10^{19}	1.8×10^{19}	1.8×10^{19}	1.8×10^{19}
Electron mobility ($cm^2/V.s$)	25	100	25	100	100
Hole mobility ($cm^2/V.s$)	100	25	100	25	25
Donor Concentration N_D (cm^{-3})	0	0	1×10^{18}	1×10^{18}	1×10^{18}
Acceptor Concentration N_A (cm^{-3})	3×10^{18}	1×10^{15}	0	1×10^{18}	0

To confirm the accuracy of the developed model, we compared the J-V characteristics obtained through simulation of the conventional LFP and CZTSSe-based solar cells (as shown in Figure IV.2 with the experimental data provided in [34-35]. This figure indicates a close match between the simulated and experimental results, demonstrating the accuracy of our numerical modeling methodology used for analyzing the electrical and optical properties of the proposed tandem cell structure.

Table IV.2: Set of the top sub-cell parameters adopted for the simulations.

Parameters	Cu_2O (HTL)	LFP (absorber)	ZnS
Thickness (µm)	0.040	0.4	0.04
Bandgap Eg(eV)	2.17	1.8	2.26
Electron affinity χ (eV)	3.2	3.58	3.5
Dielectric permittivity	7.11	6.5	9.67
CB effective density of states (cm^{-3})	2×10^{17}	2.2×10^{18}	3.7×10^{18}
VB effective density of states (cm^{-3})	1.1×10^{19}	1.8×10^{19}	1.8×10^{19}
Electron mobility ($cm^2/V.s$)	20	2	80
Hole mobility ($cm^2/V.s$)	80	2	330
Donor Concentration N_D (cm^{-3})	1×10^{7}	1×10^{13}	1×10^{16}
Acceptor Concentration N_A (cm^{-3})	1×10^{18}	1×10^{16}	0

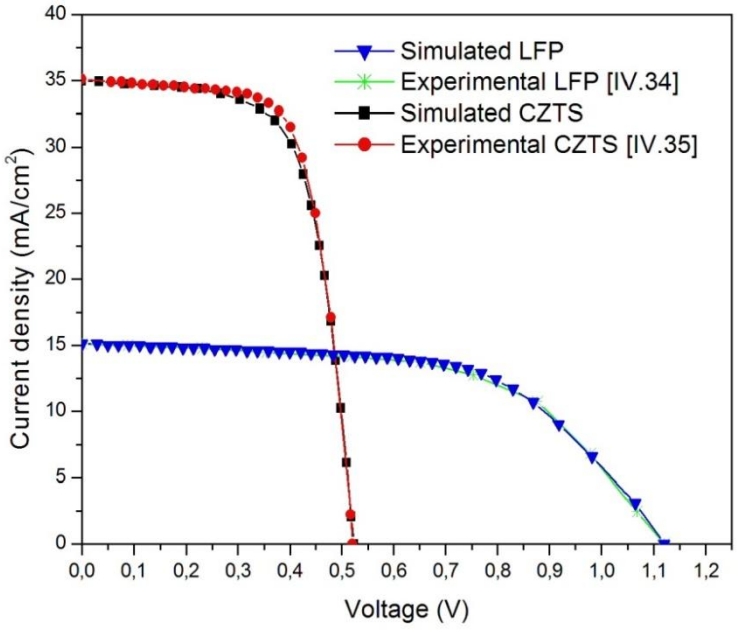

Figure IV.2: J-V characteristics of experimental data and simulation results associated with both the conventional LFP and CZTS solar cells.

IV.2.2 Numerical Method

This study uses a software tool known as SCAPS (solar cell capacitance simulator), which is adopted to simulate the electronic characteristics of tandem solar cells made from perovskite and kesterite. SCAPS is a software that utilizes important equations to simulate the capture of sunlight, as well as the generation, transport, and extraction of electron/hole pairs [35]. This adaptable tool enables the entry of a broad range of unique materials parameters for the production of a specific solar device. The outputs of simulations are then used to evaluate their impact on the device's performance and obtain crucial insights into fundamental solar characteristics like materials defect density, recombination, location and level, band-gap alignment between device layers, and more. Overall, the use of SCAPS allows answering various fundamental questions related to materials science and device physics [42-43]. The basis of the theoretical calculation for semiconductors consists of three fundamental equations, which are Poisson's equation, the carrier continuity equation, and the drift-diffusion equation,

$$\frac{dp_n}{dt} = G_p - \frac{p_n - p_{n0}}{\tau_p} - p_n u_p \frac{dE}{dx} - u_p E \frac{dp_n}{d_x} + D_p \frac{d^2 p_n}{dx^2} \quad \text{(IV.2)}$$

$$\frac{dn_p}{dt} = G_n - \frac{n_p - n_{p0}}{\tau_n} - n_p u_n \frac{dE}{dx} - u_n E \frac{dn_p}{d_x} + D_n \frac{d^2 n_p}{dx^2} \quad \text{(IV.3)}$$

$$\frac{d}{dx}\left(\varepsilon(x)\frac{d\phi}{dx}\right) = q[p(x) - n(x) + N_{d^+}(x) - N_{a^-}(x) + p_t(x) - n_t(x)] \quad \text{(IV.4)}$$

where ε stands for the dielectric permittivity, q represents the electron charge, G represents the generation rate, D designates the diffusion coefficient, φ represents the electrostatic potential, E refers to the electric field, $p(x)$ and $n(x)$ represent the free holes and electrons, and $p_t(x)$ and $n_t(x)$ denote the trapped holes and electrons. N_{d+} and N_{a-} represent the donor and acceptor ionized doping concentrations, respectively, and x represents the thickness.

IV.3 Results and discussion

perovskite is considered the best choice for creating high-performance and cost-effective tandem solar cells. The ETL and HTL layers are crucial for determining the performance of perovskite solar cells. To improve the photovoltaic efficiency of the free-lead PSC design, various ETLs and HTLs were explored. It was discovered that using cuprous oxide Cu_2O as the HTL was the most effective way to enhance the PSC's

efficiency [44]. This is due to the small activation energy of interfacial recombination, which is the difference between the band gap of the absorber layer and the valence band offset (*VBO)* [45]. The activation energy for carrier recombination can be expressed as:

$$VBO = Ev_{(HTL)} - Ev_{(Absorber\ Layer)} \quad \text{(IV.5)}$$

where $Ev_{(HTL)}$, and $Ev_{(Absorber\ Layer)}$ denote the energy valance band minimum of the HTL and the Absorber Layer, respectively. In the same way, ETL and perovskite absorber interface has a significant impact on performance of the device, if the band alignment between the perovskite absorber and the ETL is not appropriate, it can affect the shunt and series resistance, as well as recombination resistance of the device. To address these issues, it is important to carefully select materials with high electron mobility and proper band alignment for the ETL/perovskite interface to provide an excellent conduction band offset (*CBO*). This will improve electron injection and hole blocking, leading to higher current density J_{sc} and better overall device performance [46].

$$CBO = Ec_{(ETL)} - Ec_{(Absorber\ Layer)} \quad \text{(IV.6)}$$

which indicates the difference between CB level of ETL and that of the absorber layer.

It was found that the best ETL choice is the ZnS with its high electron affinity, which enables efficient electron extraction from the perovskite layer. Additionally, ZnS has a wide band-gap, which minimizes energy losses due to recombination and ensures high open-circuit voltage in the device [47]. In this perspective, Figure IV.3(a) displays the J-V curve linked to the optimized LFP solar cell compared to the conventional structure. The figure illustrates that the proposed design has better photovoltaic characteristics than the conventional design, with a higher output voltage of 1.43V, an improved efficiency of 14.83%, and a FF of 67.17%. These enhancements are due to the selection of ETL/HTL, which possesses improved band alignment, reducing interface recombination effects and allowing for a reduction in V_{OC} deficit.

Selecting narrow band-gap materials for the bottom cells is also crucial for achieving superior output voltage and high efficiency. Under standard AM1.5G illumination, in Figure IV.3(b) the J-V characteristics of the optimized design were compared to that of both the proposed structure with a random band-gap profile and the conventional structures counterparts. The main objective for utilizing a CZTSSe absorber layer with a graded band-gap profile is to improve the performance of kesterite solar cells, by enhancing the absorption characteristics across the complete solar spectrum. Besides, the usage of the graded band-gap approach creates a consistent

potential gradient in the CZTSSe absorber layer, creating an extra electric field that facilitates efficient separation of electron-hole pairs and boosts the carrier's lifetime. For further more enhancement a BSF layer of Sn_2S_3 was introduced between CZTSSe and Mo layers, to create a barrier for electrons, which can reduce the carrier recombination rate in the backside of the device. To prevent toxicity, the buffer layer used was the Zinc Selenide (ZnSe), a semiconductor compound with a direct band gap [48], which considered to be one of the most favorable options among various other possible substitute materials [49-50]. Figure IV.3(b) provides clear evidence that the suggested designs demonstrate better performance in terms of photocurrent (approximately 35.92 mA/cm^2) open circuit voltage (around 0.91 V), and a fill factor of 77.44 when compared to the standard version. Furthermore, the proposed design leads to higher conversion efficiency (approximately 24.32%) compared to the conventional design (12.30%). The photovoltaic parameters of the devices are summarized in Table IV.3 alongside comparison against experimentally fabricated perovskite and CZTS solar cells with wide band-gap and graded band-gap of top and bottom cells, respectively.

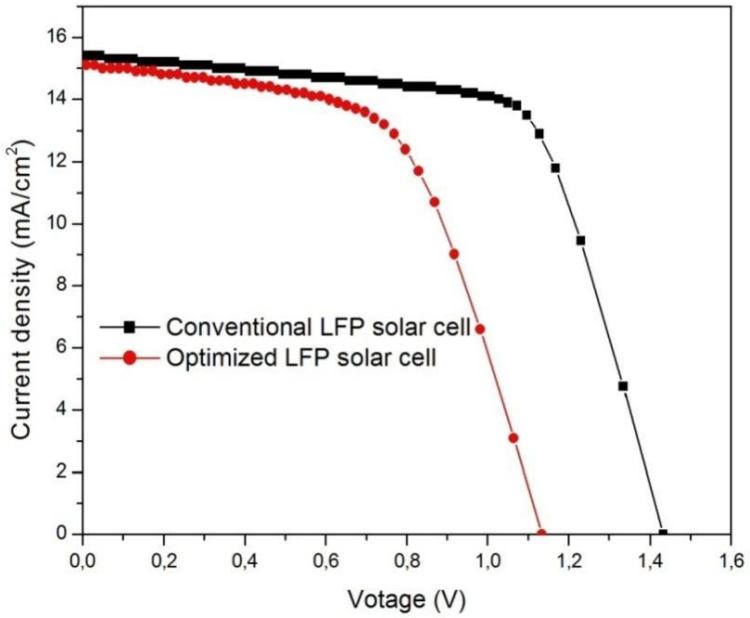

(a)

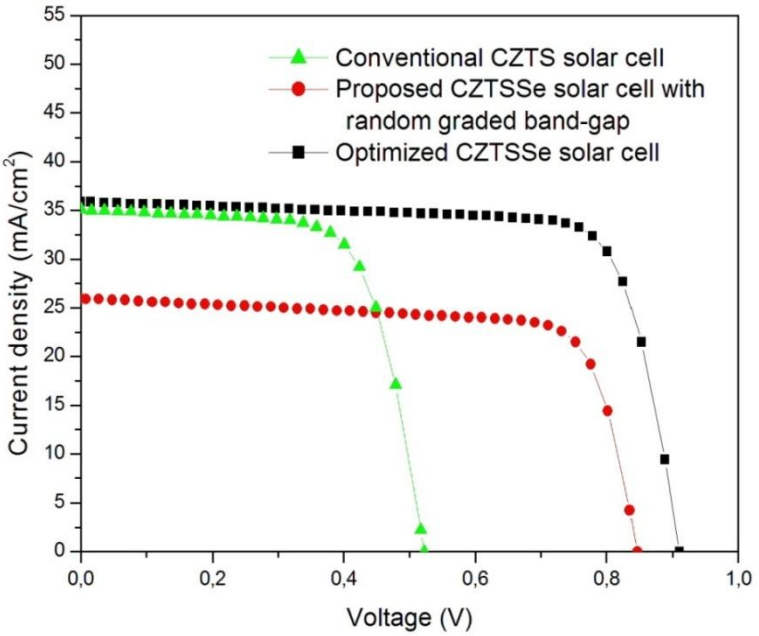

(b)

Figure IV.3: J-V characteristics comparison between: (a) the optimized LFP and the conventional structures. (b) the optimized design and that of both the proposed structure with a random band-gap profile and the conventional structures counterparts.

Table IV.3: Performance comparison between conventional and optimized structures .

Devices	V_{OC}(V)	J_{SC}(mA/cm^2)	FF(%)	PCE(%)
Experimental LFP	1.12	15.1	58.5	10.08
Optimized LFP	1.43	15.4	67.17	14.83
Experimental CZTS	0.52	34.98	67.20	12.30
Proposed GBG CZTSSe	0.84	25.97	75.41	16.56
Optimized GBG CZTSSe	0.91	34.92	77.44	24.32

IV.3.1 Current matching

The band gap has an impact on the theoretical yield of a single-junction solar cell. A large band gap can be used for a high-voltage, but this will give a low current. Conversely, if the band gap is reduced to absorb most of the spectrum, the voltage of the cell decreases. However, a multi-junction cell can efficiently collect low-energy photons while still achieving a high-voltage cell [51]. In this perspective, the top cell is exposed to an AM1.5 spectrum, and the transmitted spectrum S(λ), is determined by using the absorption coefficient and thickness of all layers in the top cell, as indicated in equation (IV.1). Firstly, the top cell is modeled by changing the absorber layer thickness from 400 nm to 1300 nm, while keeping other layers' thickness constant. As the absorber layer thickness increases in the top cell, the power of the filtered transmitted spectrum decreases, particularly at shorter wavelengths, which is due to greater absorption in the top cell with a thicker absorber layer. This filtered spectrum is then used to illuminate the bottom cell. According to reference [34], increasing the thickness of the top cell results in a decrease in the transmitted photocurrent due to the greater absorbed photocurrent.

The two-terminal tandem solar cell behaves like two diodes connected in series. As a result of this configuration, an equal amount of current must pass through each cell at all times. Furthermore, the total voltage across the tandem device is the sum of the voltage across each individual cell. Thus, in a tandem device, the cell that has a lower short current acts as the limiting cell for the overall J_{SC}, while the total open circuit voltage is the sum of the individual V_{OC} values of each cell [52]. Consequently, to ensure an equivalent J_{SC} value in tandem devices, the thickness of both the top and bottom cells are optimized, and the same tunnel recombination junctions are utilized to facilitate this [53-54]. Furthermore, if the thickness of the top cell is increased beyond the optimized value, it leads to increased parasitic absorption in the top cell and reduced optical coupling in the bottom cell, resulting in a decreased overall J_{SC} value for the tandem device. Similarly, if the thickness of the top cell is decreased below the optimized value, it results in reduced absorption in the top cell and the same consequence of decreased J_{SC}. Taking these factors into account, the conditions for current matching are determined in order to achieve equal J_{SC} values in both the top and bottom cells. This is accomplished by analyzing the computed filtered spectrum with

varying thicknesses of the absorber layer in the top cell. In order to address the variation in thickness of the top cell, ten different filtered spectra are generated (corresponding to top cell thicknesses ranging from 400nm to 1300nm) and used to illuminate the bottom cell. The photovoltaic parameters of the bottom cell are then assessed based on these spectra. Using the J_{SC} values of the bottom cell from the filtered spectrum, the current matching condition for the tandem device was determined and illustrated in Figure IV.4. The optimal current matching condition was achieved when the top cell had a thickness of 950 nm and the bottom cell had a thickness of 1000 nm. As shown in Figure IV.4, the J_{SC} values of the top and bottom sub-cells were 17.9 mA/cm^2 and 17.8 mA/cm^2, respectively.

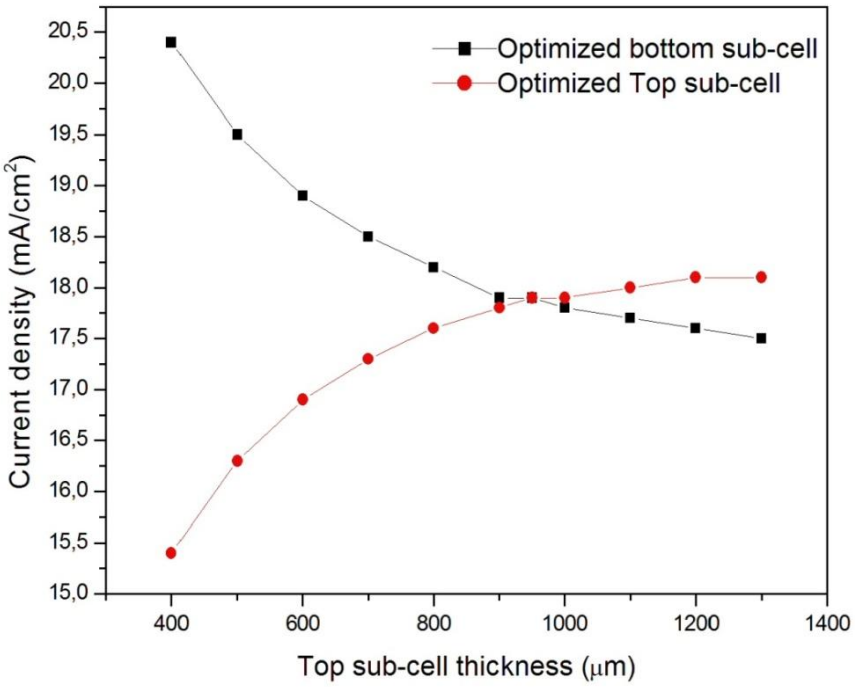

Figure IV.4: The current matching condition after optimization.

The J-V characteristics of the LFP/CZTSSe tandem solar cell can be simulated using the current matching condition determined above. The separately measured J-V curves of both the top and bottom cell at equal current are added together in series, meaning that their voltages are summed at equal current to obtain the J-V characteristics of the tandem device [52,55]. In Figure IV.5(a), The J-V curve of the tandem device is presented along with the J-V curve of the standalone top and bottom cells, which are illuminated with AM1.5sun spectrum. It can be observed from this figure that the top

cell (LFP) is the cell that restricts the current, having a higher V_{OC} (as a result of its high band-gap perovskite). In Figure IV.5(b), the J-V plot of the top sub-cell illuminated with AM1.5sun spectrum, the bottom sub-cell illuminated with the filtered spectrum, and the tandem solar cell are shown. It is clear from the plot that the V_{OC} of the tandem solar cell, which is 2.31 V, is the sum of the top and bottom solar cells' V_{OC}, which are 1.41V and 0.90 V, respectively. Furthermore, the photovoltaic parameters of the cells are presented in Table IV.4, where we found that the tandem solar cell has a J_{SC} of 17.9 mA/cm^2, FF of 69%, and PCE of 28.42%.

Table IV.4: Photovoltaic performance of top LFP sub-cell, Bottom CZTSSe sub-cell with filtered spectrum and the tandem solar cell.

Devices	V_{OC}(V)	J_{SC}(mA/cm^2)	FF(%)	PCE(%)
Top LFP SC	1.41	17.9	65.07	16.45
Bottom CZTSSe SC with filtered spectrum	0.9	17.85	74.99	11.94
Tandem SC	2.31	17.9	69	28.42

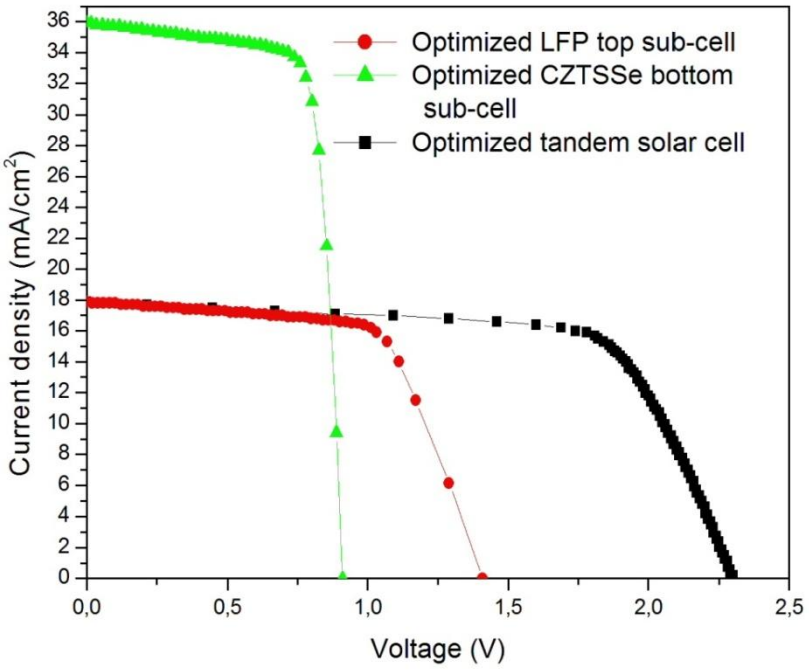

(a)

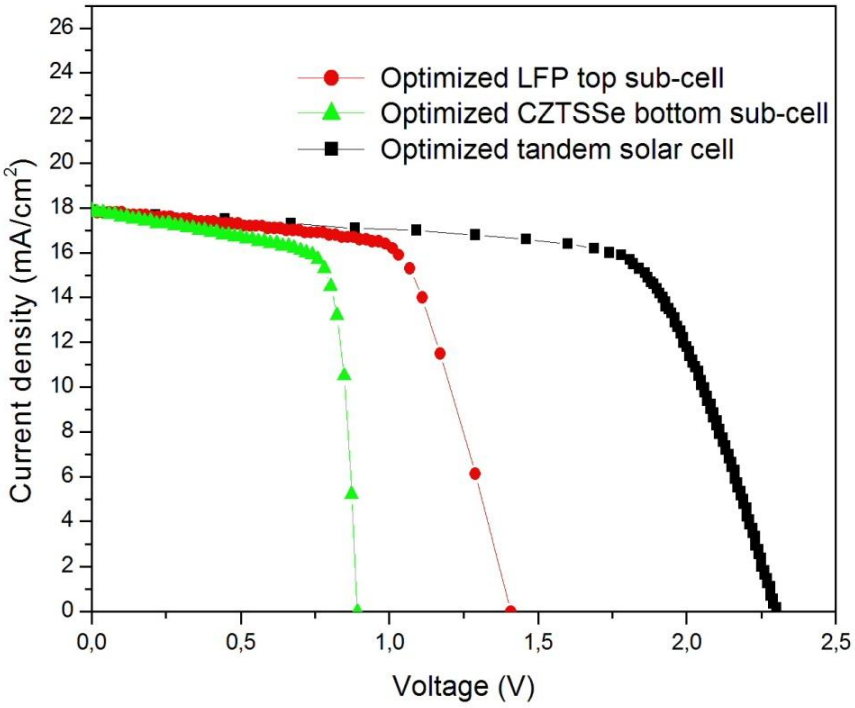

(b)

Figure IV .5: (a) J-V curve of the standalone top, standalone bottom and tandem cell. (b) J-V curve of top cell, bottom cell after fed with filtered spectrum and tandem cell.

In order to assess the effectiveness of the proposed approach in enhancing the tandem solar cell performance , the J-V curves for both the conventional structure and the optimized design with graded band-gap profiles were compared in Figure IV.6. This figure confirms that a significant improvement was achieved by using the GBG optimizer side in combination with the above optimization techniques, which has resulted in a significant enhancement in the cell performance. So that, there has been an improvement in both short circuit current, open-circuit voltage, and PCE. In Table IV.5 we have compared the results performance of our work with those of other studies, to evaluate the effectiveness of our optimized tandem cell in comparison to other research studies. This comparison is performed based on the solar cell performance metrics obtained from different tandem designs (Perovskite-CZTSSe [43], Perovskite-Perovskite [56], CZTS-CZTSSe [57], Perovskite-CIGS [58] and CZTS-Perovskite tandem solar cell [59]). The comparison indicates that our optimized design offered high Figures-of-Merit (FoMs) in comparison to that provided by other published studies

[43,56-59]. Moreover, in order to investigate the impact of top sub-cell band-gap profile on the tandem cell performances, we have implemented and optimized the graded band-gap profile of the perovskite absorber material by following the same steps, which have been previously utilized for the bottom sub-cell (kesterite material); but no improvement has been recorded using double graded band-gap optimization approach. This could be attributed to the narrow range of band-gap grading in the LFP cell (from 1.8 to 2 eV) [34, 60]. The obtained results make the proposed design methodology a potential alternative approach for developing low-cost and high performance non-toxic tandem thin film solar cells [61].

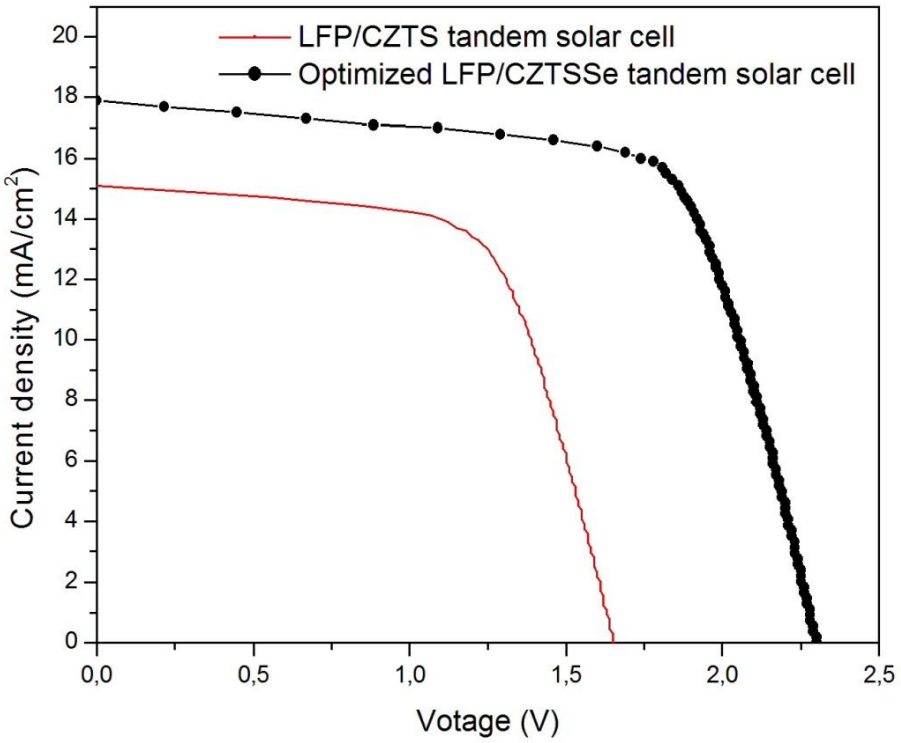

Figure IV.6: J-V characteristics of the optimized tandem design compared to the conventional tandem cell.

Table IV.5: Performance comparison between different tandem cell designs and our optimized Perovskite/CZTSSe tandem solar cell.

Devices	V_{OC}(V)	J_{SC}(mA/cm^2)	FF(%)	PCE(%)
Perovskite/perovskite tandem cell [56]	1.92	14.00	78.10	21.00
CZTS/CZTSSe tandem cell [57]	1.10	20.40	81.30	19.25
Perovskite/CIGS tandem cell [58]	1.68	19.17	71.9	24.2
CZTS/Perovskite tandem cell [59]	1.18	24.79	88.36	25.95
Perovskite/CZTSSe tandem cell [43]	1.70	14.90	65.30	16.58
This work	2.31	17.90	69	28.42

IV.4 Conclusion

In this work, we have proposed a new design methodology to improve the thin film tandem solar cells efficiency, made up of two sub-cells, a lead-free perovskite-based top sub-cell and a CZTSSe-based bottom sub-cell. The numerical analysis aimed to enhance the interfaces of the electron and hole transport layers to improve the band alignment and reduce the recombination effects, which ultimately led to a higher-performing LFP-cell. The performance of CZTSSe sub-cell was improved by introducing a graded band-gap profile, a BSF layer, and a non-toxic buffer layer (ZnSe). The simulation involved exposing the top sub-cell to the AM 1.5G sun spectrum and a filtered spectrum for the bottom sub-cell. The thickness of the two absorber layers was varied to investigate the current matching condition, where the optimized thicknesses of 950 nm and 1000 nm were found for the top and bottom absorber layers, respectively. A current-matched device with a J_{SC} of 17.9 mA/cm^2 was obtained, resulting in PCEs of 16.45% and 11.94% for the top and bottom cells, respectively, and a final tandem structure PCE of 28.42%. Therefore, this work proposed a design framework methodology offering new insights into reducing recombination losses and enhancing

absorbance efficiency, which could lead to the development of high-efficiency thin-film tandem solar cells for high-performance non-toxic photovoltaic applications. The study also highlights the importance of operating both cells at the maximum power condition to obtain an efficient tandem cell.

References

[1] International Energy Agency, Technology Roadmap: Solar Photovoltaic Energy, Technical report, International Energy Agency, 2010.

[2] K. Yoshikawa, H. Kawasaki, W. Yoshida, T. Irie, K. Konishi, K. Nakano, T. Uto, D. Adachi, M. Kanematsu, H. Uzu, K. Yamamoto, "Silicon heterojunction solar cell with interdigitated back contacts for a photoconversion efficiency over 26%," Nat. Energy, vol. 2, pp. 17032, 2017.

[3] L.C. Andreani, A. Bozzola, P. Kowalczewski, M. Liscidini, L. Redorici, "Silicon solar cells: Toward the efficiency limits," Advances in Physics: X, vol. 4, pp. 1548305, 2019.

[4] K. Kacha, F. Djeffal, H. Ferhati, M. Meguellati, "Numerical investigation of a double-junction a:SiGe thin-film solar cell including the multi-trench region," Journal of Semiconductors, vol. 36, pp. 064004-1- 064004-5, 2015.

[5] M.A. Green, E.D. Dunlop, J. Hohl-Ebinger, M. Yoshita, N. Kopidakis, X. Hao, C.A. Martin Green, "Solar cell efficiency tables (version 59)," Prog. Photovoltaics Res. Appl, vol. 30, pp.3–12, 2022.

[6] W. Shockley, H.J. Queisser, "Detailed balance limit of efficiency of p-n junction solar cells," J. Appl. Phys, vol. 32, pp. 510–519, 1961.

[7] H. Ferhati, F. Djeffal, A. Bendjerad, A. Benhaya, A. Saidi, " Perovskite/InGaAs tandem cell exceeding 29% efficiency via optimizing spectral splitter based on RF sputtered ITO/Ag/ITO ultra-thin structure, ". Physica E: Low-dimensional Systems and Nanostructures, vol. 128, pp. 114618, 2021.

[8] H. Ferhati, F Djeffal, "Exceeding 30% efficiency for an environment-friendly tandem solar cell based on earth-abundant Se/CZTS materials," Physica E: Low-dimensional Systems and Nanostructures Vol. 109, 52-58, 2019.

[9] T. Todorov, et al., "Monolithic perovskite-CIGS tandem solar cells via in situ band gap engineering," Adv. Energy Mater, vol. 5, pp. 1500799, 2015.

[10] U. Saha, M.K. Alam, "Proposition and computational analysis of a kesterite/kesterite tandem solar cell with enhanced efficiency," RSC Adv, vol. 7, pp. 4806, 2017.

[11] A.D. Vos, "Detailed balance limit of the efficiency of tandem solar cells," J. Phys. D. Appl. Phys, vol. 13, pp. 839–846, 1980.

[12] S. Abdul Hadi, E.A. Fitzgerald, A. Nayfeh, "Theoretical efficiency limit for a two-terminal multi-junction "step-cell," using detailed balance method," J. Appl. Phys, vol. 119, pp. 073104, 2016.

[13] K. Kacha, F. Djeffal, H. Ferhati, L. Foughali, A. Bendjerad, A.Benhaya, A. Saidi, "Efficiency improvement of CIGS solar cells using RF sputtered TCO/Ag/TCO thin-film as prospective buffer layer," Ceramics International, vol. 48, pp. 20194-20200, 2022.

[14] H. Ferhati, F. Djeffal, B.L. Drissi, "Performance improvement of Perovskite/CZTS tandem solar cell using low-cost ZnS/Ag/ITO multilayer spectrum splitter, Superlattices and Microstructures," Vol. 148, pp.106727, 2020.

[15] H. Ferhati, F. Djeffal, A. Bendjerad, A. Benhaya, A. Saidi, "Perovskite/InGaAs tandem cell exceeding 29% efficiency via optimizing spectral splitter based on RF sputtered ITO/Ag/ITO ultra-thin structure," Physica E: Low-dimensional Systems and Nanostructures, Vol. 128, pp.114618, 2021.

[16] G. Nazir, S.-Y. Lee, J.-H. Lee, A. Rehman, J.-K. Lee, S. I. Seok, S.-J. Park , "Stabilization of Perovskite Solar Cells: Recent Developments and Future Perspectives," Adv. Mater, vol. 34, pp. 2204380, 2022.

[17] H. Ferhati, F. Djeffal and L. B. Drissi, "A new approach to the modeling and simulation of multi-junction solar cells," Optik, vol. 200, pp.163452, 2020.

[18] S.P. Bremner, et al., "Analysis of tandem solar cell efficiencies under AM1.5G spectrum using a rapid flux calculation method," Prog. Photovoltaics Res. Appl, vol. 16, pp. 225–233, 2008.

[19] H. Ferhati, F. Djeffal, "An efficient analytical model for tandem solar cells," Materials Research Express, vol. 6, pp. 076424, 2019.

[20] Su Geun Ji, Ik Jae Park, et al, "Stable pure-iodide wide-band-gap perovskites for efficient Si tandem cells via kinetically controlled phase evolution," Joule, Vol. 6, pp. 2390-2405, 2022,.

[21] A. Zekry, I. Yahyaoui, F. Tadeo, "Generic Analytical Models for Organic and Perovskite Solar Cells," 10th International Renewable Energy Congress (IREC), Sousse, Tunisia, pp. 1–6, 2019.

[22] T. Leijtens, K.A. Bush, R. Prasanna, et al., "Opportunities and challenges for tandem solar cells using metal halide perovskite semiconductors," Nat. Energy, vol. 3, pp. 828–838, 2018.

[23] R. Lin, J. Xu, M. Wei, et al. "All-perovskite tandem solar cells with improved grain surface passivation," Nature, vol. 603, pp.73–78, 2022.

[24] P. Tockhorn, J. Sutter, A. Cruz, et al. "Nano-optical designs for high-efficiency monolithic perovskite–silicon tandem solar cells," Nat. Nanotechnol, vol. 17, pp. 1214–1221, 2022.

[25] F. Esmaeili and S. Khosroabadi, " A novel design of high efficiency perovskite solar cell using electron reflector strategy and transport layers optimization," the European Physical Journal Plus, vol. 136, pp.915, 2021.

[26] D.A. Chalkias, A. Karavioti, G.C. Papanicolaou, E. Stathatos, "Stability assessment of carbon-based hole-transport-layer-free perovskite solar cells under accelerated ageing: A combined experimental and predictive modelling analysis," Electrochimica Acta, vol. 427, pp. 140905, 2022.

[27] F.Z. Ramadan, F. Djeffal, L.B. Drissi, S. Saidi, H. Ferhati, "Highly efficient ACdTS kesterite solar cell based on a new photovoltaic material," Journal of Physics and Chemistry of Solids, vol.161, pp.110458, 2022.

[28] H. Ferhati, F. Djeffal, "Role of intermediate metallic sub-layers in improving the efficiency of kesterite solar cells: concept and optimization," Mater. Res. Express, vol. 5, pp. 036417, 2018.

[29] M. Minbashi, A. Ghobadi, E. Yazdani, et al. “Efficiency enhancement of CZTSSe solar cells via screening the absorber layer by examining of different possible defects,” Sci Rep, vol. 10, pp. 21813, 2020.

[30] M. Nakamura, K. Yamaguchi, Y. Kimoto, Y. Yasaki, T. Kato and H. Sugimoto, "Cd-Free Cu(In,Ga)(Se,S)2 Thin-Film Solar Cell With Record Efficiency of 23.35%," *IEEE Journal of Photovoltaics*, vol. 9, pp. 1863-1867, 2019,

[31] C. Zeng, Y. Liang, L. Zeng, L. Zhang, J. Zhou, P. Huang, R. Hong, “Effect of S/(S+Se) ratio during the annealing process on the performance of Cu2ZnSn(S,Se)4 solar cells prepared by sputtering from a quaternary target,” Solar Energy Materials and Solar Cells, vol. 203, pp. 110167, 2019.

[32] H. Ferhati, F. Djeffal, “Graded band-gap engineering for increased efficiency in CZTS solar cells,” Optical Materials, vol.76, pp.393-399, 2018.

[33] S. Chen, et al., “Compositional dependence of structural and electronic properties of Cu2ZnSn(S,Se)4 alloys for thin film solar cells,” Phys. Rev. B, vol. 83, pp.125201, 2011.

[34] J. Madan, Shivani, R. Pandey, R. Sharma, “Device simulation of 17.3% efficient lead-free all-perovskite tandem solar cell,” Solar Energy, vol 197, pp 212-221, 2020.

[35] K.-J. Yang, et al., “A band-gap-graded CZTSSe solar cell with 12.3% efficiency,” J. Mater. Chem. A, vol 4, pp.10151-10158, 2016.

[36] K. Kim, J. Gwak, S.K. Ahn, Y.J. Eo, J.H. Park, J.S. Cho, M.G. Kang, H.E. Song, J.H. Yun, “Simulations of chalcopyrite/c-Si tandem cells using SCAPS-1D,” Sol. Energy, vol. 145, pp. 52-58, 2017.

[37] D. Kumari, S. K. Pandey, “Effect of an ultra-thin 2D transport layer on eco-friendly Perovskite/CIGS tandem solar cell: A numerical study,” Micro and Nanostructures, Vol. 170, pp. 207398, 2022.

[38] A. Bouzidi, I. Bouchama , M. Hadjab, M. A. Saeed, “Numerical simulation of tandem solar cells based-CIGS and C-Si sub-cells using SCAPS -1D,” International Journal of advanced studies in computer science and engineering, vol. 11, pp. 17-27, 2022.

[39] S. Gohri, J. Madan, R. Pandey, R. Sharma, "Performance Analysis for SnS and Sn2S3-Based Back Surface Field CZTSSe Solar Cell: A Simulation Study," Journal of Electronic Materials, vol 50, pp. 6318-6328, 2021.

[40] Et-taya. Lhoussayne, A. Benami, and T. Ouslimane, "Study of CZTSSe-Based Solar Cells with Different ETMs by SCAPS," Sustainability, vol. 14, pp. 1916, 2022.

[41] S. Gohri, J. Madan, R. Pandey, R. Sharma, "Design and analysis of lead‑free perovskite‑CZTSSe based tandem solar cell," Optical and Quantum Electronics, vol. 171, pp. 1-11, 2023.

[42] M. Burgelman, P. Nollet, S. Degrave, " Modelling polycrystalline semiconductor solar cells," Thin Solid Films, vols: 361-362, pp. 527-532, 2000.

[43] M. Burgelman, K. Decock, A. Niemegeers, J. Verschraegen, S. Degrave, SCAPS Manual, pp. 1-111, 2016.

[44] H. Sabbah, "Numerical Simulation of 30% Efficient Lead-Free Perovskite CsSnGeI3-Based Solar Cells," Materials, vol. 15, pp. 3229, 2022.

[45] Y. He, L. Xu, C.Yang, X.Guo, S. Li, "Design and Numerical Investigation of a Lead-Free Inorganic Layered Double Perovskite Cs4CuSb2Cl12 Nanocrystal Solar Cell by SCAPS-1D," Nanomaterials, vol. 11, pp. 2321-2340, 2021.

[46] T. Kim, J. Lim, S. Song, "Recent Progress and Challenges of Electron Transport Layers in Organic-Inorganic Perovskite Solar Cells," Energies, vol. 13, pp. 5572, 2020.

[47] N. Touafek, R. Mahamdi, C. Dridi, "Impact of the secondary phase ZnS on CZTS performance solar cells," International Journal of Control. Energy and Electrical Engineering (CEEE), Vol. 9, pp. 6-9, 2019.

[48] M.A. Hines and Ph. Guyot-Sionnest, "Bright UV-Blue Luminescent Colloidal ZnSe Nanocrystals," The journal of physical chemistry, vol. 102 , pp. 3655-3657, 1998.

[49] M.N. Tousif, Md. Nahian Rabbi Ushan, Abdullah Al Joha, Sakib Mohammad, "A comprehensive study of CZTS solar cell simulation with ZnSe buffer layer," 2017 IEEE Region 10 Humanitarian Technology Conference (R10-HTC), Dhaka, Bangladesh, pp. 193-197, 2017.

[50] Md Abu Sayeed, H.K. Rouf, K. Md, A. Hussain, "Effect of thickness on characteristics of ZnSe thin film synthesized by vacuum thermal evaporation," J. Theor. Appl. Phys. vol. 14, pp. 251-259, 2020.

[51] S.R. Kurtz, P. Faine, and J.M. Olson , "Modeling of two-junction, series-connected tandem solar cells using top-cell thickness as an adjustable parameter," Journal of Applied Physics, vol. 68, pp. 1890-1895, 1990.

[52] J. Burdick, T. Glatfelter, "Spectral response and I-V measurements of tandem amorphous-silicon alloy solar cells," Solar Cells, vol. 18, pp. 301-314, 1986.

[53] B. Chen, Z. Yu, K. Liu, X. Zheng, Y. Liu, J. Shi, D. Spronk, P.N. Rudd, Z. Holman, J. Huang, " Grain engineering for perovskite/silicon monolithic tandem solar cells with efficiency of 25.4%," Joule, vol. 3, pp. 177-190, 2019.

[54] Ramírez Quiroz et al, "Interface molecular engineering for laminated monolithic perovskite/silicon tandem solar cells with 80.4% fill factor," Adv. Funct. Mater, vol. 29, pp. 1901476, 2019.

[55] K. Kim, J. Gwak, S.K. Ahn, Y.-J. Eo, J.H. Park, J.-S. Cho, M.G. Kang, H.-E. Song, J.H. Yun, "Simulations of chalcopyrite/c-Si tandem cells using SCAPS-1D," Sol. Energy, vol. 145, pp. 52-58, 2017.

[56] D. Zhao, C. Chen, C. Wang, et al., "Efficient two-terminal all-perovskite tandem solar cells enabled by high-quality low-bandgap absorber layers," Nat. Energy, vol. 3, pp. 1093-1100, 2018.

[57] A. Benzetta, M. Abderrezek , M. Djeghlal "Numerical study of CZTS/CZTSSe tandem thin film solar cell using SCAPS-1D," Optic, vol.242, pp.167320, 2021.

[58] Al. Amran, et. al., "Conformal monolayer contacts with lossless interfaces for perovskite single junction and monolithic tandem solar cells," Energy Environ. Sci, vol.12, pp. 3356-3369, 2019.

[59] M.A. Shafi, L. Khan, Shafi Ullah, Muhammad Yasir. Shafi, Amal. Bouich, Hanif Ullah, Bernabe Mari, "Novel compositional engineering for ~26% efficient CZTS-perovskite tandem solar cell," Optik, vol. 253, pp. 168568, 2022.

[60] E. Meyer, D. bMutukwa, N. Zingwe, R. Taziwa, "Lead-Free Halide Double Perovskites: A Review of the Structural, Optical, and Stability Properties as Well as Their Viability to Replace Lead Halide Perovskites," Metals, vol. 8, pp. 667, 2018.

[61] A. Maoucha, F. Djeffal, H. Ferhati, and F. AbdelMalek, "Eco-friendly perovskite/CZTSSe tandem cell exceeding 28% efficiency through current matching and bandgap optimization: a numerical investigation," The European Physical Journal Plus, vol. 138, 2023.

Conclusion

This dissertation has investigated the potential of soft-computing-based approaches for the study and modeling of semiconductor devices. The focus was on developing new models that can accurately represent the complex physical processes involved in these devices and on optimizing their performance. The objectives of this dissertation were to review the state of the art in the field, to develop new accurate models, to validate these models using experimental data, and to demonstrate their potential for the optimization of semiconductor device performance. The application of both analytical and numerical modeling techniques, combined with metaheuristic-based optimization approaches, can significantly improve the performance of semiconductor devices. Furthermore, the use of novel design strategies, such as hybrid GBG-PSO-approach and double-layered perovskite absorbers, can further enhance the efficiency and stability of thin-film solar cells based on non-toxic elements. The proposed design methodology also offers new insights into reducing recombination losses and enhancing absorbance efficiency, which could lead to the development of high-efficiency thin-film tandem solar cells for high-performance non-toxic photovoltaic applications. Overall, the work highlights the potential of various modeling techniques and design strategies to optimize the performance of semiconductor devices and advance the development of sustainable and eco-friendly energy technologies.

In the first chapter, the various equations that govern the physical behavior of a semiconductor have been presented. We have examined the use of analytical and numerical modeling techniques in the field of semiconductor devices, and their respective strengths and weaknesses. Analytical modeling can deliver faster closed-form solutions, but it may not capture complex or nonlinear phenomena with precision. In contrast, numerical modeling can provide more accurate results, but it can be computationally expensive and require iterative methods. Using both techniques jointly can lead to a better understanding of the system and enable optimization of device performance. The second section of this chapter has given an extensive review of metaheuristic-based optimization techniques and their categorization. The various global optimization methods, such as MOGA, PSO, ML, and ABC-based algorithms, have been carefully explained, and their fundamental concepts have been elucidated in detail. Moreover, the application of these metaheuristic methods to optimize semiconductor devices has been introduced. By utilizing these techniques, the

performance of semiconductor devices can be significantly enhanced besides the support of the design and optimization of new devices. The chapter has effectively described the fundamental concepts of these methods and provided insights into their potential applications in the field of semiconductor device optimization.

In chapter II, a new modeling framework design strategy has been proposed to enhance the performance of CIGS-based thin-film solar cells (TFSCs) using a hybrid GBG-PSO approach. The solar cell behavior has been investigated using new analytical models, and the accuracy of the obtained results has been confirmed by numerical simulations. Additionally, instead of the conventional toxic CdS buffer layer, ZnMgO has been employed, which includes graded band-gap engineering aspects that make it compatible with the CIGS absorber layer in terms of band alignment and light management behavior. The combination of the metaheuristic-based approach and the GBG aspect for both CIGS and ZnMgO layers has opened up new roads for improving TFSC performance. The optimized design using the GBG paradigm has yielded relatively a high improvement compared to the conventional CdS-based design, resulting in very satisfactory outcomes. Therefore, the proposed strategy will provide new guidelines for developing high-performance thin-film solar cells based on non-toxic elements.

A novel high-efficiency design for a lead-free perovskite solar cell is presented in chapter III, optimizing both the double-absorber material and charge carrier transport layers. Lead-free materials that are both eco-friendly and stable are used for this design. The double layered PSC performance is exhaustively studied to investigate the effect of different HTL and ETL materials. The appropriate absorbers thicknesses is selected based on the best ratio of the two perovskite layers thicknesses. The proposed PSC design with a double-absorber aspect demonstrates high photovoltaic performances by selecting Cu2O and SnO2 as the most suitable HTL and ETL, respectively. This leads to an optimized band alignment and reduced recombination effects that enhance the performance of the solar cell. Furthermore, using a double layered perovskite absorber with an optimized thickness configuration allows for better absorption capabilities and greater freedom to optimize the band alignment at the ETL/absorber/HTL interfaces.

The last chapter has presented a novel design approach aimed at enhancing the efficiency of thin film tandem solar cells, which is composed of two sub-cells: a lead-free perovskite-based top sub-cell and a CZTSSe-based bottom sub-cell. The numerical

analysis focused on improving the band alignment and minimizing the recombination effects at the interfaces of the electron and hole transport layers to enhance the performance of the lead-free perovskite sub-cell. Where the performance of the CZTSSe sub-cell was improved by incorporating a graded band-gap profile, a BSF layer, and a non-toxic buffer layer (ZnSe). During simulation, the top sub-cell was exposed to the AM 1.5G sun spectrum, while the bottom sub-cell was exposed to a filtered spectrum. Therefore, this research introduced a design framework methodology that shed light on reducing recombination losses and enhancing absorbance efficiency, which could pave the way for the development of high-efficiency thin-film tandem solar cells suitable for non-toxic photovoltaic applications. The study has also emphasized the importance of operating both sub-cells at their maximum power condition to achieve an efficient tandem cell.

This dissertation represents a significant contribution to the field of semiconductor device modeling and optimization based on soft computing and numerical modeling to study and design of high performance and reliable semiconductor devices. The results of this research will be valuable for both academic and industrial researchers working in various fields and can open new path ways for developing microelectronics circuits for future research applications. It is to note that this work can be extended by elaborating the proposed devices using appropriate experimental facilities.